Petrogenesis and geodynamic setting ~~implications~~ of Ediacaran rocks from the Sirwa massif, ~~(~~Central Anti-Atlas of Morocco~~); insights from U-Pb geochronology, whole-rock geochemistry, and Sm-Nd isotopes.~~

Abdelhay Ben-Tami[1,2], Said Belkacim[1,6], Jamal El Kabouri[1], Bouchra Baidada[3], Joshua H.F.L. Davies[4], Morgann G. Perrot[5], Mohamed Bhilisse[2], Mohamed Assalmi[2], Mariam Ferraq[1,6], Mohamed Bouabdellah[7,8], ~~David Lalonde[2].~~

[1] Laboratoire de Géologie Appliquée et Géo-Environnement, Département de la Géologie, Faculté des Sciences, Université Ibn Zohr, B.P.8106, Agadir, Maroc.
[2] Zgounder Millennium Silver Mining, Aya Gold and Silver Group, Rue De L'epargne, Quartier Racine, Casablanca, Maroc.
[3] Higher school of Technology, Fkih Ben Salah, Beni Mellal, Morocco.
[4] Department of Earth and Atmosphere Sciences, University of Quebec in Montreal, Montreal, QC H3C 3P8, Canada.
[5] Department of Earth and Planetary Sciences, McGill University, Montreal, Quebec H3A 0E8, Canada.
[6] Mining and Environmental Research Institute, University of Quebec in Abitibi-Timiskaming, Rouyn-Noranda, QC J9X 5E4, Canada.
[7] Laboratoire des Gîtes Minéraux, Hydrogéologie et Environnement, Faculté des Sciences, Université Mohammed Premier, 60000, Oujda, Maroc.
[8] Geology and Sustainable Mining Institute, Mohammed VI Polytechnic University, Benguerir 43150, Morocco.

Correspondence to: Abdelhay Ben-Tami (abdelhaybentami@gmail.com)

Abstract.

The geodynamic evolution of the post-Pan-African Anti-Atlas belt Orogeny ~~Anti-Atlas belt post-Pan-African orogeny~~ (~650 Ma) remains debated, particularly regarding the basement beneath the Central Anti-Atlas, and the geological processes leading to the formation of the Ediacaran Saghro Group (SG), and Ouarzazate Group (OG). New LA-ICP-MS U-Pb ages of 575 ± 3 Ma and 564 ± 2 Ma were obtained ~~respectively from samples Zg-106, and Zg-119~~ from two magmatic rocks of the OG. In addition, detrital zircons from SG ~~sediments~~ yield a 2025 Ma maximum depositional age (MDA) and a prominent ~~2.1 G~~2100 Ma ~~age~~ peak, indicating exclusive~~local~~ recycling of Paleoproterozoic basement into the Ediacaran SG bain.~~material~~. Geochemically, two magmatic series are identified : (i) ~~a~~ SG mafic~~-intermediate~~ rocks displaying a calc-alkaline ~~series~~ signature of within plate character with Nb-Ta and Ti negative anomalies from ~~early~~ a back-arc basin setting; and (ii) a felsic-intermediate high-K calc-alkaline to shoshonitic series of the OG of a post-collisional character.~~, exhibiting continental magmatic arc signatures~~. Isotope data (εNd_{620}: +3.2 to +4.6, TDM = 1.02-0.91 Ga for SG; εNd_{570}: -0.8 to +1.1, TDM = 1.30-1.15 Ga for OG), indicate that the SG formed from a near-pristine mantle source, with limited crustal input; whereas the younger OG involved significant reworking of older, evolved continental crustal material.~~(εNd (t): +3.2 to +4.5, TDM = 1431 – 1197 Ma for SG; εNd (t): -0.9 to +1.1, TDM = 1526 – 1252 Ma for OG), indicates that the SG formed from a dominantly juvenile, mantle-derived source, with limited crustal contribution; while the slightly younger OG involved significant reworking of older, evolved continental crustal material.~~

These findings sustain a model where Early Ediacaran SG sediments and associated magmatic rocks ~~mafic-intermediate volcanics~~ were ~~formed~~ deposited in a back-arc basin. During this basin development, its shoulders were locally formed by the 2~~.~~100 M~~G~~a Paleoproterozoic basement, supplying Paleoproterozoic zircons to the Saghro ~~host~~ basin~~. This, further supports the occurrence~~ , and corroborating the extension of the Eburnian basement north of the Anti-Atlas Major Fault (AAMF). ~~Additionally~~Subsequently, the younger OG ~~reflects~~ recorded a Late Ediacaran post-collisional ~~continental~~ crustal collapse event, where lithospheric delamination and potential slab break-off drove ~~involving~~ widespread crustal reworking and the emplacement of a Silicic Large Igneous Province (SLIP).

Keywords

Anti-Atlas; Ediacaran; ~~Saghro Group; Ouarzazate Group; Sirwa massif;~~ LA-ICP-MS U-Pb ~~on zircon~~geochronology; Saghro Group (SG); Ouarzazate Group (OG); 2~~.~~100 M~~G~~a Paleoproterozoic crust

1 Introduction

The Anti-Atlas belt of Morocco in the northern margin of the West African Craton (WAC) bears witness to a long-lived geological evolution ~~started~~ since the break-up of Rodinia (Hefferan et al., 2014; Gasquet et al., 2008; Thomas et al., 2002). ~~The Tonian - Cryogenian evolution of this belt record the establishment of a passive margin, and island arc which were accreted to the WAC margin at ca. 650 Ma, with the emplacement of syn-tectonic granitoids (Linnemann et al., 2019, 2014; Pereira et al., 2012a; Abati et al., 2010; Liégeois et al., 2006; Gasquet et al., 2005)~~. Accordingly, the initial rifting at ca. 900–700 Ma was evidenced by the 885 Ma Tonian mafic dikes. The rifting in question generated a WAC passive margin and the eventual development of a Cryogenian ocean lithosphere (Hefferan et al., 2014). This period is characterized by the deposition of the Lkest-Taghdout Group, a thick sequence of quartzites and carbonates (Alvaro et al., 2014b) (Fig. 1B). The subsequent evolution of the Anti-Atlas belt during the Ediacaran is still debated despite the improvements in the understanding of the multiple events that prevailed during Neoproterozoic times (D'Lemos et al. 2006; Samson et al. 2004; Gasquet et al. 2008, 2005, 2004; Thomas et al. 2004, 2002; Ennih and Liégeois, 2008, 2001; Walsh et al. 2002), and led to the final amalgamation of Gondwana (D'Lemos et al., 2006; Gasquet et al., 2008, 2005). Within this time frame, and based on paleogeographic reconstruction and lithostratigraphic correlations (Linnemann et al., 2014; Errami et al., 2021a; Walsh et al., 2012)~~;~~, the Anti-Atlas belt was close to the Cadomian subduction system. While the internal amalgamation of Gondwana was driven by large-scale Pan-African collisions between major cratonic blocks, the northern margin of the WAC experienced a synchronous but distinct tectonic regime (Rojo-Pérez et al., 2024; Stern, 2024; Hefferan et al., 2014). ~~In liaison, this subduction is responsible for the accretion of peri-Gondwana terranes and the final amalgamation of the Gondwana (El Kabouri et al., 2025; Rojo-Pérez et al., 2024; Stern, 2024; Garfunkel, 2015; Hefferan et al., 2014)~~. During the Ediacaran, this margin was proximal to the Cadomian accretionary system, a long-lived subduction-related orogen that developed along the Gondwana periphery (Linnemann et al., 2014; Nance et al., 2008).

HoweverMoreover, it is still debated whether the Anti-Atlas records the post-collisional phase of the Pan-African belt, or if it is related to the establishment of a back-arc basin induced by the southward-dipping Cadomian subduction beneath the amalgamated WAC-Iriri/Tazigzaout arc complex at ca. 620 Ma (Errami et al., 2021a; Walsh et al., 2012; El Hadi et al., 2010; Abati et al., 2010). Furthermore, the basement nature of the basement north of the AAMF Anti-Atlas Pan-African suture zone, known as the Anti-Atlas Major Fault is also still a matter of debate (Ennih and Liégeois, 2008, 2001). However, Iin the Zgounder Mine Region (ZGMR), a well-preserved section of Ediacaran sedimentation and magmatism provides key insights into the final stages of Pan-African tectono-magmatic evolution along the northern margin of the WAC.

The study area, so-called the “Zgounder Mine Region” in this contribution corresponds to the vicinity of the Zgounder Ag-Hg deposit (Ben-Tami et al., 2024). The Zgounder deposit is situated at approximately 265 km east of Agadir, and 220 km west of Ouarzazate, along the southern flank of the Ouzellagh-Sirwa Salient in the Central Anti-Atlas Mountains of the WAC. The Ediacaran period of the Zgounder Mine Region (630-539 Ma), is represented by : (i) the Saghro Group (SG) sedimentary successions and coeval mafic to intermediate units deposited at around 630 to 600 Ma (Abati et al., 2010); (ii) large felsic plutons, subvolcanic formations, along with coeval pyroclastic rocks referred to as the Ouarzazate Group (600 Ma - 539 Ma (Thomas et al., 2002).

Commenté [CM1]: Moved to section 2.1 on “Field characteristics and sample distribution”

We present new whole-rock geochemistrygeochemical, and Sm-Nd isotopes isotopic data for the Ediacaran successions of the Zgounder Mine Region. The aims areof these rocks in order to decipher their petrogenesis, explore magma sources, and investigate their geodynamic significance in Ediacaran evolution of the WAC. We also report new LA-ICP-MS U-Pb dating on magmatic and detrital zircons to constrain the lower Ediacaran magmatism and challenge the source of the Saghro Group's sedimentary units, hence, refining existing geodynamic models.

2 Geological backgroundsetting

2.1 The Anti-Atlas belt

The Anti-Atlas Mountainsbelt, located on the northern edge of the WAC, and consist of a Proterozoic basement and a Late Ediacaran to Paleozoic cover (Leblanc and Lancelot, 1980) (Fig. 1B). These mountains record two major orogenic cycles: the Paleoproterozoic Eburnean and the Neoproterozoic Pan-African, classically separated by the AAMF (Fig. 1B). orogenies. The Paleoproterozoic Eburnean Oorogeny is preserved in the Western Anti-Atlas, where low-- to high-grade metamorphic rocks are intruded by a series of granitoids dated at ~2.2 Ga (Hefferan et al., 2014, and references therein; O’Connor et al., 2010; El Hadi et al., 2010; Ennih and Liégeois, 2008; Gasquet et al., 2008, 2005; Thomas et al., 2002; Walsh et al., 2002; Aït Malek et al., 1998). The Central Anti-Atlas features the ophiolitic sequences and island-arc complexes of the Bou Azzer and Sirwa massifs (Admou et al., 2012; D’Lemos et al., 2006; Thomas et al., 2002, 2004). To the east, the Eastern Anti-Atlas comprises the Jbel Saghro and Ougnat massifs, which are composed exclusively of Neoproterozoic Pan-African units (Fig. 1B). These include an early Ediacaran basement of SG, consisting of folded meta-sedimentary rocks metamorphosed under greenschist facies conditions, and unconformably overlain by the late Ediacaran OG successions of volcanic and volcano-sedimentary nature (Ouabid and Garrido, 2023; Errami et al., 2021a; Yajioui et al., 2020; Michard et al., 2017; Blein et al., 2014; Álvaro et al., 2014, 2014b; Walsh et al., 2012; Abati et al., 2010; Errami et al., 2009; Gasquet et al., 2008; Liégeois et al., 2006; Thomas et al., 2002; Fekkak et al., 2001; Bajja, 2001; Ouguir et al., 1996).

Overlying these terranes, is the carbonate and quartzite succession of the Taghdout Group deposited in a passive margin (Errami et al., 2021a; Álvaro et al., 2014; Abati et al., 2010; Thomas et al., 2004). U-Pb ages on a quartzite sample from the Taghdout Group provided ages spanning from 2182 to 1987 Ma (Walsh et al., 2012). Moreover, undeformed Doleritic dikes intrude the Taghdout Group in the Ighrem and Zenaga inliers, and were dated between 1710 and 1630 Ma by Ikenne et al., (2017), and Ait Lahna et al., (2020), respectively. Overall, this implies that the Taghdout Group is in fact of Paleoproterozoic in age (Ikenne et al., 2017; Abati et al., 2010).

Commenté [CM2]: This chapter is completely rewritten. All regional names that are not shown in Fig. 1B are removed to facilitate understanding.

The Neoproterozoic episode known as the Pan-African orogeny is well established in the Central and Eastern Anti-Atlas (ca. 760 to 550 Ma) in numerous studies (Bouougri et al., 2020; Soulaimani et al., 2018; Triantafyllou et al., 2016; Karaoui et al., 2015; Blein et al., 2014; Álvaro et al., 2014; Hefferan et al., 2014; Walsh et al., 2012; El Hadi et al., 2010; Errami et al., 2009; Michard et al., 2008; Gasquet et al., 2008, 2005; Ennih and Liégeois 2008, 2001; Thomas et al., 2004, 2002). These Pan-African successions start with an early Tonian - Cryogenian syn-rift units, consisting of carbonates and quartzites known as the Jbel Lkst Group (Kerdous inlier), the Tachdamt Group (Zenaga inlier), and the Bleida quartzites (Bou-Azzer-El Graara inlier) (Álvaro et al., 2014). The rifting process is evidenced by the formation of oceanic basement now preserved as ophiolitic sequences in the Bou-Azzer and Sirwa inliers (Thomas et al., 2002, 2004). Concurrently, a long-lived island arc complex formed north of the WAC (Admou et al., 2012; D'Lemos et al., 2006; Thomas et al., 2002, 2004). This arc is now preserved as the 743 ± 14 Ma Iriri Arc in the Sirwa inlier (Thomas et al., 2002), and its equivalent, the Tazigzaout-Bougmane Complex in the Bou-Azzer inlier, dated at 752 ± $^{+}_{2}$ Ma (D'Lemos et al., 2006). Following this, and as the north dipping subduction ceased, these latter terranes were subsequently deformed and obducted to the northern margin of the WAC around 650 Ma during the main Pan-African orogeny (Hefferan et al., 2014, and references therein; Thomas et al., 2002). Further, widespread calc-alkaline magmatic intrusions and regional metamorphism affected the Anti-Atlas belt (Hefferan et al., 2014, and references therein), with several syn-orogenic granitoids dated between 680 and 640 Ma (Hefferan et al., 2012; Walsh et al., 2012; El Hadi et al., 2010; Inglis et al., 2005; Thomas et al., 2002).

In the northeastern domain of the Anti-Atlas, the Ediacaran stratigraphy (630 – 539 Ma) comprises an early Ediacaran basement of Saghro Group, consisting of folded meta-sedimentary units under greenschist facies conditions, and covered by a late-Ediacaran Ouarzazate Group sequence of volcanic and volcano-sedimentary nature (Ouabid and Garrido, 2023; Errami et al., 2021a; Yajioui et al., 2020; Michard et al., 2017; Blein et al., 2014; Álvaro et al., 2014, 2014b; Walsh et al., 2012; Abati et al., 2010; Errami et al., 2009; Gasquet et al., 2008; Liégeois et al., 2006; Thomas et al., 2002; Fekkak et al., 2001; Bajja, 2001; Ouguir et al., 1996). The transition from volcanic dominated successions of the Ouarzazate Group to the establishment of a stable platform series is recorded during the Ediacaran - Cambrian transition, with the deposition of the Taroudante and Tata groups in an anorogenic setting (Álvaro et al., 2014).

This study focuses on the Ediacaran period (630–539 Ma) within the Sirwa massif. The recent geological mapping of 1/50 000 scale sheet maps of Douar Çour, Assarrag, Tachoukacht, Tamallakout, Sirwa, Taghdout, and Açdif (see Fig. 1C for relevant sheets) has subdivided the Sirwa massif into several distinct groups (Thomas et al., 2000a; De Beer et al., 2000; Gresse et al., 2000). The oldest mapped units belong to the Bleida Group, comprising schists and orthogneisses dated at 743 ± 14 Ma (Fig. 1C) (Thomas et al., 2002). This is overlain by the SG (Thomas et al., 2002), a thick succession of deformed sedimentary, volcanoclastic, and volcanic rocks characterized by a calc-alkaline composition, and metamorphosed under greenschist-facies metamorphism. The SG includes six formations: Tittalt, Agchtim, Imghi, Tizoula, Azarwas, and Tafiat (Thomas et al., 2002). The lower sequence features greywacke/turbidites with volcanic rocks, while the upper formations consist of coarse-grained clastic rocks (Thomas et al., 2002). U-Pb dating on detrital zircons indicates a maximum depositional age at ca. 610 Ma (Abati et al., 2010; Liégeois et al., 2006), with more recent detrital ages around 607 ± 6 Ma and 604 ± 5 Ma (Errami et al., 2021a). Crucially, in the Sirwa inlier, the SG is significantly older as it is intruded by the Mzil granite dated at 614 Ma (Thomas et al., 2002, 2004).

The Bou Salda Group, a volcano-sedimentary succession from 610 to 580 Ma (Gasquet et al., 2008), represents basin infills of grabens and pull-apart basins within the AAMF (Errami et al., 2021a; Gasquet et al., 2008; Thomas et al., 2002). The age of Bou Salda Group is derived from the Tadmant and Tamriwine rhyolites, dated respectively at 606 ± 6 Ma and 605 ± 9 Ma (Thomas et al., 2002) (Fig. 1C, and Fig. 2). Pelleter et al. (2016), also dated the Tadmant rhyolite at 610 ± 7 Ma (Fig. 2). Nonetheless, Abati et al. (2010) reported detrital zircon ages of 600 ± 12, and 603 ± 13, establishing a maximum depositional age for the Bou Salda Group.

The OG sequences (580–539 Ma; Blein et al., 2014b; Toummite et al., 2013; Thomas et al., 2002, 2004) of immature, coarse clastic sedimentary rocks (conglomerates, arkoses, reworked volcanic rocks) acid to intermediate volcaniclastic rocks (lapilli tuff, volcanic breccias, ignimbrites, etc.) and lavas (minor basalt, andesite and rhyolite) are associated with post-collisional high-K calc-alkaline to shoshonitic magmatism (Soulaimani et al., 2018). Briefly, throughout the Sirwa inlier, the OG is subdivided into four subgroups (Fig. 1C for relevant subgroups) (Tiouin, Bouljama, Tafrant and Achkoukchi) (Thomas et al., 2000a; Gresse et al., 2000; De Beer et al., 2000). Under an extensional regime, typical foreland basin successions of Tata Group were deposited, following the post-orogenic molasse volcaniclastic rocks of the OG (Thomas et al., 2002) (Fig. 1C).

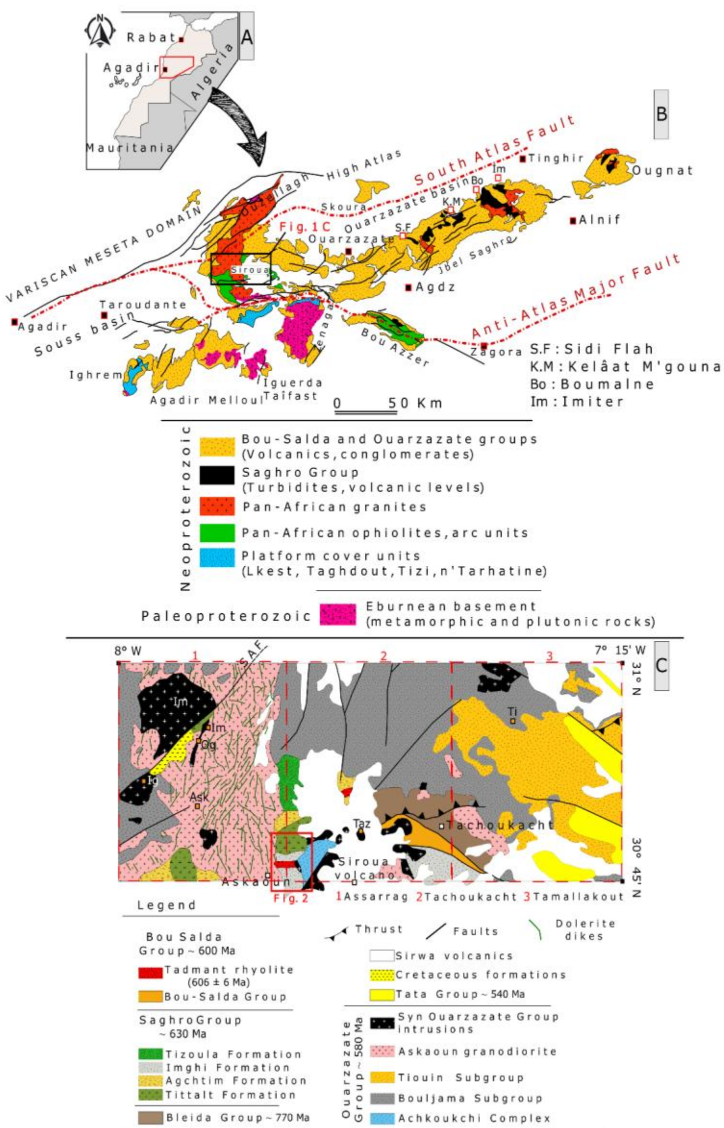
A
B
C
Rabat
Agadir
Algeria
Mauritania
High Atlas
South Atlas Fault
Anti-Atlas Major Fault
VARISCAN MESETA DOMAIN
Ouzellagh
Fig.1C
Siroua
Skoura
Ouarzazate basin
Ouarzazate
S.F
K.M
Bo
Im
Tinghir
Ougnat
Alnif
Jbel Saghro
Agdz
Taroudante
Agadir
Souss basin
Zenaga
Bou Azzer
Zagora
Ighrem
Agadir Melloul
Iguerda Taifast
0 50 Km
S.F: Sidi Flah
K.M: Kelâat M'gouna
Bo: Boumalne
Im: Imiter
Neoproterozoic
Bou-Salda and Ouarzazate groups (Volcanics, conglomerates)
Saghro Group (Turbidites, volcanic levels)
Pan-African granites
Pan-African ophiolites, arc units
Platform cover units (Lkest, Taghdout, Tizi, n'Tarhatine)
Paleoproterozoic
Eburnean basement (metamorphic and plutonic rocks)
8° W
7° 15' W
31° N
30° 45' N
S.A.F
Ti
Taz
Tachoukacht
Siroua volcano
Askaoun
Fig. 2
1 Assarrag 2 Tachoukacht 3 Tamallakout
Legend
Thrust
Faults
Dolerite dikes
Bou Salda Group ~ 600 Ma
Tadmant rhyolite (606 ± 6 Ma)
Bou-Salda Group
Saghro Group ~ 630 Ma
Tizoula Formation
Imghi Formation
Agchtim Formation
Tittalt Formation
Bleida Group ~ 770 Ma
Sirwa volcanics
Cretaceous formations
Tata Group ~ 540 Ma
Ouarzazate Group ~ 580 Ma
Syn Ouarzazate Group intrusions
Askaoun granodiorite
Tiouin Subgroup
Bouljama Subgroup
Achkoukchi Complex

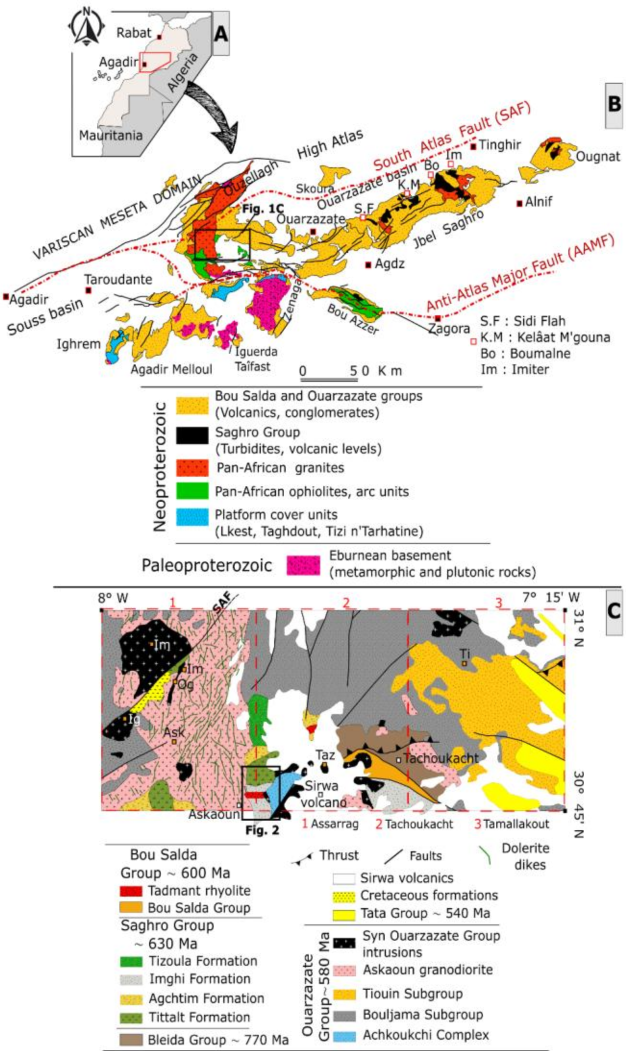

Figure 1 has been corrected based on the comments from Reviewers 1 and 2.

Mis en forme : Couleur de police : Accent 6

Figure 1: (A) Sketch map locating the Anti-Atlas belt in respect to Morocco (Saadi, 1985). (B): geological map of the Central and Eastern Anti-Atlas Proterozoic inliers (redrawn and modified after Michard et al., (2017)). (C): Schematic representation of the geology of the Sirwa (We have corrected Siroua to Sirwa in Fig. 1C, based on RC2) massif (compiled and redrawn after Thomas et al., (2002)); location of the Zgounder Mine Region in red square (see Fig. 2). Abbreviations: Taz : Tazoult quartz-porphyry (559 ± 6 Ma); Im: Imourkhssen granite (562 ± 5 Ma); Ti: Tikhfist rhyolite (571 ± 8 Ma); Ask: Askaoun granodiorite (575 ± 8 Ma); Ig: Ighrem granite; Og: Ougougane granite; and SAF: South Atlas Fault. U-Pb ages are from Thomas et al., (2002).

2.2 Sirwa inlier

Commenté [CM3]: This chapter has been rewritten based on recommendations from Reviewer 2.

The recent geological mapping of 1/50 000 scale sheet maps of Douar Çour, Assarrag, Tachoukacht, Tamallakout, Sirwa, Taghdout, and Açdif (see Fig. 1C for relevant sheets) has subdivided the Sirwa inlier into various groups (Thomas et al., 2000a; De Beer et al., 2000; Gresse et al., 2000).

Paleoproterozoic rocks are the oldest in the Sirwa inlier, mainly composed of altered iron-rich gneiss and schist fragments from the Zenaga Complex (Thomas et al., 2002). The Tachdamt Group's sedimentary and volcanic rocks were deposited after Rodinia's breakup (Thomas et al., 2002). Interbedded Tachdamt Group volcaniclastic deposits date to ca. 883 Ma (Bouougri et al., 2020). This Group is overlain by the Khzama Complex, which includes the Tasriwine ophiolite, the Iriri Migmatite, and Tachoukacht schists formed during island arc development and associated back-arc oceanic crust (Thomas et al., 2002).

The Saghro Group, as defined by Thomas et al., (2002), is a thick, ~8000 m pile of deformed sedimentary, volcanoclastic, and volcanic rocks with a calc-alkaline composition and greenschist-facies metamorphism. It includes six lithostratigraphic formations: Tittalt, Agchtim, Tizoula, Imghi, Azarwas, and Tafiat. The lower sequence features greywacke/turbidites with volcanic rocks, while the upper formations consist of coarse-grained clastic rocks (Thomas et al., 2002). The age of the Saghro Group has been constrained by Liégeois et al., (2006) and Abati et al., (2010) using U-Pb dating on detrital zircons from both the Sirwa and Saghro massifs. These studies established a maximum depositional age at approximately 610 Ma. More recent data from the Eastern Saghro massif reported by Errami et al., (2021a), provided slightly younger detrital ages clustering around 607 ± 6 Ma and 604 ± 5 Ma. In addition, the entire Saghro series was intruded by syn-tectonic granitoids dated at 603 ± 6 Ma and 600 ± 3 Ma (Errami et al., 2021a). Crucially, in the Sirwa inlier, the Saghro Group is significantly older as it is intruded by the Mzil granite dated at 614 Ma (Thomas et al., 2002, 2004).

The Bou Salda Group is a thick volcano-sedimentary succession from 610 to 580 Ma (Belkacim et al, 2017; Gasquet et al., 2008), interpreted as basin infills of grabens and pull-apart basins within the AAMF (Errami et al., 2021a; Gasquet et al., 2008; Thomas et al., 2002). In the Sirwa inlier, it mainly comprises the Lmakhzene and Ighil members (Thomas et al., 2002). The Lmakhzene Member features arkosic gritstones, sandstones, and conglomerates, while the volcanic Ighil Member includes basalt, rhyolite, and andesite. Ages for the Bou Salda Group in the Sirwa inlier are derived from the Tadmant and Tamriwine rhyolites, dated respectively at 606 ± 6 Ma and 605 ± 9 Ma (Thomas et al., 2002) (Fig. 1C, and Fig. 2). Pelleter et al. (2016), also dated the Tadmant rhyolite at 610 ± 7 Ma (Fig. 2). Nonetheless, Abati et al., (2010) reported detrital zircon ages of 600 ± 12, 603 ± 13, and 625 ± 12 Ma, suggesting a maximum age for quartzite clasts in a conglomerate and, hence for the Bou Salda Group.

The Ouarzazate Group sequences (580-539 Ma; Blein et al., 2014b; Toummite et al., 2013; Thomas et al., 2004) of immature, coarse clastic sedimentary rocks (conglomerates, arkoses, reworked volcanic rocks) acid to intermediate volcaniclastic rocks (lapilli tuff, volcanic breccias, ignimbrites, etc.) and lavas (minor basalt, andesite and rhyolite) are associated with post-collisional high-K calc-alkaline to shoshonitic magmatism (Soulaimani et al., 2018). Briefly, throughout the Sirwa inlier, the Ouarzazate Group is subdivided into four subgroups (Fig. 1C for relevant groups) (Tiouin, Bouljama, Tafrant and Achkoukchi) (Thomas et al., 2000a; Gresse et al., 2000; De Beer et al., 2000). Under an extensional regime, typical foreland basin successions of Tata Group were deposited, following the post-orogenic molasse volcaniclastic rocks of the Ouarzazate Group (Thomas et al., 2002) (Fig. 1C).

2.1 Field characteristics and sample distribution

Commenté [CM4]: We have added this chapter after deleting the old chapter on 2.2 Sirwa inlier. This new sub-section was based on the recommendations from Reviewer 2.

The study area (Fig. 2), so-called the ZGMR "Zgounder Mine Region" in this contribution corresponds to the vicinity of the Zgounder Ag-Hg deposit. The Zgounder deposit is situated at approximately 265 km east of Agadir, and 220 km west of Ouarzazate, along the southern flank of the Ouzellagh-Sirwa Salient in the Central Anti-Atlas Mountains (Ben-Tami et al., 2024). Detailed geological mapping was conducted across the ZGMR to establish the primary lithostratigraphic relationships (Fig. 2). The Ediacaran period of the ZGMR (630–539 Ma), is represented by : (i) the SG sedimentary successions and coeval magmatic rocks deposited at around 630 to 600 Ma (Errami et al., 2021a; Abati et al., 2010); (ii) large felsic plutons, subvolcanic formations, along with coeval pyroclastic rocks referred to as the OG (600–539 Ma; Thomas et al., (2002)).

The oldest rocks in the study area belong to the SG, represented by the northern, E-W-striking Tittalt Formation and the southern Imghi Formation (Fig. 2). The lowermost Tittalt Formation consists of basaltic and andesitic volcanic rocks associated with a gabbroic intrusion, bounded to the south by the Imghi Formation. The Imghi Formation features poorly graded, thick-bedded greywacke composed of stacked fine- to very fine-grained sandstone beds and greyish-green, well-bedded, graded turbidites that strike east and dip steeply south at 70° (Fig. 2). Felsic magmatism is represented by the E-W-trending Tadmant rhyolite (Bou Salda Group; Thomas et al., 2002), which forms the core of the area between the western Askaoun granodiorite and the eastern OG sequences (Fig. 2). Other subvolcanic activities include the E-W-trending rhyolitic dikes and plugs of the Assarrag suite (Thomas et al., 2002). Post-SG and post-Bou Salda magmatism includes the Askaoun granodiorite, which intrudes the western Imghi Formation, and the syn- to late-Ouarzazate Bou-Tazart granite (Amassine Suite; Thomas et al., 2002). To the east, the sub-horizontal volcano-sedimentary packages of the OG consist of laminated ignimbrites, ignimbritic rhyolites, andesites, and lapilli tuffs containing volcanic glass lenses. Associated mafic activity is recorded by an intermittent, fault-offset dolerite/diabase sill-like body (~25 m surface width) running parallel to the rhyolite-sediment contact (Fig. 2).

For the purpose of this study, a total of 32 samples were collected from the Saghro and Ouarzazate groups for petrographic and geochemical analysis. For each sample, lithostratigraphic position, sample type, drill core name and depth, short description and analytical methods applied are reported in supplementary table 1. For U-Pb geochronology, three specific samples were selected: (i): a laminated, light-pink to brownish rhyolitic dike crosscutting the Tittalt Formation (Zg-106; 46 m long, 4–5 m thick; Fig. 2); (ii): a fine- to medium-grained, light grey granite (Zg-119) from drill hole ZG-20-21 at 555.30–

568.50 m intruding the Imghi Formation; and (iii): a fine- to medium-grained greenish SG sandstone collected near the Zgounder Mine main entrance for detrital zircon analysis (Zg-132; Fig. 2) (Supplementary table 2).

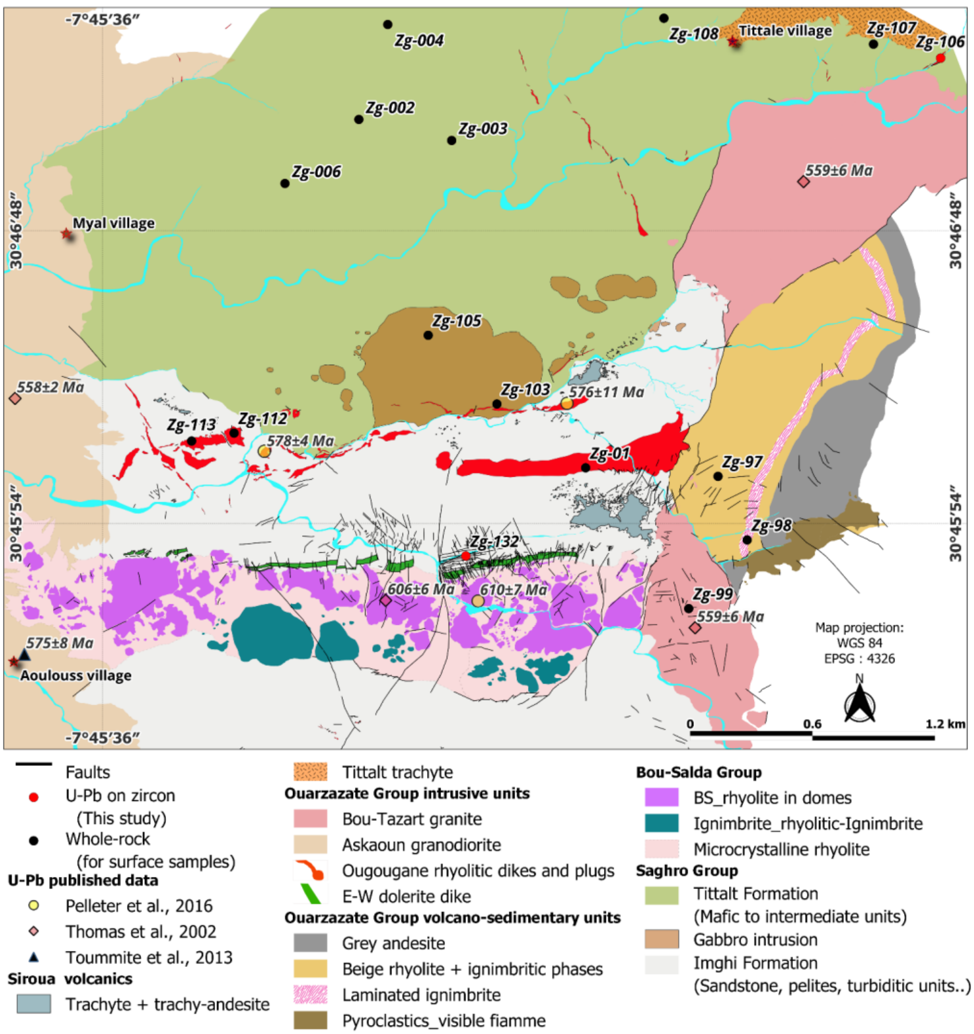
-7°45'36"
Zg-004
Zg-108
Tittale village
Zg-107
Zg-106
Zg-002
Zg-003
Zg-006
559±6 Ma
Myal village
30°46'48"
Zg-105
558±2 Ma
Zg-103
576±11 Ma
Zg-113
Zg-112
578±4 Ma
Zg-01
Zg-97
30°45'54"
Zg-98
Zg-132
606±6 Ma
610±7 Ma
Zg-99
559±6 Ma
575±8 Ma
Aoulouss village
Map projection:
WGS 84
EPSG : 4326
N
0
0.6
1.2 km
Faults
U-Pb on zircon (This study)
Whole-rock (for surface samples)
U-Pb published data
Pelleter et al., 2016
Thomas et al., 2002
Toummite et al., 2013
Siroua volcanics
Trachyte + trachy-andesite
Tittalt trachyte
Ouarzazate Group intrusive units
Bou-Tazart granite
Askaoun granodiorite
Ougougane rhyolitic dikes and plugs
E-W dolerite dike
Ouarzazate Group volcano-sedimentary units
Grey andesite
Beige rhyolite + ignimbritic phases
Laminated ignimbrite
Pyroclastics_visible fiamme
Bou-Salda Group
BS_rhyolite in domes
Ignimbrite_rhyolitic-Ignimbrite
Microcrystalline rhyolite
Saghro Group
Tittalt Formation
(Mafic to intermediate units)
Gabbro intrusion
Imghi Formation
(Sandstone, pelites, turbiditic units..)

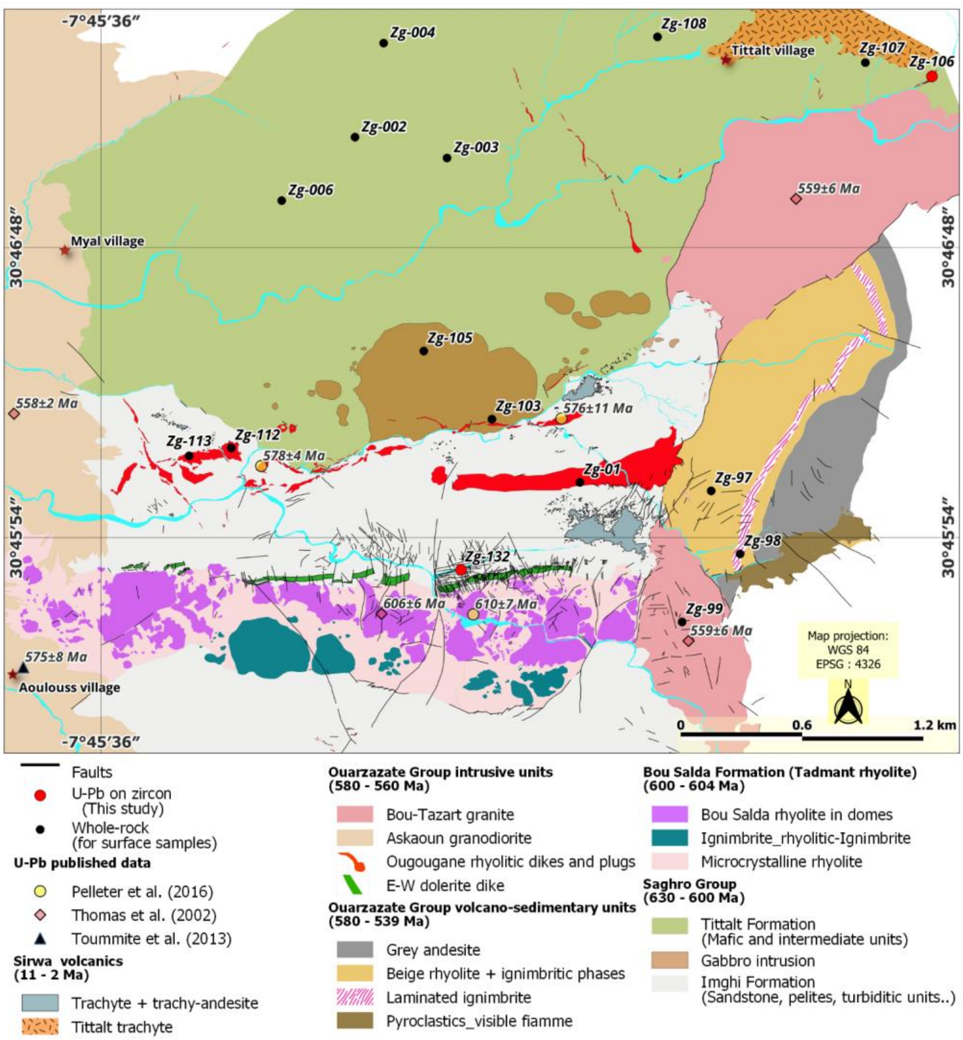

We have corrected Fig. 2 based on comments from Reviewers 1 and 2. BS (Bou-Salda) abbreviation was removed in respect to comment from Reviewer 1. Plus, ages were assigned to different groups based on Reviewer 2 comments.

Figure 2: Detailed geological map of the Zgounder Mine Region (this study). Locations of surface samples are indicated on the map. Underground samples (e.g. Mine levels, drill holes) including the dated Zg-119 are not represented on the map.

Commenté [CM5]: We have corrected Tittale to Tittalt

3 Data and methodology

3.1 U-Pb zircon geochronology

Three samples from the Zgounder Mine Region (Zg-106; Zg-119; Zg-132) were selected for U-Pb zircon geochronology (~~see~~ Fig. 2 for location: Zg-106, and Zg-132). They were crushed, sieved to 50–~~-~~250 µm, and weighed (1.4 kg for Zg-106; 1.5 kg for Zg-119; 2.3 kg for Zg-132), at the preparation unit of the Département de Géologie, Faculté des Sciences, Université Ibn Zohr, Maroc. Samples were then shipped to the Geotop Research Center, Université de Québec à Montréal (UQAM), Canada. Analytical parameters are detailed in supplementary data 1, following Horstwood et al. (2016~~) (refer to table 1 in supplementary data 1)~~. Ages of intrusive rocks are reported as weighted mean $^{206}Pb/^{238}U$ dates, and detrital zircon data as concordia dates. LA-ICP-MS U-Pb data are in supplementary table ~~5~~2.

3.2 Whole-rock geochemistry and Sm-Nd isotopes

Fresh rock samples were collected for whole-rock geochemistry and Sm-Nd isotopes from outcrops (surface and underground), as well in various diamond drill holes from the ZGMR ~~Zgounder Mine Region~~. Crushing and powdering of the rock samples were performed at the facilities of the Zgounder Millennium Silver Mining Company (ZMSM).~~ For each sample, lithostratigraphic position, sample type, drill core name and depth, short description and analytical methods applied are reported in supplementary table 3.~~ Further details on the analytical procedures are given as supplementary data ~~2~~1, and the results are shown in supplementary table 3.

4 Results

4.1 Petrography

4.1.1 The ~~Saghro Group~~SG magmatic rocks

- The ~~Saghro Group~~SG is mainly represented by fine to medium-grained, ~~and dark to olive green mafic volcanic rocks~~dolerite to basaltic-andesite samples. A medium- to coarse-grained equigranular and dark green gabbroic facies is also present, and shows heavily altered pyroxenes and amphiboles (Fig. 3a). The~~y~~ SG mafic volcanics contain fine-grained plagioclase and clinopyroxene phenocrysts dispersed in the groundmass~~ (Fig. 3)~~. ~~A medium- to coarse-grained equigranular and dark green gabbroic facies is also present, and shows heavily altered pyroxenes and amphiboles (Fig. 3a).~~ Dolerite sample (Fig. 3b) ha~~ve~~s an intergranular texture, with ~~lath shaped plagioclase,~~ primary Fe-Ti oxides,~~ and~~ clinopyroxene aggregates, and lath-shaped plagioclase,. Sample Zg-108 is andesitic in composition

(Fig. 3c), ~~and shows a medium-grained intergranular~~with an ophitic texture. The texture is microlitic to microlitic-porphyritic for basalt and basaltic-andesite samples (Fig. 3d).

4.1.2 The SG sedimentary sample

- The dated sandstone sample (Zg-132), displays alternating patterns with distinct well-defined, millimeter-scale laminations, controlled by compositional variations. Darker bands are enriched in chlorite, whereas lighter laminae are mainly composed of quartz and muscovite (Fig. 3e). ~~Such alternating patterns suggest fluctuating depositional conditions, specifically changes in hydrodynamic energy and the amount of clay input, consistent with a low-energy, suspension-dominated sedimentation typical of distal turbidites or quiet shallow-marine environment.~~

Commenté [CM6]: Moved to discussion as recommended by reviewer 2.

- 4.1.3~~2~~ The ~~Ouarzazate Group~~OG magmatic rocks
- Rhyolite samples show a microcrystalline locally glassy texture. Primary mineral assemblages are composed of quartz megacrysts and, K-feldspar altered to albite, and embedded in a devitrified matrix. Secondary alteration minerals are sericite, albite, with some local carbonate veinlets (Fig. 3f). Dolerite samples (Zg-13, Zg-15; Fig. 3g) are fine-grained, exhibiting an intergranular texture. It shows equant opaque grains enclosed in the primary minerals (plagioclase, pyroxene), with Plagioclase crystals, locally transformed to albite are moderately sericitized and ~~rarely~~ locally altered to epidote.~~, with equant opaque grains enclosed in the primary minerals (plagioclase, pyroxene)~~. A dolerite sample (Zg-14) collected next to the mineralized zone has~~ve~~ an intergranular texture in which laths of black oxidized plagioclase were included in pyroxene crystals (Fig. 3h). Clinopyroxene is mainly replaced by hornblende and actinolite, and partially by pyrite, while ~~T~~the plagioclase crystals are strongly altered and replaced by a mixture of blue chlorite, weak and sparse grains of epidote. ~~Clinopyroxene is mainly replaced by hornblende and actinolite, and partially by pyrite~~. Ignimbrite samples show an eutaxitic texture with remarkable fiamme and dense welded volcanic glass, along with cryptocrystalline facies locally fluidal, mainly composed of quartz, opaque minerals, sericitized phenocrysts of plagioclase and K-feldspars (Fig. 3i).
- Granodiorite and quartz-diorite samples are grey to light brown with a moderate pinkish tint related to K-feldspar alteration, and they show a homogenous coarse-grained texture. Opaque minerals are enclosed in hornblende, biotite and plagioclase. Sericite and clay minerals replace lath-shaped plagioclase phenocrysts, and are associated with chlorite and iron oxides (Fig. 3j~~g~~). Chlorite replaces biotite, which locally substitutes hornblende crystals. ~~Opaque minerals are enclosed in hornblende, biotite and plagioclase~~. Granite is medium- to locally fine-grained; it is distinguished from the granodiorite and quartz-diorite by its white to pink color (Fig. 3k).

More details regarding the mineralogical compositions of the studied samples for both Saghro and the Ouarzazate groups are given as supplementary table 4.

Lithology	Sample code	Texture	Primary minerals and accessory phases (size + %)	Alteration minerals
Saghro Group rocks				
Gabbro	Zg-103	medium to coarse-grained/ locally equigranular	Olivine (<0,1mm; <2%); Pyroxene (up to 0,25mm; less than 5%); hornblende;(5-13%); Ca-rich plagioclase (20-35%); Fe-Ti oxides (up to 9%); accessory sulfides (pyrite); <2%)	Secondary Amphibole; Green Chlorite as patches (10%); Sericite (up to 15%); epidote (2%)
	Zg-105			
Dolerite	Zg-107	intergranular	Clinopyroxene, up to 0,5mm; up to 15%); Plagioclase (20-35%); primary Fe-Ti oxides (up to 12%).	Chlorite; minor epidote; rare albite; minor sericite (green schist alteration package)/ secondary amphibole,
Andesite	Zg-108	Medium-grained intergranular	Primary Fe-Ti oxides (up to 10%); Pyroxene (up to 0,2mm; less than 5%); Plagioclase (up to 35%)	Minor sericite, oxides.
Basaltic-andesite	Zg-002	Microlitic-porphyritic	Clinopyroxenes as fine aggregates (0,1mm; up to 10%); Automorphic plagioclase as micro and phenocrysts locally zoned (0,4 - up 1,4 mm; up to 40%); Opaque minerals (<5%)	Chlorite (micro-patches); Sericite (13%); Argillic alteration, minor kaolinite in plagioclase, oxides altering plagioclase.
	Zg-003		Micro and local phenocrysts of Pyroxene (0,1 – to up to 1 mm; up to 13%); Plagioclase as micro and phenocrysts locally zoned (0,4 - up to 1,4 mm; 35%); oxides altering plagioclase phenocrysts; rare apatite	Chlorite; dispersed calcite (up to 5%), oxide orioles surrounding pyroxenes; Sericite (14%);
	Zg-004			
Basalt	Zg-006	Microlitic-porphyritic	Pyroxene (0,1 - 0,8 mm; less than 10%); Micro plagioclase in the mesostasis + phenocrysts (0,2-1,5mm; 30-38%); Fe-Ti oxides.	Abundant calcite, secondary quartz (amygdales); Sericite.
Sandstone	Zg-132	Fine to medium-grained	Compositional variation for darker/lighter laminations: Quartz (0,2-0,4mm; up to 70%); muscovite flakes (10 to 30 %); chlorite (10 to 25 % or more); feldspar (up to 0,3mm); iron oxides (7%).	
Ouarzazate Group rocks				
Rhyolite	Zg-04	Cryptocrystalline, locally glassy with visible fiamme	Quartz (0, 2-0,4mm; up to 30%); Plagioclase (0, 15-0,6mm; 20-30%); K-feldspar (0, 15-0,8mm; up to 55%); Biotite (~0,1mm; less than 4%); Primary opaque minerals; Zircon (<1%) + xenoliths (1-2mm; 6%)	Slight albitization; Chlorite/muscovite (micro-patches); Sericite;
	Zg-06			
	Zg-117			
Rhyolitic-ignimbrite	Zg-05	vitroclastic to cryptocrystalline texture, locally fluidal	Quartz (0,1-1,8 mm; up to 30%); Plagioclase (up to 2,2mm); K-feldspar (0,8-1,9mm); Fe-Ti oxides (less than 4%); + xenoliths (meta-sedimentary facies)	Sericite (4-8%)
	Zg-111			
Porphyritic rhyolite	Zg-110	porphyritic	Quartz in phenocrysts (1-4,5mm; 18-28%); K-feldspar (up to 4,5 mm); Plagioclase (up to 4,3 mm); Opaque minerals (Less than 5%); + visible xenoliths (up to 2,6mm)	Sericite (3-6%); Muscovite (1-2%)
Quartz-diorite	Zg-07	medium to coarse-grained	Amphibole (0, 15-1mm; 2-8%) ; Biotite (0,25-2mm ; 4-9%) ; Plagioclase (1,3 – 3.4 mm; 32-60%); K-feldspar (up to 1,6m ; up to 8%) ;	Chlorite (5-8%); Muscovite (3%); Epidote (<2%)

			interstitial quartz (0.2 -1.2 mm; up to 25 %); Primary opaque minerals (inclusion in amphibole crystals; <6%); Zircon (<1%)	Sericite (10-15%); Kaolinite and Clay minerals (2%); Oxides (6%);
Granodiorite	Zg-08 Zg-09	medium to coarse-grained, isogranular texture	Hornblende (0,15-1,2mm ; 6-10%) ; minor Biotite (0,25-2mm ; 4-18%) ; Plagioclase phenocrysts (0.25 – 2.6 mm; 45-55%); Orthoclase (1-2,2m ; 20-35%) ; Quartz (0.4 -2.5 mm; 10-30 %); +xenoliths ; Primary + secondary opaque minerals ; Zircon in biotite (<1%)	Chlorite (less than 10%); Sericite (up to 25%); Epidote (2%);; Clay minerals (2%); Kaolinite (<2%); Oxides (4%)
Dolerite	Zg-13 Zg-15	intergranular	Clinopyroxene (augite) (0,1mm; up to 6%); brown hornblende (up to 14%); automorphic plagioclase (0,4 – less than 1,4 mm; up to 43%); Biotite (<4%); secondary Quartz (0,1-0,4mm; <4%); Primary opaque minerals (<5%); accessory sulfides (pyrite); <2%)	Intense Chlorite (patches); Sericite (20%); Muscovite (up to 2%)
Diabase	Zg-14	intergranular	Pyroxene (0,03-0,1mm; less than 10%); Plagioclase (0,25-2,5mm; 35-40%); Fe-Ti oxides (magnetite+ilmenite prisms, <6%)	Patches of blue chlorite (0,25-1,1 mm; up to 38%); sericite (up to 8%); clay minerals (<6%); Secondary amphibole
Ignimbrite	Zg-97 Zg-98	eutaxitic texture with visible fiamme	Quartz (less than 0,7mm; 45-60%); Plagioclase; K-feldspar (sanidine; up to 23%, 0,4mm); Opaque minerals (euhedral to subhedral) (5-10%); + Xenoliths (anhedral); Zircon in inclusion in k-feldspar crystals (<1%)	Sericite (less than 5%); Scarce chlorite (2%); Kaolinite (5%)
Granophyre	Zg-99	coarse grained	Amphibole; sub-automorphic Biotite (0,4-0,9mm) ; Plagioclase (up to 8%; 0,5–1mm) ; K-feldspar (microcline) ; Quartz (rounded and eye-shaped (0,4-3,2mm)); Magnetite + apatite+ Zircon (<2%) (; +xenoliths (mafic)	Chlorite; Sericite ; Muscovite
Rhyolite	Zg-106	Microcrystalline, locally fluidal	Quartz (0,2-0,4mm) ; K-feldspar (up to 0,3mm); Plagioclase (< 0,4mm); + rare xenoliths (mafic to intermediate). Mesostasis forms more than 85% of the rock.	Albite; Chlorite (3-5%); Sericite (up to 25%); Calcite (veinlets) (2%)
Granite	Zg-115 Zg-119	medium to fine-grained, equigranular	Amphibole (rare 2% (<0,2mm); Biotite (up to 2%); Microcline with visible twinning (20-30% (0,5 to 1,2 mm)); Plagioclase (6-10% (=0,7mm)); Quartz (35-45% (0,4 to 1,3 mm)) ; +metasedimentary xenoliths (0,5-1cm; 3%) ; Opaque minerals; Zircon (<2%);	Chlorite (moderate); Actinolite (less amount); Sericite (15%); Muscovite (less than 4%)
Rhyolite	Zg-01 Zg-112 Zg-113	microcrystalline porphyritic texture,	Quartz phenocrysts (0,4-0,9mm); Plagioclase; K-feldspar; rare biotite Opaque minerals + rare xenoliths	Muscovite rare micro-patches; Sericite (up to 12%)
Micro-granite	Zg-02 Zg-03	fine to medium-grained texture	Amphibole (0,1-0,4mm; rare: less than 3%); Biotite (<0,9mm; 2-4%); Quartz (0,4-3,2mm; less than 40%); K-feldspar (up to 32%); Plagioclase (1-2,9mm; up to 20%); Opaque minerals (<4%); + xenoliths (up to 4,5mm)	Abundant Sericite (up to 10%); chlorite (<3%); rare epidote (<1%)
	Zg-109	fine grained texture	Amphibole (0,1-0,4mm; rare: less than 3%); Biotite (<0,5mm; 2-4%); Quartz (0,4-0,9mm; less	Abundant Sericite (up to 10%); chlorite (<3%); rare epidote (<1%)

			~~than 48%); K-feldspar (up to 30%); Plagioclase (0,5-1,4mm; up to 22%); Opaque minerals (<4%)~~	

~~**Table 1: Mineralogical compositions of the studied rocks of the Saghro Group and Ouarzazate Group from the Sirwa massif (Zgounder Mine Region; 33 samples), refer to Fig. 2 for surface sample's locations.**~~

Commenté [CM7]: Table 1 is moved to supplements (supplementary table 4), as requested by reviewer 1.

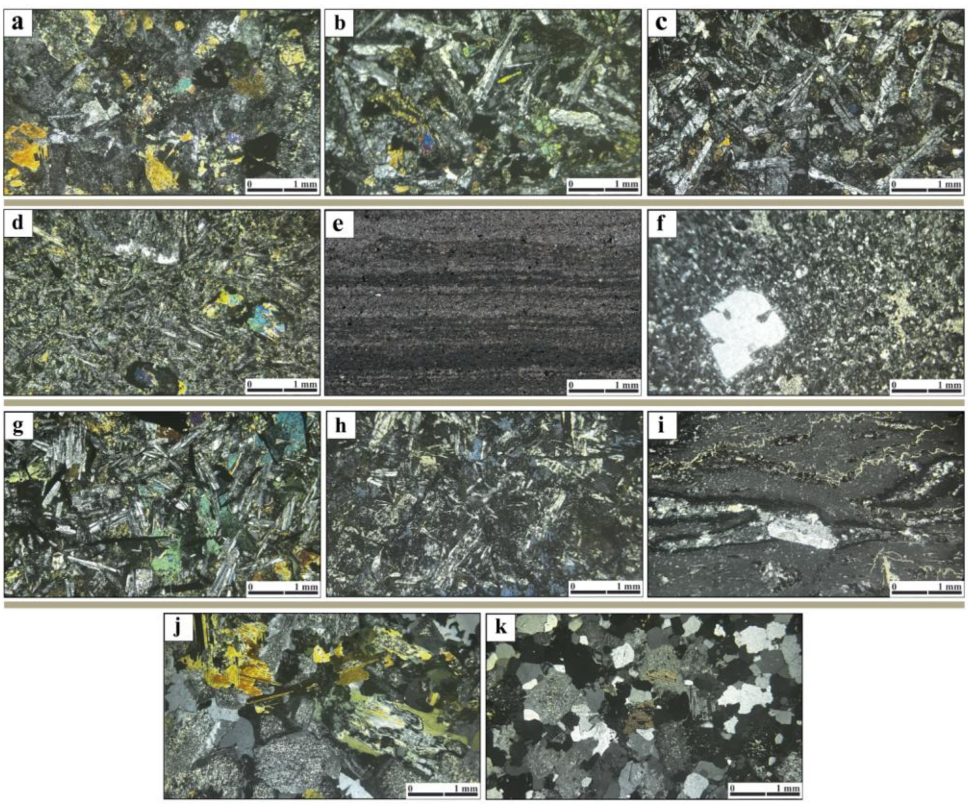

Figure 3: Photomicrographs (all in cross-polarized light) of the studied ~~Saghro Group~~SG and ~~Ouarzazate Group~~OG rocks. (a) Gabbro sample showcasing a medium to coarse- grained locally equigranular texture;~~.~~ (b) An intergranular texture for dolerite~~.~~; (c) Andesite ~~with a medium grained intergranular~~showcasing an ophitic texture;~~.~~ (d) Microlitic-porphyritic texture for basaltic-andesite;~~.~~ (e) Sandstone (Zg-132) exhibiting millimetre-scale laminations showcasing darker bands enriched in chlorite, with quartz-muscovite lighter laminations;~~.~~ (f) Microcrystalline texture for rhyolite with embayed quartz phenocrysts~~.~~; (g) Dolerite exhibiting an intergranular texture;~~.~~ (h) Diabase characterized by an intergranular texture with patches of blue chlorite~~.~~; (i) Welded ignimbrite with an eutaxitic texture displaying flow textures with feldspars (sanidine) crystals embedded in a glassy fiamme;~~.~~ (j) Quartz diorite with subhedral to anhedral amphiboles and sericitized plagioclase;~~.~~ (k) Medium to locally fine-grained granite, with an anhedral to subhedral equigranular texture.

4.2 Cathodoluminescence (CL) imaging and LA-ICP-MS U-Pb zircon geochronology

We have added Fig. 4 based on a recommendations from Reviewers 1 and 2. We enhanced the quality of zircon images, and refined the interpretations. Plus, the three dated samples were rearranged to go in parallel with Fig. 4 and Fig. 5.

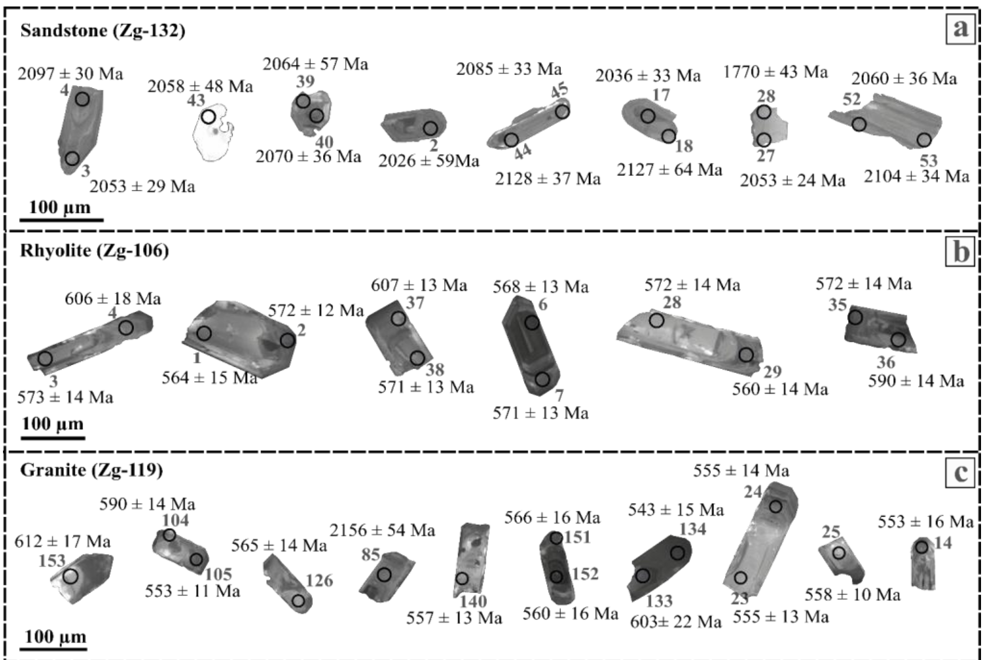

Figure 4. Cathodoluminescence (CL) images of representative zircon grains from the (a): SG sandstone (Zg-132); (b): OG rhyolite (Zg-106); and (c): OG granite (Zg-119). Black circles indicate analytical spots, with corresponding $^{206}Pb/^{238}U$ ages.

4.2.1 Sandstone (Zg-132)~~Tittalt rhyolite (Zg-106)~~

Most zircons from sample Zg-132 (sandstone) are uniformly rounded and fragmented, with some being subhedral and showing rounded borders. They measure ca. 75–200 µm. They are distinguishable by their low CL signal with some being preferentially zoned (Fig. 4a). A total of hundred and thirty-eight analysis were obtained from ninety-three zircons (rims and cores) from this sample, of which 90 are concordant (Fig. 5A; supplementary data 2). The dated zircon grains have Th and U contents of 13–908 ppm and 9–3462 ppm, respectively; Th/U ratios range between 0.03 and 2. For the detrital zircons, we calculated a maximum depositional age (MDA) using the weighted mean of the youngest zircon cluster of three grains with a 98–100% concordance and overlapping in age at 1σ (YC1σ [2+]) (Dickinson and Gehrels, 2009). This yielded a MDA age of

Mis en forme : Police :9 pt, Gras, Couleur de police : Rouge, Police de script complexe :11 pt, Gras

2025 Ma (MSWD = 1.4; n = 3; (Fig. 5A-1)). Moreover, the ages distribution is dominated by one single population, with one uniform peak at 2100 Ma, and one zircon recording an age at 3700 Ma (Fig. 5A-2). The significance of the detrital age will be discussed below (see section 5.4.1).

The rhyolite sample Zg-106 was taken from the Tittalt Formation as the lower unit that represents the Saghro Group in the Sirwa massif (Thomas et al., 2002, 2004). For context, this rhyolite is represented as a compact and homogenous body of approximately 46 m length, and 4 to 5 m thick. On the field, it corresponds to a rhyolitic dike crosscutting the mafic to intermediate units of the Tittalt Formation (Fig. 2). Admittedly, similar subvolcanic activity represented by E-W-trending rhyolitic dikes and related plugs was previously reported in the Zgounder Mine Region by Pelleter et al., (2016), and attributed to the Assarrag suite of Thomas et al., (2002). On the outcrop, it has a light pink to brownish taint with visible laminations. U-Th ratios range between 0.3 and 1. Most of the zircon crystals in this sample are euhedral and moderate in size. CL images reveal that zircon grains exhibit typical oscillatory zoning with rare and limited dark rim overgrowths (Fig. 4-1a), with no indication of inherited zircon grains. For filtering the data, only zircons with 95% to 105% concordance were used for age calculation (Fig. 4-1b). Thus, the weighted mean age for this sample gave 575 ± 3 Ma (MSWD = 1.5; n = 21/40), which is interpreted as the crystallization age (Fig.4-1c).

4.2.2 Rhyolite (Zg-106)Granite (Zg-119)

Zircon grains from the Zg-106 (rhyolite) are transparent with subhedral to euhedral habitus. They measure ca. 100–350 µm in length. CL images reveal that zircon grains exhibit typical oscillatory zoning with rare and limited dark rim overgrowths (Fig. 4b). Forty analyses were obtained on twenty-eight zircon grains from this sample (Supplementary data 2). The dated zircon grains have Th and U contents of 20–556 ppm and 40–833 ppm, respectively; Th/U ratios range between 0.3 and 0.7. These data yield a ^{206}Pb/^{238}U weighted mean age of 575 ± 3 Ma (MSWD = 1.5; n = 21/40), which is interpreted as the crystallization age of the rhyolite (Fig.5B).

The sample Zg-119 was sampled from the diamond drill hole (DDH) ZG-20-21 (interval in meters: 555,30m to 568,50m), representing the Zgounder Mine exploration program from 2020, and referred to as the 'Deep Intrusion' (Mine terminology). On hand, the sample corresponds to a fine to medium-grained light grey granite with pink passes. Zircon grains from this sample are homogenous in size, mostly euhedral to subhedral with some rounded zircon grains. CL images show visible oscillatory zoning with local moderately fractured zircons showing dark overgrowths (Fig. 4-2a). The discordance filter used for this sample was the same as for Zg-106; thus, zircons falling outside 95% to 105% concordance were omitted from the age calculation. A total of high-quality zircon analyses yielded a reliable concordia age of 564 ± 2 Ma (MSWD = 1.6; n = 34/37). We also calculated a weighted mean age using a broader selection of concordant zircons within error, which gave an equivalent age of 564 ± 2 Ma (MSWD = 1.1; n = 76/160) (Fig. 4-2b). However, the zircon U-Pb are quite complicated and seem to spread over ~80 Ma which is likely due to the combined effects of Pb loss and inheritance (Fig. 4. 2-b). Hence both were omitted from the age calculation. We interpret the youngest tail of ages (~ 520 Ma) which are clearly outside of the main population reflecting analysis that have been affected by Pb loss (Sharman and Malkowski, 2024). Whilst oldest zircons are probably

~~inherited (~ 620 Ma), and referring to a detrital signature. However, the analyzed detrital sample (Zg-132), that represents the sedimentary succession in which this granite is intruded has no zircons of this age (see supplementary table 5 for Zg-132). Moreover, the inheritance signature cannot be supported as no xenocrystic zircons were observed in the CL images. Overall, as both ages are statistically identical, we interpret the 564 ± 2 Ma as the robust crystallization age for the granite (Fig. 4-2c).~~

4.2.3 Granite (Zg-119)~~Sandstone (Zg-132)~~

Zircon grains from sample Zg-119 (granite) are mostly euhedral to subhedral with some being rounded. They measure ca. 100–300 µm in length. CL images show visible oscillatory zoning with local moderately fractured zircons showing dark overgrowths (Fig. 4c). A hundred and sixty analyses were obtained on a hundred and twenty-two zircon grains from this sample (Supplementary data 2). The dated zircon grains have Th and U contents of 12–619 ppm and 39–934 ppm, respectively; Th/U ratios range between 0.1 and 1.3, supporting their magmatic origin. A total of high-quality concordant zircon analyses yielded a reliable concordia age of 564 ± 2 Ma (MSWD = 1.6; n = 34/37). One zircon with a $^{206}Pb/^{238}U$ age of 2156 ± 54 Ma (103.5 % concordance) was excluded from the age calculation after being identified by IsoplotR as a statistical outlier (Fig. 4c). We also calculated a $^{206}Pb/^{238}U$ weighted mean age using a broader selection of concordant zircons within error, which gave an equivalent age of 564 ± 2 Ma (MSWD = 1.1; n = 76/160) (Fig. 5C). As both ages are statistically identical, we interpret the 564 ± 2 Ma as the crystallization age for the granite.

~~This sample was collected from the Ag-Hg hosting sedimentary units from the Imghi Formation of Saghro Group near the Zgounder Mine entrance (Fig. 2). It is a fine to medium-grained greenish sandstone. On the outcrop, it follows the E-W-trending direction of the Imghi Formation, dipping at 70° to the south. For Thomas et al., (2002), the Imghi Formation represents the lower thick beds of greywacke/turbiditic section of Saghro Group, and seems to represent a typical flysch succession, which is interpreted as the primary sedimentary fill of a back-arc basin associated with the Khzama ophiolite complex. Most zircons from this sample are uniformly rounded and fragmented. They are distinguishable by their low CL signal with some being preferentially zoned (Fig. 4-3a). The age calculation utilized a filtered dataset, specifically incorporating only zircons that fell within the 95% to 105% concordance range. A total of 139 analyses were obtained on zircons from this sample, of which 91 are concordant (Fig. 4-3b). The ages distribution is dominated by one single population. For the detrital zircons, one uniform peak at around 2100 Ma, with one zircon recording an age at 3700 Ma (Fig. 4-3c).~~

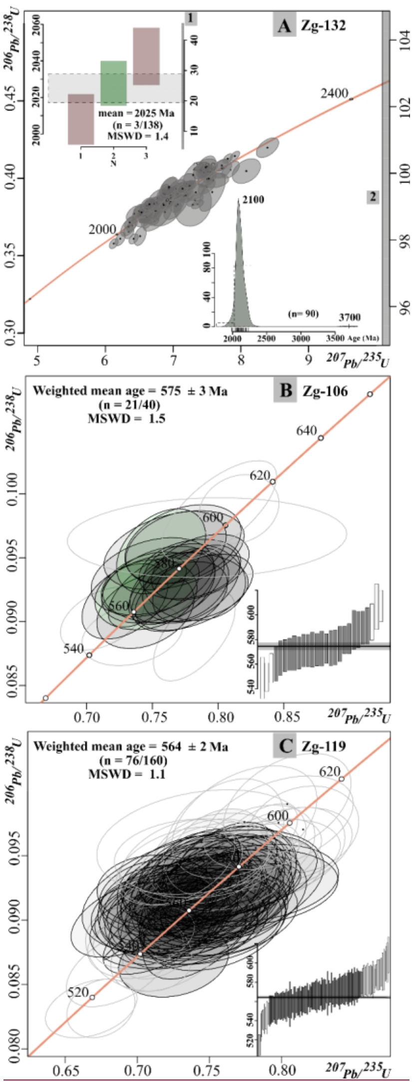
A Zg-132
mean = 2025 Ma
(n = 3/138)
MSWD = 1.4
2400
2100
2000
(n= 90)
3700
Age (Ma)
B Zg-106
Weighted mean age = 575 ± 3 Ma
(n = 21/40)
MSWD = 1.5
640
620
600
580
560
540
C Zg-119
Weighted mean age = 564 ± 2 Ma
(n = 76/160)
MSWD = 1.1
620
600
520
$^{206}Pb/^{238}U$
$^{207}Pb/^{235}U$

Figure 5. Pb^{206}/U^{238} weighted mean age of three concordant grains, U-Pb concordia, and Kernel Density Estimate (KDE) diagram for (A) Zg-132 (sandstone). Along with U-Pb concordia diagrams, and Pb^{206}/U^{238} weighted mean ages for (B) Zg-106 (rhyolite), and (C) Zg-119 (granite). Ages were calculated using Isoplot R 1.0 (Vermeesch, 2018).

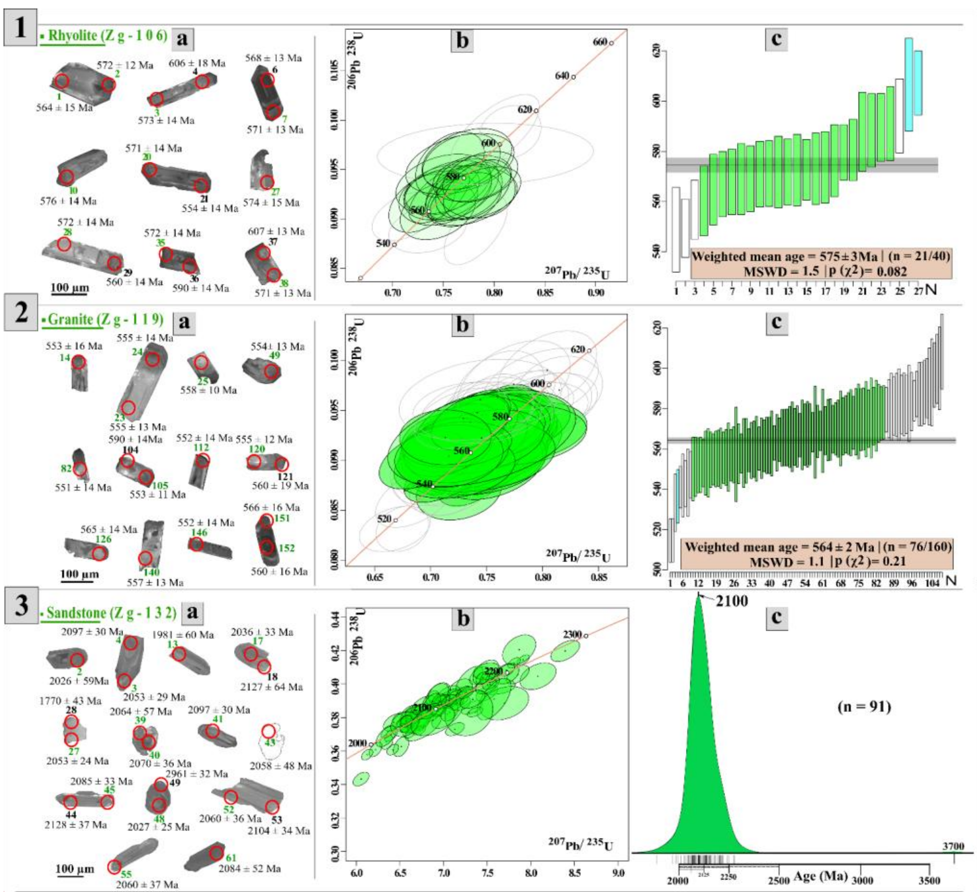

~~Figure 4: Cathodoluminescence (CL) images for selected zircons, U-Pb concordia and Pb^{206}/ U^{238} weighted mean diagrams for samples (1) Zg-106 (rhyolite), and (2) Zg-119 (granite); along with U-Pb concordia diagram and KDE for (3) Zg-132 (sandstone). Error ellipses are plotted at 2σ. Ages were calculated using Isoplot R 1.0 (Vermeesch, 2018).~~

4.3 Whole-rock ~~geochemistry~~geochemical compositions

4.3.1 Effects of weathering

Commenté [CM8]: This figure has been changed, as the zircon images were given as Fig. 4 in the revised version. In addition, all the necessary modifications and corrections from both reviewers were adopted.
We have reproduced Fig. 5 based on recommendations from Reviewer 2, and interpreted accordingly. Please refer to Reply on RC2 for the U-Pb geochronology section.

Due toGiven samples distribution and geological diversity, the selected samples are organized in respectaccording to their lithostratigraphic position (Supplementary table 1), and hence treated accordingly. The whole-rock data for 32 samples are listed in supplementary table 4. For a start, we assessed the behavior of mobile elements and how it relates with the formed alteration minerals, using the diagram of Large et al., (2001); and samples are plotted in (Fig. 5). The rock material Lloss onf iIgnition (LOI) values at 1100 °C is are generally low for most samples (less than < 2 wt.-%), except for the mafic and intermediate terms of the SGSaghro Group where it is close towhich reach approximately 4 wt.-% (Supplementary table 3; n = 32e.g. basalt, gabbro and andesite samples). On plotting our data in this diagram, a homogenous hydrothermal trend is clearly defined for all samples except for sample (Zg-106). Its trend is more directed towards sericite alteration, typical of a distal ore environment (Large et al., 2001). Overall, the plot confirms that most of our samples plot in the domain of ‘‘‘Least altered rocks’’’.When plotted on the alteration box plot of Hughes (1972) (Fig. 6a), most samples fall within the igneous spectrum, defining a homogenous hydrothermal trend. However, sample Zg-106 deviates, plotting in the K-altered zone, reflecting localized potassium enrichment. Conversely, two granite samples (Zg-02 and Zg-109) plot in the Na-altered field, suggesting sodium metasomatism.

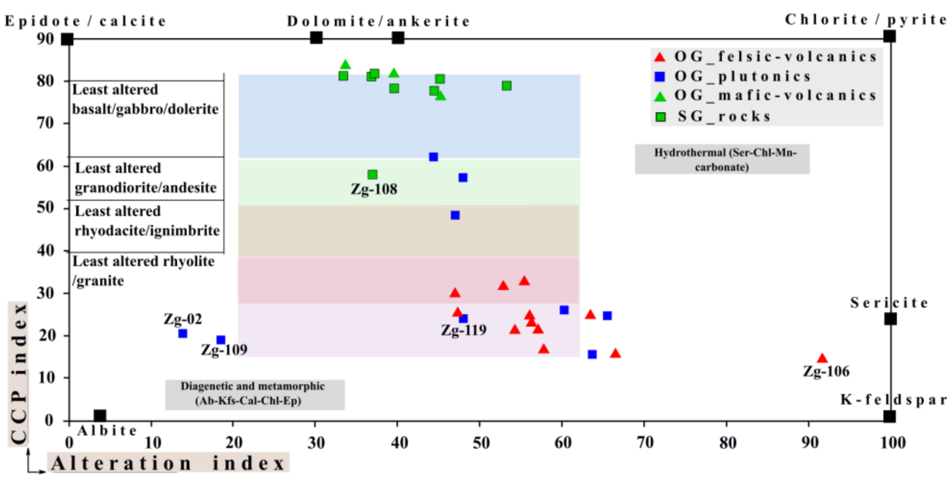

Figure 5: Plots of the studied rocks on the alteration box diagram (Large et al., 2001). Alteration Index (AI) = 100 x (K_2O + MgO) / (K_2O + MgO + Na_2O + CaO), Chlorite-carbonate-pyrite index (CCPI) = 100 x (MgO + FeO) / (MgO + FeO + Na_2O + K_2O).

Commenté [CM9]: Fig. 5 is now reproduced to Fig. 6a

Mis en forme : Couleur de police : Noir

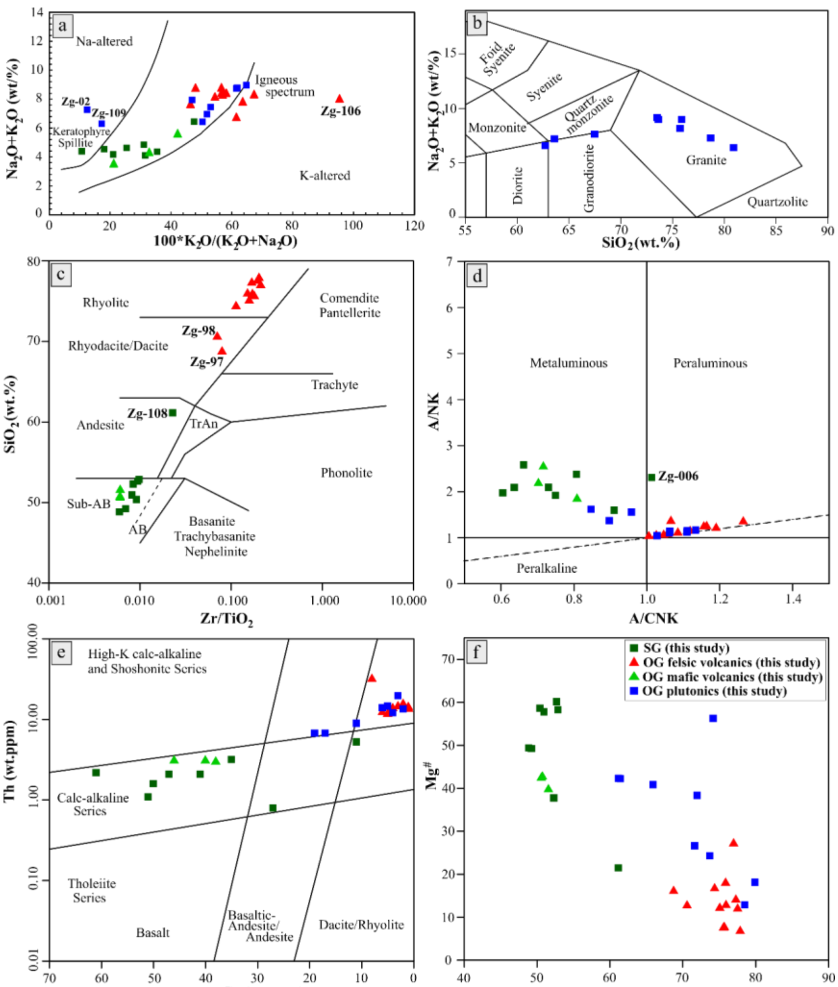

Figure 6. (a) Na_2O+K_2O (wt.%) versus $100*K_2O/(K_2O+Na_2O)$ plot of Hughes (1972); (b) TAS diagram (after Middlemost, 1994); (c) SiO_2 (wt.%) versus Zr/TiO_2 (Winchester and Floyd, 1977); (d) Plot of A/NK versus A/CNK [A/CNK = molar ratio Al_2O_3 / ($CaO + Na_2O + K_2O$) and A/NK = molar ratio Al_2O_3 / ($Na_2O + K_2O$)] (Shand, 1943); (e) Plot of Th (ppm) versus Co (ppm) of Hastie et al. (2007); (f) Mg# value versus SiO_2 contents (wt.%).

Mis en forme : Couleur de police : Texte 1

4.3.12 The Saghro GroupSG magmatic rocks

The analyzed Saghro GroupSG rocks belong to the Tittalt Formation of the Saghro GroupSG in the study area (Fig. 1C; Fig. 2; Thomas et al., 20042, 20042). Geochemically, they define a narrow range of compositions, with SiO_2 contents from 48.85 wt.% to 52.87 wt.%, except for sample (Zg-108) with SiO_2 of 61.15 wt.%. They contain 1.08 – 7.45 wt.% MgO,; 13.44 – 15.65 wt.% Al_2O_3,; 2.82 – 3.95 wt.%, Na_2O and 0.47 – 3.07 wt.% K_2O. Based on the SiO_2 (wt.%) vs Nb/Y vs Zr/TiO_2 diagram (Fig. 6a), all samples plot within a sub-alkaline basalt, except for one sample (Zg-108) with andesitic composition, all samples plot within a sub-alkaline basalt,; similar to contemporaneous mafic-intermediate rocks from the Saghro (Errami et al., 2009) and Sirwa inliers (Thomas et al., 2002). Most rocks are metaluminous except for one sample (Zg-006) which is peraluminous (Fig. 6db). In addition, the Saghro GroupSG rocks display a calc-alkaline signature (Fig. 6ee). Mg# (Mg# = (MgO+FeO)/MgO×100) values range from 21.50 to 60.20 (Fig. 6f).

Using rare earth elements (REE) (Fig. 6d), tThe Saghro GroupSG samples show a total rare earth elements (∑REE) varying between 60.94 to 231.77 ppm with coherent patterns characterized by a slight enrichments in light rare earth elements (LREEs) enrichments and heavy rare earth elements (HREEs) depletion (Fig. 7a), with $(La/Yb)_N$ ratios ranging from 1.83 to 6.42 (N subscript denotes normalization to Chondrite). Almost all samples have slight/no importantnegligible negative Eu anomalies (Eu/Eu* δEu = 0.898 0.998) to less positive anomaly for one sample offor gabbro (Zg-105; (Eu/Eu*)N = 1.28; Fig. 67ad); (Eu/Eu* = 2EuN / (SmN + GdN, subscript N denotes normalization against chondrite Sm and Gd contents)). For the NMORB-normalized multi-elements diagram (Fig. 7b)multi-elements diagram (Fig. 6e), the Saghro GroupSG rocks exhibit an enrichment of large ion lithophile elements (LILEs, like Cs, Rb, Ba, K) over high field strength elements (HFSEs) with negative anomalies in Nb, Ta, and a prominent positive Pb anomaly. They do compare in the most part with basaltic rocks from the Saghro Group of Kelâat M'gouna inlier (Benziane et al., 2008; Fekkak et al., 2001), and the early gabbro sample from Sirwa (Touil et al., 2008; Fig. 6d).

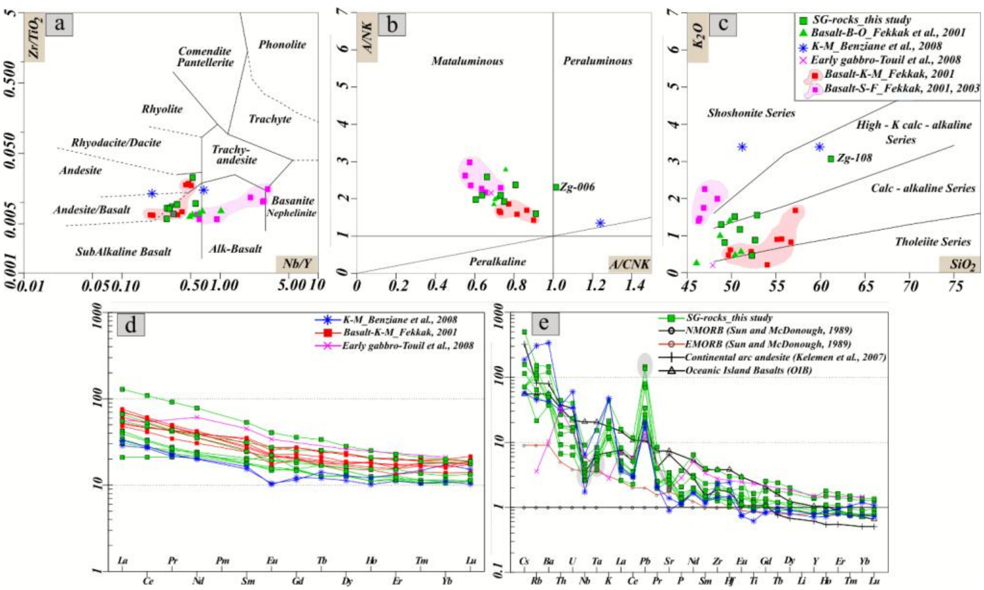

~~**Figure 6: Saghro Group:(a) Nb/Y versus Zr/TiO$_2$ (Winchester and Floyd, 1977). (b) Plot of A/NK vs. A/CNK [A/CNK = molar ratio Al$_2$O$_3$ / (CaO + Na$_2$O + K$_2$O) and A/NK = molar ratio Al2O3 / (Na$_2$O + K$_2$O)](Shand, 1943). (c) K$_2$O versus SiO$_2$. (d) Chondrite-normalized REE diagram of Boynton, (1984). (e) NMORB normalized diagram; normalization values are sourced from Sun and McDonough, (1989). SG samples are plotted against reference rocks from the literature. Abbreviations: B-O : Boumalne; K-M: Kelâat M'gouna; S-F: Sidi Flah.**~~

Commenté [CM10]: Figure 6 has been reproduced into Fig. 6, and Fig. 7.

4.3.2 The ~~Ouarzazate Group~~OG magmatic rocks

The studied samples ~~representing~~ of the ~~Ouarzazate Group~~OG are composed of both volcanic and plutonic rocks. The felsic volcanic and plutonic samples have high contents ~~in~~ of SiO$_2$ (61.16 – 79.89 wt.%), Al$_2$O$_3$ (10.83 – 15.18 wt.%), and CaO (0.1 – 4.42 wt.%) and low MgO (0.06 – 2.83 wt.%), ~~(79.89 – 61.16 wt.%), Al$_2$O$_3$ (15.18 – 10.83 wt.%), and CaO (4.42 – 0.1 wt.%) and low MgO (2.83 – 0.06 wt.%),~~ Ni (2~~6~~0 – ~~–~~ 6~~2~~0 ppm) and Co content (1~~9~~ – ~~–~~ 1~~9~~ ppm), except for one granite (Zg-119) that ~~have~~ has relatively high Co content of 109 ppm (Supplementary table 3). Moreover, they have a Na$_2$O~~-~~+~~-~~K$_2$O (wt.%) = 6.31 to 8.97 ~~to 6.31~~ with a K$_2$O/Na$_2$O ratio of 0.14 to 20.75 ~~to 0.14~~. The plutonic rocks occupy the granite field, with three distinctive granodiorites (Fig. 6b). Furthermore, r~~R~~ock types for felsic volcanics are as follows: ignimbrites (e.g., Zg-97, Zg-98) are represented as rhyodacite and dacite, while rhyolites and rhyolitic-ignimbrites plot inside the rhyolite field (Fig. 6c~~7a~~). Furthermore, ~~the plutonic rocks occupy the granite field, with three distinctive granodiorites (not shown).~~ t~~T~~he whole set consists of ~~high-K calc-alkaline to shoshonitic rocks (Fig. 7b), and are~~ peraluminous rocks, except for the granodiorite samples (Zg-07, Zg-08, and Zg-09) that exhibit a metaluminous character (Fig. 6d~~7c~~). ~~Overall, all samples plot within the calc-alkaline~~

~~and alkali-calcic slightly migrating towards alkaline field (Fig.7d).~~ They showcase a high-K calc-alkaline to shoshonitic signature (Fig. 6e).

Mafic volcanics (~~e.g.~~ dolerite) have moderate SiO_2 contents of (~~51.56 –~~ 50.58 – 51.56 wt.%), Al_2O_3 (~~14.69 –~~ 13.9 – 14.69 wt.%), moderate CaO (~~7.67 –~~ 5.61 – 7.67 wt.%) and moderate MgO (~~5.3 –~~ 4.56 – 5.3 wt.%). K_2O/Na_2O ratio values are 0.~~73~~26 to 0.73~~26~~, along with Na_2O+K_2O ~~ratio~~ sum = ~~5.64~~3.58 to ~~3.58~~ 5.64 (supplementary table 3~~4~~). They are sub-alkaline basalts (Fig. 6c~~7a~~), with a metaluminous character (Fig. 6d~~7c~~)~~,~~, and a calc-alkaline signature (Fig. 6e~~7b~~), and a ~~metaluminous character (Fig. 7c).~~ Mg# values range from 37.19 to 40.16 (Fig. 6f).

The OG samples show a total rare earth elements (∑REE) varying between 93.52 to 646.17 ppm. In the REE diagram (Fig. 7c~~e~~), all felsic volcanic and plutonic samples show homogeneous patterns, with enriched LREEs over HREEs. $(La/Yb)_N$ ratio varies between ~~17.93~~2.91 and 17.93~~2.1~~, except for one rhyolitic sample Zg-106 with $(La/Yb)_N$ of 0.89. All samples have high Eu negative anomaly (Eu/Eu* = ~~0.61~~0.34 – 0.61~~34~~, except for the same Zg-106 sample, that exhibits a prominent Eu anomaly with Eu/Eu* = 0.04.~~, controlled by advanced plagioclase crystallization.~~ In the multi-element spider diagram, all samples display enrichments in LILEs (Cs, Rb, Ba, Th, and U) and depletion in HFSEs (Zr, Nb, Hf and Ta), relative to Primitive Mantle (Fig. 7~~f~~d). Plus, samples show a prominent negative anomaly in Nb, Ta, P and Ti along a positive anomaly in Pb, Ba and Th, except for sample Zg-106 that lacks negative Nb anomaly (Fig. 7d).

For the ~~mafic volcanics~~OG dolerites, the REE normalized to chondrite (Fig. 7c~~e~~) show moderate LREEs enrichments over HREEs with less fractional patterns ($(La/Yb)_N$ = ~~6.22~~5.94 to 6.22~~5.94~~) and very low/absent Eu anomaly (Eu/Eu* = 0.8~~9~~8 to 0.9~~8~~8). However, ~~our dolerites are distinguished~~they are distinguished by their homogenous pattern with a prominent Pb enrichment, with less significant Sr anomaly (Fig. 7d~~f~~). ~~Our dolerites resemble those of the Tifnout Valley (TV), Group A and B, and Zaghar mafic dikes from the Sirwa massif by Belkacim et al., (2017); Touil et al., (1999); Toummite et al., (2013), respectively. Even so, minor differences related to prominent negative Nb and Ti anomaly are observed for reference samples compared to our dolerites' positive Ti anomaly (Fig. 7f). However, they differ from the Bas Drâa inlier mafic-intermediate bodies, which lack Pb enrichment and Sr depletion Karaoui et al., (2014).~~

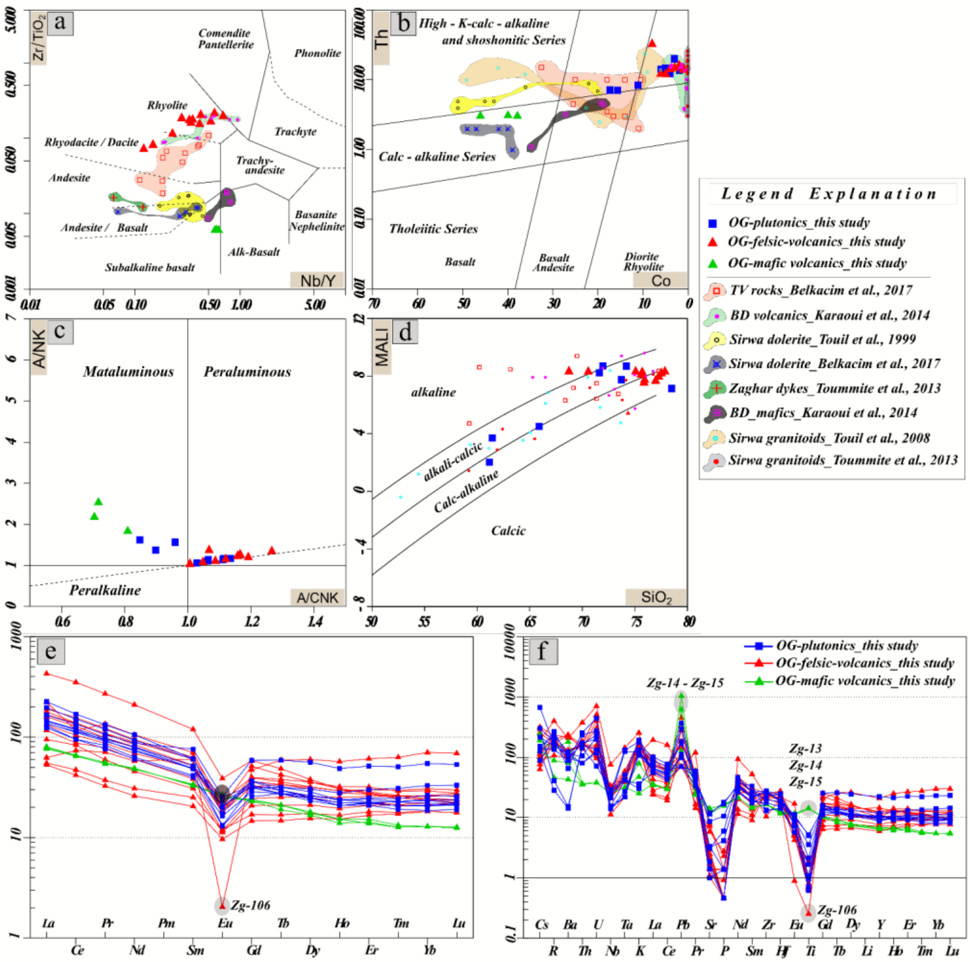

470 Figure 7: Ouarzazate Group: (a) Nb/Y versus Zr/TiO_2 (Winchester and Floyd, 1977). (b) Th vs Co plot of Hastie et al., (2007). (c) Plot of A/NK vs. A/CNK of Shand, (1943). (d) MALI diagram of Frost et al., (2001). (e) Chondrite-normalized REE diagram of Boynton, (1984). (f) Primitive mantle normalized diagram of Sun and McDonough, (1989). OG samples are plotted against reference rocks from the literature. Abbreviations: TV: Tifnoute Valley; BD: Bas Draâ.

Commenté [CM11]: Figure 6 has been reproduced into Fig. 6, and Fig. 7 in the new revised version.

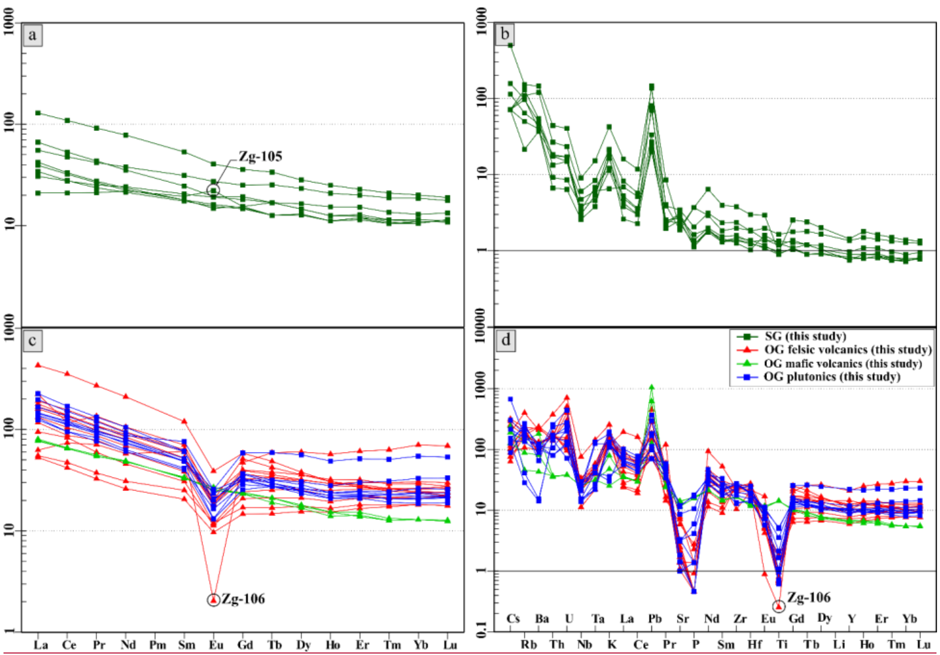

Figure 7. (a) Chondrite-normalized REE diagram of Boynton, (1984) for SG; (b) NMORB normalized diagram of Sun and McDonough (1989) for SG; (c) Chondrite-normalized REE diagram of Boynton, (1984) for OG; (d) Primitive-mantle normalized diagram of Sun and McDonough (1989) for OG.

4.4 Whole-rock Sm-Nd isotope compositions~~Significance of Sm-Nd isotopic data~~

Sm-Nd isotopic studies of seven representative samples covering the Ediacaran record of the Sirwa massif reveal petrogenesis processes and orogenic evolution between the 630 to 53~~8~~9 Ma evolution of the Anti-Atlas belt post-Bou Azzer-Sirwa ophiolite accretion. Results are listed in table ~~2~~1.

~~Lithology~~	~~Sample code~~	~~Sm (ppm)~~	~~Nd (ppm)~~	~~147Sm/144Nd~~	~~143Nd/144Nd~~	~~± 2 SE~~	~~ƐNd(0)~~	~~ƐNd(570)~~	~~TDM (Goldstein) Ma~~	~~TDM Ga~~
~~**Ouarzazate Group rocks**~~										
~~Granodiorite~~	~~Zg-09~~	~~10.23~~	~~50.70~~	~~0.1220~~	~~0.512414~~	~~0.000005~~	~~−4,4~~	~~+ 1,1~~	~~1252,8~~	~~1,24~~
~~Dolerite~~	~~Zg-14~~	~~6.518~~	~~28.99~~	~~0.1359~~	~~0.512390~~	~~0.000010~~	~~−4,8~~	~~−0,4~~	~~1526,7~~	~~1,51~~
~~Rhyolite~~	~~Zg-106~~	~~11.50~~	~~32.75~~	~~0.2124~~	~~0.512693~~	~~0.000007~~	~~+ 1,1~~	~~−0,1~~	~~0~~	~~N/A~~
~~Rhyolite~~	~~Zg-117~~	~~10.69~~	~~50.59~~	~~0.1278~~	~~0.512332~~	~~0.000011~~	~~−6,0~~	~~−0,9~~	~~1483,7~~	~~1,47~~
~~Granite~~	~~Zg-119~~	~~9.106~~	~~42.92~~	~~0.1283~~	~~0.512381~~	~~0.000009~~	~~−5,0~~	~~0,0~~	~~1404,8~~	~~1,39~~
~~**Saghro Group rocks**~~										

Gabbro	Zg-105	3.739	13.27	0.1704	0.512762	0.000011	+ 2,4	+ 4,5	1431,6	N/A
Andesite	Zg-108	8.943	40.03	0.1351	0.512550	0.000007	- 1,7	+ 3,2	1197,3	1,19

Table 12: Whole-rock Sm-Nd isotopic data compositions for the analyzed Saghro GroupSG and Ouarzazate GroupOG rocks. TDM Goldstein is the Depleted Mantle Age in Ga calculated using the linear model of Goldstein et al., (1984); and is not calculated for samples with $^{147}Sm/^{144}Nd$ ratios greater than 0.145 (e.g. Zg-106, Zg-105). Abbreviations: ± 2 SE: Standard Errors (Uncertainty in Nd isotopic composition); N/A : Not Available.

Sample	Lithology	Age (Ma)	Sm (ppm)	Nd (ppm)	$^{147}Sm/^{144}Nd$	$^{143}Nd/^{144}Nd$ measured	± 2SE	$^{143}Nd/^{144}Nd_{(t)}$	$\varepsilon Nd^{(t)}$	TDM (Goldstein) Ga	TDM (2stage) Ga
SG rocks											
Zg-105	Gabbro	620	3.73	13.27	0.1704	0.512762	0.000011	0.512071	+4.6	1.36	0.91
Zg-108	Andesite	620	9.94	40.03	0.1351	0.512550	0.000007	0.512002	+3.2	1.16	1.02
OG rocks											
Zg-09	Granodiorite	570	10.23	50.70	0.1220	0.512414	0.000005	0.511959	+1.1	1.22	1.15
Zg-119	Granite	570	9.10	42.92	0.1283	0.512381	0.000009	0.511903	+0.0	1.37	1.24
Zg-14	Dolerite	570	6.51	28.99	0.1359	0.512390	0.000010	0.511884	-0.3	1.50	1.26
Zg-106	Rhyolite	570	11.50	32.75	0.2124	0.512693	0.000007	0.511902	+0.0	N/A	1.25
Zg-117	Rhyolite	570	10.69	50.59	0.1278	0.512332	0.000011	0.511856	-0.8	1.45	1.30

$(^{143}Nd/^{144}Nd)_t = (^{143}Nd / ^{144}Nd)_0 + (^{147}Sm / ^{144}Nd)_t \times (e^{\lambda t} - 1)$

$\varepsilon Nd^{(t)} = [(^{143}Nd/^{144}Nd_{sample}{}^{t} / ^{143}Nd/^{144}Nd_{CHUR}{}^{t}) - 1] \times 10000$

$T_{DM2} = 1/\lambda \times \mathrm{Ln}\ \{1 + [(^{143}Nd/^{144}Nd)_{DM} - (^{143}Nd / ^{144}Nd)_{sample} + ((^{147}Sm / ^{144}Nd)_{sample} - (^{147}Sm / ^{144}Nd)_{CC)} \times (e^{\lambda t} - 1)] / ((^{147}Sm / ^{144}Nd)_{DM} - (^{147}Sm / ^{144}Nd)_{CC)}\}$

$\lambda\ ^{147}Sm = 0.654 \times 10^{-11}\ a^{-1}$: the decay constant of ^{147}Sm.

$(^{143}Nd/^{144}Nd)_{DM} = 0.51315$: present-day ratio of the Depleted Mantle (DM).

$(^{147}Sm / ^{144}Nd)_{DM} = 0.2137$: present-day parent/daughter ratio of the DM.

$(^{147}Sm / ^{144}Nd)_{CC)} = 0.12$: average parent/daughter ratio assigned to the Continental Crust (CC).

Error of initial ratio is calculated from the measurement of error of the isotope ratio, the estimated concentration error and the age error. The decay constant is considered to be a fixed value.

$$\sigma_{Nd(t)} = \sqrt{\sigma_{Nd}^2 + \sigma_{Sm}^2\ (e^{\lambda t} - 1)^2\ +\ \sigma_t^2\ \left(\lambda e^{\lambda t}\left(\frac{^{147}Sm}{^{144}Nd}\right)\right)^2}$$

$\sigma_{Nd(t)}$ is mean-square deviation of $(^{143}Nd/^{144}Nd)_t$

σ_{Sm} is mean-square deviation of $(^{143}Sm/^{144}Nd)_{sample}$

σ_t is mean-square deviation of age

Based on field relationships, Aan angular unconformity (Errami et al., 2009; Thomas et al., 2002), and a significant sedimentary/magmatic gap exist between the 630 –– 600 Ma Saghro GroupSG and the overlaying 570 –– 538 Ma Ouarzazate GroupOG (Errami et al., 2021a). We have used the 620 Ma as a reference age for εNd analyses of Saghro GroupSG samples (Zg-105, and Zg-108). They show narrow (^{143}Nd /^{144}Nd) 620 Ma ratios, ~ from 0.512001 to 0.512070, and positive εNd_{620} εNd (at 620 Ma) values between of +-3.2 to and +-4.65. Additionally, the TDM model ages (Fig. 8a), ranging fromof 1.02 and 0.91 Ga 1431 – 1197 Ma, exceed the individual maximum depositional ages of 630 to 600 Ma, and the crystallization ages of pre to contemporaneous igneous intrusions found elsewhere in the Anti-Atlas belt that fall within the bracket of 640 Ma to 580 Ma, respectively (Errami et al., 2021a; O'Connor et al., 2010; Liégeois et al., 2006; Gasquet et al., 2005; Mrini, 1993). Overall, the Saghro Group samples show a mixed origin with εNd (620 Ma) ranging from + 3.2 to + 4.5, indicating a blend of mantle-derived magma and moderate contribution of an old crust (Paleoproterozoic ?). This contrasts the basaltic rocks studied in the

Commenté [CM12]: Table 1 is reproduced after the recommendations from reviewer 1.

Saghro region by Errami et al., (2009), for which εNd (at 640 Ma) vary between + 7.63 to + 8.08, suggesting a juvenile source, with no Paleoproterozoic influence. Consequently, authors argued that the Saghro Group's sedimentary and volcanic deposits attest to an active back-arc basin, with the arc itself located north of the Saghro mountains in the Saghro inlier (Errami et al., 2009).

The OGOuarzazate Group rocks calculated at 570 Ma exhibit a mostly uniform distribution with ($^{143}Nd/^{144}Nd$) 570 Ma values from 0.51185555 to 0.51195858. These ratios are close to or slightly lower than the Chondritic Uniform Reservoir (CHUR) values. (εNd_{570} = -0.8 to +1.1). Moreover, for all samples, the εNd570 values range from - 0.9 to + 1.1. Volcanic rocks show negative εNd_{570}εNd570 values: -0.98 (Tadmant rhyolite), +–0.10 (Ouarzazate GroupOG rhyolite), and - 0.34 (dolerite). Granitoids have εNd_{570}εNd570 values of +-0.0 to and +-1.1 for Zg-119 and Zg-09, respectively. This range in values suggests mixing or variable degrees of interaction between a mantle source and an older crustal component. In addition, the TDM model ages for all of these samples range from 1.30 to 1.15 Ga (Fig. 8a). 1526 to 1252 Ma (Fig. 8c), indicating a Mesoproterozoic affinity, even though the effect is limited. Admitting that Mesoproterozoic rocks are scarce to absent in the Anti-Atlas, these Proterozoic TDM ages, in conjunction with the mixed (near zero) εNd (570 Ma) values for both volcanic and plutonic rocks, strongly suggest that the magma for the Ouarzazate Group are likely to represent mixed values involving a Pan-African juvenile mantle together with moderate but discernible contribution from an older crustal material of Mesoproterozoic in age, which itself incorporated some even older (Paleoproterozoic ?) material (Baidada et al., 2017; El Bahat et al., 2017; Blein et al., 2014b; Gasquet et al., 2005; Thomas et al., 2002) (Fig. 8d). All in all, these results do confirm the presence of an old cratonic basement beneath the Central Anti-Atlas. Overall, the distinct $\varepsilon Nd_{(t)}$ isotopic signatures for both groups is further supported by the negative correlation of $\varepsilon Nd_{(t)}$ values with SiO_2 (Fig. 8b).

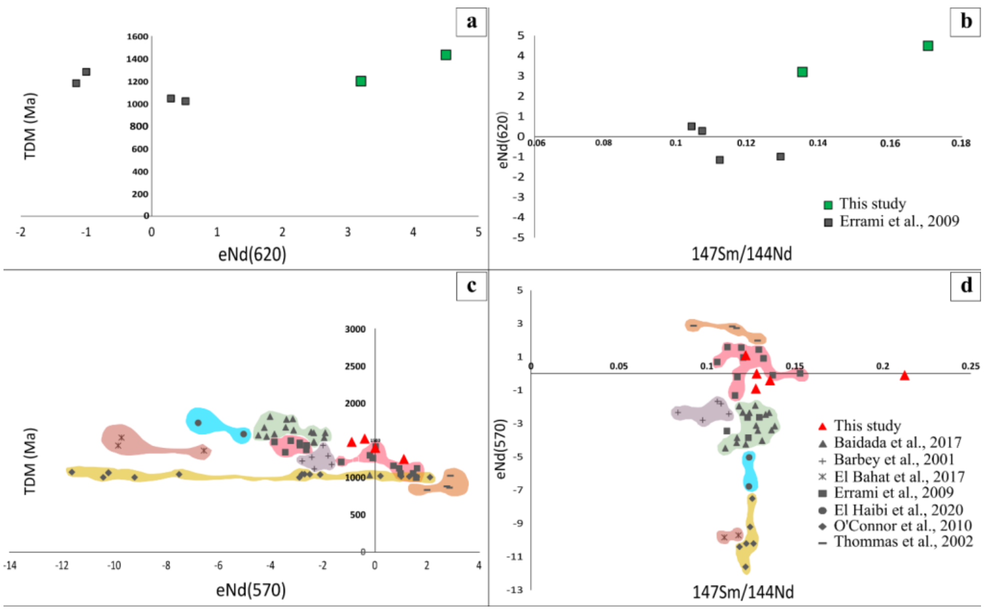

~~Figure 8: (a) εNd_{620} vs TDM model ages for SG. (b) εNd_{620} vs $^{147}Sm/^{144}Nd$ diagram for SG. (c) εNd_{570} vs TDM model ages for OG. (d) εNd_{570} vs $^{147}Sm/^{144}Nd$ diagram for OG rocks. All samples are compared with selected and available reference rocks from the literature.~~

Commenté [CM13]: Figure 8 is reproduced based on the propositions from Reviewers 1 and 2. Detailed modifications were adopted for RC1 comments.

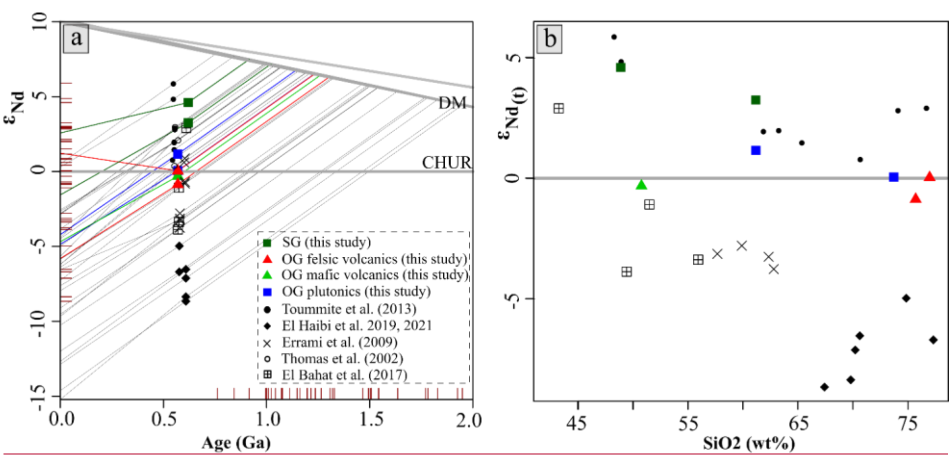

Figure 8. (a) two-stage εNd isotope growth diagram for SG and OG rocks versus Age (Ga). DM, Depleted Mantle evolution lines after Goldstein et al. (1984) and Liew and Hofmann (1988); CHUR, Chondritic Uniform Reservoir. The tick marks on the axes denote two-stage Nd model ages along the x-axis and initial εNd values along the y-axis; (b) Initial εNd versus SiO2 (wt.%) for SG and OG rocks. All samples are compared with selected and available reference rocks from the literature. Calculations and diagrams are produced using GCDkit (Janoušek et al., 2006).

Further, to quantify the mixing proportions for the Saghro and Ouarzazate groups, this study employs a binary mixing model based on the equations of Faure (1986), utilizing the computational approach detailed by Janoušek et al. (2016). In this model, the isotopic ratio of a mixture (I_M) is defined as the mean of the isotopic ratios of two end-members (I_1 and I_2), weighted by their respective mass fractions and elemental concentrations. f_1 represents the mass fraction of end-member 1 (where $f_1 + f_2 = 1$), while C_1, C_2, and C_M represent the elemental concentrations of the end-members and the resulting mixture. The mantle end-member 1 is defined by a metasomatized lithospheric source with values of $I_1 = 0.512265$; $C_1 = 13.27$ ppm, and $\varepsilon Nd_{620} = +8$ from Errami et al. (2009), reflecting an enriched mantle by prior subduction processes. For the crustal end-member 2, we utilized parameters from Ennih and Liégeois, (2008) ($I_2 = 0.511472$; $C_2 = 47$ ppm; $\varepsilon Nd_{620} = -16$), representing the Paleoproterozoic basement of the WAC.

The mixing equations are defined as :

$$I_M = I_1 \left(\frac{C_1}{C_M}\right) f_1 + I_2 \left(\frac{C_2}{C_M}\right)(1 - f_1)$$

Where:

(1)

$$C_M = f_1 C_1 + (1 - f_1) C_2$$

(2)

$$f_1 = \frac{C_2(I_M - I_2)}{C_1(I_1 - I_M) + C_2(I_M - I_2)})$$

Applying this mixing model reveals that SG rocks are characterized by a dominantly mantle origin; the andesite (Zg-108) and gabbro (Zg-105) yield high mantle-derived mass fractions (f_1) of 88 % and 92 %, respectively, with minor crustal inputs ($f_2 \approx$ 8 % to 12 %). Conversely, the OG magmas have mantle mass fractions (f_1) ranging from 75 % to 85 %. Moreover, the calculated crustal contribution (f_2) increases from 15 % in granodiorite (Zg-09) to 25 % in the rhyolite (Zg-117).

5 Discussions

5.1 Petrogenesis

~~5.1.1 The Saghro Group rocks~~

The SG and OG rocks exhibit chemical evolution that can be explained by fractional crystallization. The general trends for major elements (e.g., Al_2O_3, CaO, and TiO_2) show positive correlations versus Mg# (Fig. 9a,b, and c). For instance, Al_2O_3

Commenté [CM14]: We have added this paragraph on the binary mixing proportions based on the corrected calculations as requested by Reviewer 1, and interpreted accordingly (see sub-section 5.2).

Commenté [CM15]: Please be aware that the discussion part has been completely rewritten based on the constructive comments from Reviewer 1.

contents decrease with decreasing Mg# suggesting the crystallization of plagioclase (Fig. 9a). CaO contents exhibit a sharp drop as Mg# decreases (below ~40), indicating clinopyroxene or calcic plagioclase fractionation (Fig. 9b). TiO_2 also decreases with decreasing Mg#, pointing to the early crystallization of Fe-Ti oxides (e.g., ilmenite or titanomagnetite) (Fig. 9c).

On the A/CNK versus Mg# plot (Fig. 9d), the SG rocks are metaluminous (A/CNK < 1.0), while the OG felsic and plutonic rocks are peraluminous (A/CNK > 1.0). This shift to peraluminous composition suggests that the felsic rocks involved the melting of aluminum-rich material or the fractionation of aluminum-poor minerals (e.g., hornblende, pyroxene). In Figure. 9e, the SG rocks retain the highest Sr concentrations (~200–350 ppm), indicating a more aluminum enriched source or less plagioclase removal. Furthermore, this is supported by the absence of a negative Eu anomaly (Eu/Eu* = 0.89–1.28), to positive one for gabbro Zg-105 (Eu/Eu* = 1.28) indicating limited plagioclase fractionation (Fig. 7a). On the contrary, the OG rocks showcase a dramatic drop in Sr from the OG mafic volcanics, passing through the OG plutonics to the OG felsic volcanics. This steep decline proves that plagioclase crystallization was the dominant driver for OG differentiation (Fig. 9e). This is corroborated by the prominent negative Eu anomaly in rhyolite Zg-106, while the absence of an Eu anomaly in dolerites suggests limited plagioclase involvement (Fig. 7c).

On the Th (ppm) versus Mg# (Fig. 9f), both the SG rocks and OG mafic volcanics showcase low Th concentrations (<5 ppm) typical of mantle-derived melts. However, for the SG, the Mg# values of 21.50 to 60.20, reflect early fractionation of ferromagnesian minerals, and suggest that rocks are not derived from a primitive melt. For the OG, Th levels spike to up to 32 ppm for the OG felsic volcanics and plutonics, suggesting possible influence by crustal melting or assimilation during magma ascent (Fig. 9f). The lack of a negative Eu anomaly in the SG rocks (Fig. 7a), despite the evolved nature of the magmas, is likely due to the mixing of evolved basaltic magmas, with more primitive magmas that lacked plagioclase fractionation. The OG felsic volcanics and plutonics show Sr and P depletion that can be explained by plagioclase and apatite fractionation (Fig. 7d).

Eu/Eu* values versus Sr contents (ppm) evince a clear positive correlation (Fig. 9g). The mafic rocks of the Saghro and the Ouarzazate groups have high Sr and Eu/Eu* values near 1.0 suggesting plagioclase accumulation in relation to their more primitive nature. On the contrary, the OG felsic volcanics and plutonics have significantly lower Sr and Eu/Eu* values, providing evidence that fractionation of plagioclase from the melt was significant (Fig. 9g). Whole rock Zr/Sm versus Zr and Rb/Nb versus Rb correlations are as expected for a fractional crystallization process (Fig. 9h-i). The localized spike in Zr/Sm at high Zr contents (~350 ppm) indicates late stage mineralogical control, involving zircon or amphibole fractionation in the more evolved magmas of the OG, distinct to the relatively stable ratios for most samples (Fig. 9h). This implies that the magmatic evolution of the SG and the OG rocks was characterized by both fractional crystallization and progressive crustal contamination or a subduction modified source (Fig. 9i).

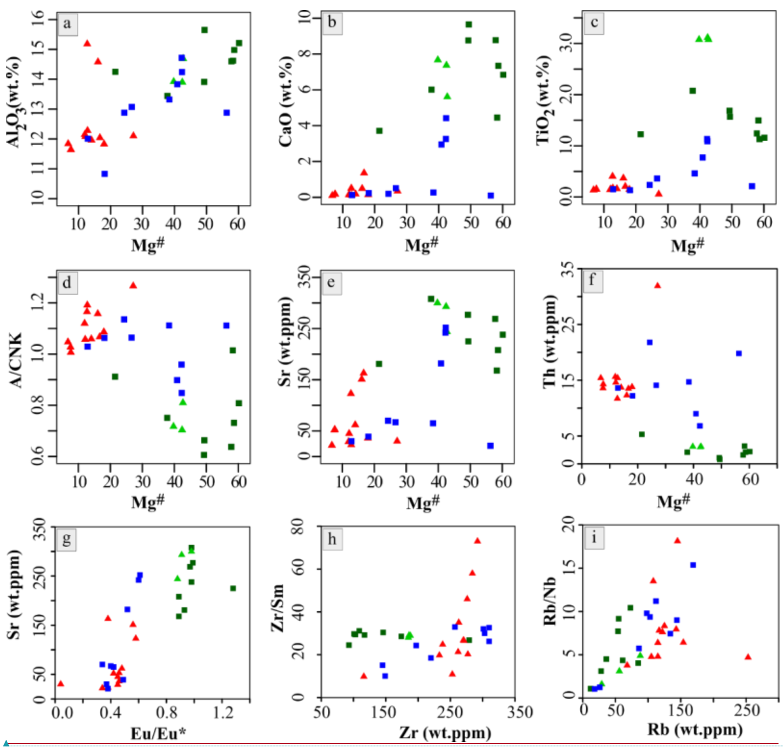

Figure 9. (a) Al_2O_3 (wt.%) versus Mg#; (b) CaO (wt.%) versus Mg#; (c) TiO_2 (wt.%) versus Mg#; (d) A/CNK (A/CNK = molar ratio Al_2O_3 / (CaO + Na_2O + K_2O)) versus Mg#; (e) Sr (ppm) versus Mg#; (f) Th (ppm) versus Mg#; (g) Zr / Sm value versus Zr content (ppm); (h) Rb / Nb value versus Rb content (ppm); (i) Eu / Eu* value versus Sr (ppm). Symbols as those in Figure 6.

The εNd_i versus $^{147}Sm/^{144}Nd$ plot evince a clear distinction between the SG and the OG rocks (Fig. 10a). The SG rocks exhibit strongly positive εNd_i values of +3.2 and +4.6, indicating a juvenile, depleted mantle origin with minimal crustal interaction. In contrast, the OG rocks cluster near or below the CHUR line (εNd_i values of -0.8 to +1.1), signaling a hybrid source involving the significant reworking of older, evolved continental crust. Notably, while sample Zg-106 shares this near-zero isotopic signature, its unusually high $^{147}Sm/^{144}Nd$ ratio of ~0.21 confirms it underwent a distinct petrogenetic process, likely a low degree of partial melting that fractionated REE without significantly altering the initial Nd isotopic composition of its source (Fig. 10a).

The geochemical fingerprints for the SG and OG are distinct. For samples with Nb < 25 ppm (Fig. 10b), a significant vertical spread in Nb/Ta ratios (~3–15) is observed; specifically, the OG plutonics exhibit a sharp decline in Nb/Ta (~3), indicating

Mis en forme : Couleur de police : Vert advanced fractional crystallization of ferromagnesian and accessory minerals. Conversely, the SG mafic rocks maintain higher, stable ratios (~10–15), identifying them as more primitive melts. While Nb and Ta typically behave as geochemical twins, they can fractionate during subduction (Hofmann et al., 1986). The OG rocks cluster below a Nb/Ta ratio of 14, well under the mantle value of 17.5 (Sun and McDonough, 1989), matching the bulk continental crust value of ~11 (Green, 1995) and confirming a dominant crustal signature. This is further corroborated by an enrichment in LILEs (like Rb, Ba, and Th), coupled with prominent negative Nb-Ta and Ti anomalies (Fig. 7d), signature of subduction-related magmatism or the recycling of metasomatized lithosphere (Ikenne et al., 2007). Finally, the OG rhyolite (Zg-106) displays a horizontal shift toward higher Nb contents at a fixed Nb/Ta ratio (~9) (Fig. 10b), suggesting magma enrichment via a low degree of partial melting from a source already characterized by a low Nb/Ta ratio and a pre-existing subduction-modified signature.

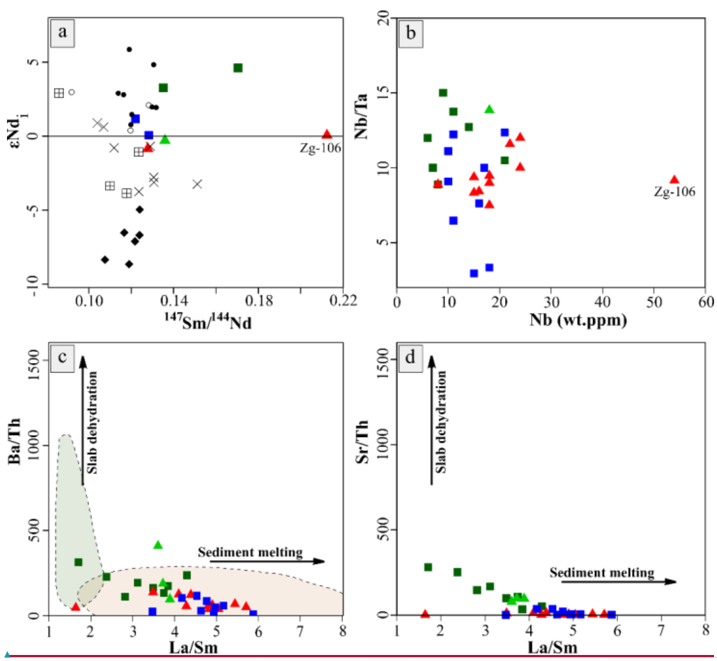

Figure 10. Plots (a) Initial εNd versus ^{147}Sm/^{144}Nd; (b) Nb/Ta versus Nb contents (ppm); (c) Ba/Th versus La/Sm and (d) Sr/Th versus La/Sm (domains are modified from Labanieh et al. (2012). Legend is the same as in Figure 8.

The SG and OG rocks show enrichment in LILEs and LREEs relative to HFSEs and HREEs. They also exhibit pronounced negative anomalies in Nb, Ta, and Ti (Fig. 7), suggesting a subduction zone fluids influence (Wilson, 1989). Admittedly, for

Mis en forme : Police :9 pt, Gras, Couleur de police : Texte 1, Police de script complexe :11 pt, Gras the OG rocks, this inherited geochemical signature is attributed to oceanic arc rocks previously subducted into the mantle (Toummite et al., 2013; Gasquet et al., 2008; Ikenne et al., 2007; Thomas et al., 2002).

Trace elements can clarify subduction input versus crustal contamination. As shown in the Ba/Th versus La/Sm diagram (Fig. 10c), most samples display low Ba/Th, high and variable La/Sm ratios, favoring the dominant role of the sediment melting process. Similarly, the role of the sediment melt is also observed for all samples in the Sr/Th versus La/Sm diagram (Fig. 10d). For the SG rocks, their relatively high Sr/Th ratios are attributed to plagioclase accumulation. Furthermore, high La/Sm ratios indicate a sediment-dominated influence, suggesting that the slab pressure-temperature conditions were sufficient to trigger sediment melting (Labanieh et al., 2012). The melting process acted as the primary mechanism for transferring the slab signature into the analyzed samples.

5.2 Initial Sm-Nd isotopes composition and magma source characteristics

The whole-rock Sm-Nd isotope compositions of the Saghro and Ouarzazate groups suggest a heterogeneous magma source, exhibiting negative correlation of $\varepsilon Nd_{(t)}$ values versus SiO2 (Fig. 8b). For instance, the SG maintains high $\varepsilon Nd_{(620)}$ values (+3.2 and +4.6) even as silica increase, reinforcing their juvenile mantle source with minimal crustal input,. Eventually, the obtained TDM model ages of 1.02 and 0.91 Ga confirm a depleted mantle source. Within the OG, the decreasing trend of εNd_{570} = +1.1 to -0.8 with increasing SiO_2 is a classic signature of Assimilation-Fractional Crystallization (AFC), where the cooling magma is simultaneously evolving toward a felsic composition and incorporating more evolved, negative εNd continental crust. Notably, the calculated TDM model ages clustering around 1.30 to 1.15 Ga indicates that the OG magmas were not purely mantle-derived but involved the significant recycling of much older underlying basement (Mesoproterozoic and/or Paleoproterozoic).

Indeed, quantitative binary mixing model validates these isotopic trends. the SG rocks showcase a near-pristine mantle signature (f_1 = 88–92 %). However, the increase in the crustal contribution (f_2) of the OG rocks from 15 % in granodiorite (Zg-09) to 25 % in the rhyolite (Zg-117) confirm a coupling of increasingly felsic compositions with higher crustal input. The 25 % contribution from an ancient Paleoproterozoic source with εNd_{620} = -16 constitutes a major contamination event, exerting a significant isotopic pull by shifting the εNd values of the samples to near zero. Normally, without the recycling of this ancient basement, a purely mantle-derived magma at 570 Ma would exhibit strongly positive values up to +7 to +8. This hybridization is further supported by the TDM model ages of 1.30 to 1.15 Ga, proving the significant involvement of the underlying Eburnean WAC basement.

5.3 Tectonic implications

Previously, the SG basin was interpreted as consisting of distal deep marine sediments equivalent to the platform series of Tachdamt Group, formed during the initial rifting associated with the Rodinia breakup (Thomas et al., 2002). However, recent zircon data from the SG sediments in the Sirwa and Saghro inliers suggest its deposition occurred post the Bou Azzer–Sirwa ophiolite accretion, during the main Pan-African Orogeny (Abati et al., 2010; Errami et al., 2009; Liégeois et al., 2006). Furthermore, the Ediacaran magmatism of the OG is still debated as being fully post-collisional and linked to asthenospheric rise (upwelling) beneath the WAC during its metacratonic evolution (Gasquet et al., 2008, 2005; Liégeois et al., 2006; Thomas et al., 2002), or related to subduction (Walsh et al., 2012; Benziane, 2007; El Baghdadi et al., 2003), or even representing the Iapetus Ocean opening with ties to the Ediacaran Central Iapetus Magmatic Province (CIMP; Youbi et al., 2020). Based on similarities in ages and chemical characteristics, this magmatism is associated with the Avalonian-Cadomian marginal belt along the Northwestern edge of Gondwana, and constitutes a major magmatic flare-up spanning roughly 590–540 Ma (Letsch et al., 2018; Tahiri et al., 2010; Linnemann et al., 2008).

For our samples, the multi-elemental discrimination plots (Fig. 11a–f) provide a framework for deciphering the petrogenesis and tectonic transition of the Ediacaran magmatic sequences in the Anti-Atlas. For a start, the SG basalts feature high Zr and relatively low Y concentrations, classifying them as within-plate basalts (WPB) (Fig. 11a), indicating an extensional or transtensional geodynamic setting. On the Th/Nb versus Ti/V diagram of Shervais (2022), these samples plot in the Continental Flood Basalts (CFB) field (Fig. 11b). Admittedly, and placed in the regional context of the Anti-Atlas; the geodynamic setting of the SG has been interpreted as an intracontinental rift evolving into either a mature back-arc basin (Errami et al., 2009; Fekkak et al., 2001) or a continental passive margin (Fekkak et al., 2002). This evolution is characterized by a transition from early, sediment-influenced tholeiites to more evolved magmatic suites rather than a massive subaerial flood province. The calc-alkaline character for the SG mafic rocks reflects an enrichmentt in Th, typical of subduction-influenced or crustally contaminated suites (Fig. 6e). This apparent transitional character exhibiting a calc-alkaline affinity (Fig. 6e) but a within-plate (Fig. 11a), continental tholeiites (Fig. 11e) character represents an early Ediacaran extensional phase where advanced lithospheric thinning allowed asthenospheric decompression triggering large-scale melting of the Sub-Continental Lithospheric Mantle (SCLM). In contrast, the younger OG volcanic and plutonic rocks plot at higher Th/Nb ratios (>0.5) along the Upper Continental Crust (UCC) and Andean Arc fields, with extreme Th enrichment pointing to a regional thermal regime shift (Fig. 11b). The OG magmatism marks a massive crustal melting event, which we interpret as a response to post-collisional lithospheric delamination and possible slab break-off. This process generated highly differentiated and evolved magmatic suites with wide variations in Ti/V ratios (Fig. 11b).

Furthermore, there is a clear lithospheric transition between the SG and the OG rocks based on their trace element enrichments. For instance, the SG mafic rocks follow the MORB-OIB array (Fig. 11c), indicating a magma source derived directly from an enriched mantle source akin to the source of enriched mid-ocean ridge basalt (E-MORB). This infers that the primary magmas were derived via partial melting of an enriched lithospheric mantle that carried a fossil subduction signature from earlier Cryogenian cycles. Conversely, the younger OG volcanic and plutonic rocks evince a considerable crustal contamination. This shift toward higher Th/Yb ratios reflects an input of continental crust or the widespread tapping of a SCLM domain deeply metasomatized by subduction-related sediments (Fig. 11c). Moreover, for SG rocks, their lower Th/Nb ratios suggest a more primitive mantle-dominated source modified by an ancient subduction-preconditioned lithospheric root rather than an active deep-mantle plume head, as they cluster within the vertical Subduction Zone-Modified Lithospheric Mantle (SZLM) array, near the LCC (Lower Continental Crust) (Fig. 11d).

In addition, the OG rocks plot within the upper limits of the SZLM array, clustering inside the IAB and CAB fields. This geochemical footprint might signifies slab break-off where the crustal recycling or the melting of the thickened lithospheric root was driven directly by the severe thermal anomaly of the upwelling asthenospheric mantle (Fig. 11d).

Ultimately, a coherent geodynamic transition emerges between both Saghro and Ouarzazate groups. On Figure. 11e, the SG mafic rocks cluster within the Continental Tholeiites (CT) field, adjacent to the Back-Arc Basin (BAB) domain. This position, combined with their calc-alkaline signature (Fig. 6e), and a within-plate character (Fig. 11a) confirms that these rocks were formed in an extensional continental setting. The proximity to the BAB field suggests that while the crust was thinning, the magmatism still retained a slight transitional character, typical of a maturing continental rift or a back-arc basin environment, with a distinct geochemical overprint from a pre-modified lithospheric root. Finally, the OG felsic and plutonic samples plot decisively within the A2-type granite field, supporting their post-collisional nature (Fig. 11f). Eby (1992) suggests that A2-type granites originate from the partial melting of continental or underplated mafic crust, typically within extensional environments. In this context, crustal recycling was driven by the mechanical and thermal effects of lithospheric delamination and potential slab failure (Blein et al., 2023; Ougadire et al., 2023). This triggered the rapid basin development and the accumulation of the thick volcano-sedimentary sequences characteristic the OG across the already rigid and fractured metacratonic margin of the WAC, providing preferential pathways for the rapid upward migration of deep-sourced magmas (Walsh et al., 2012, and references therein; Ennih and Liégeois, 2001, 2008; Gasquet et al., 2008).

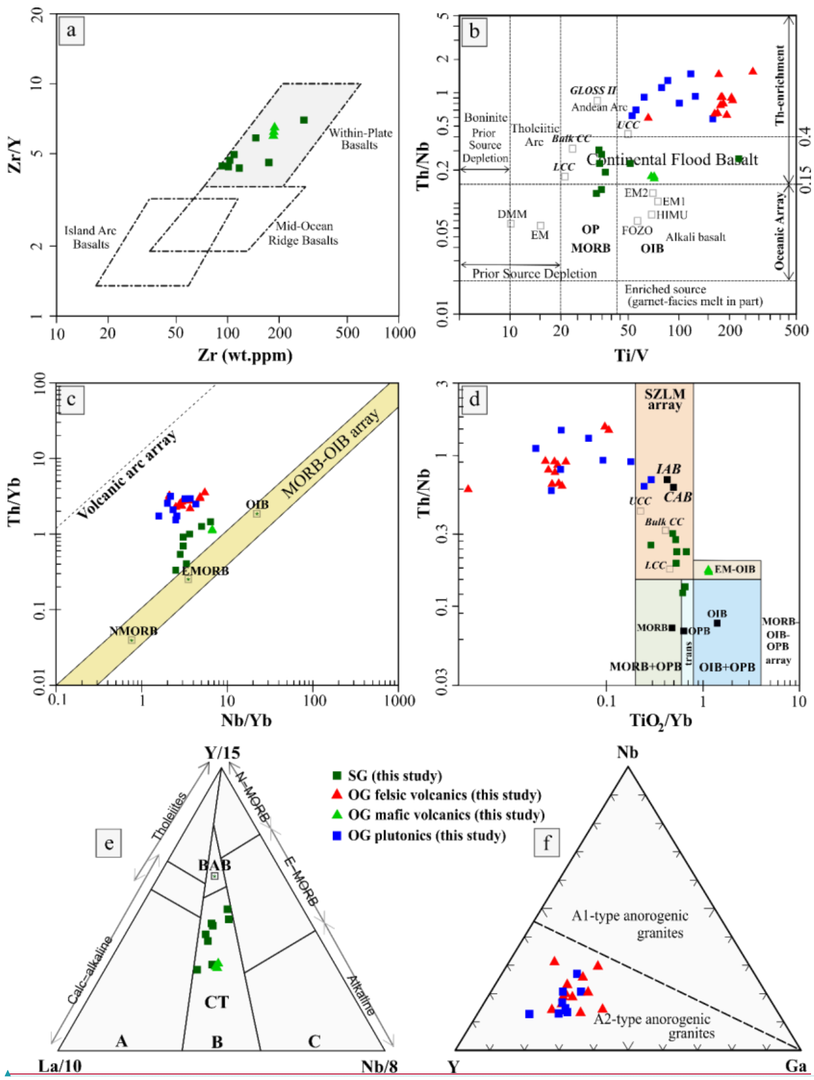

Mis en forme : Police :8 pt, Police de script complexe :8 pt

Figure 11. (a) Zr/Y vs Zr (ppm) plot for SG rocks and OG mafic volcanics (Pearce and Norry, 1979); (b) Th/Nb versus Ti/V diagram of Shervais (2022); (c) Th/Yb versus Nb/Yb diagram of Pearce (2008); (d) Th/Nb versus TiO_2/Yb plot of Pearce et al. (2021); (e) La/10 – Y/15 – Nb/8 ternary diagram for the tectonic discrimination of basaltic rocks (Cabanis and Lecolle, 1989); (f) Nb – Y – Ga ternary diagram for the classification of A1 and A2-type anorogenic granites (Eby, 1992). Abbreviations: Bulk CC: Bulk Continental Crust; GLOSS: Global Subducting Sediment; LCC: Lower Continental Crust; UCC: Upper Continental Crust; EM1 / EM2: Enriched Mantle (Type 1 & 2); DMM: Depleted MORB Mantle; HIMU: High μ (high $^{238}U/^{204}Pb$ ratio) mantle reservoir; OIB: Ocean Island Basalt; SZLM: Subduction Zone-Modified Lithospheric Mantle; CAB: Calc-Alkaline Basalt; IAB: Island Arc Basalt; OPB: Oceanic Plateau Basalt; MORB: Mid-Ocean Ridge Basalt; N-MORB: Normal Mid-Ocean Ridge Basalt; E-MORB: Enriched Mid-Ocean Ridge Basalt; EM: Enriched Mantle; OP MORB: BAB: Back-Arc Basin; CFB: Continental Flood Basalt; CT: Continental Tholeiites; A: Orogenic (compressive) domains (island arc, active margins); B: Late to post-orogenic (compressive to distensive) intra-continent domains; C: Anorogenic (distensive) domains.

The Saghro Group rocks consist of basaltic lava flows interbedded with marine, low-grade metasediments. The geochemical fingerprint of the mafic rocks is well-suited for investigating the orogenic processes involved in magma genesis (Pearce, 1983; Wood, 1980). However, it is crucial to evaluate the effects of alteration, metamorphism, and crustal contamination before exploring the magmatic evolution.

- **Alteration effect**

The analyzed samples exhibit loss on ignition (LOI) values of 2 to 4 wt.%, implying major elements and LILE mobility during alteration process (supplementary table 4). Saghro Group basalt samples display scattered large-ion lithophile elements (LILEs; e.g., K, Rb, Na, Sr, Pb) vs. Zr, suggesting alteration variances. In contrast, binary plots of high-field-strength elements (HFSEs; e.g., Nb, Ta, Ti, Hf) and rare earth elements (REEs) against Zr exhibit consistent linear trends, reflecting their immobile nature (Pearce, 1996; supplementary table 4). All samples from this Group are classified as minimally altered basalts (Large et al., 2001) (Fig. 5).

- **Fractional crystallization and crustal contamination**

The analyzed samples predominantly consist of basalts displaying negative correlations for Al_2O_3, CaO, MgO, Fe_2O_3, and TiO_2 vs. Zr, and a positive correlation for P_2O_5, indicating fractional crystallization during magma evolution. The Mg# values (12.13 to 43.26), reflect early fractionation of ferromagnesian minerals, and suggest that the Saghro Group samples are not derived from a primitive melt. Furthermore, the absence of a significant Eu anomaly (δEu = 0.88–1.28) indicates limited plagioclase fractionation (Fig. 6d). The lack of a negative Eu anomaly, despite the evolved nature of the magmas (low Mg#), is likely due to the mixing of evolved basaltic magmas (low Mg#), with more primitive magmas that lacked plagioclase fractionation.

In a contamination-sensitive trace element diagram (Th/Ce and Th/La) (Fig. 9a), our samples show ratios of 0.047 to 0.080 and 0.115 to 0.172, respectively. The trend suggest that crustal contamination played a significant role in magma genesis (Taylor and McLennan, 1995). Additionally, the low Ce/Pb ratio (~ 4.3) further highlights continental crustal influence (Hofmann et al., 1986; supplementary table 4 for calculation). Further, a binary mixing model with Nd isotopic data (supplementary table 4 for calculation; De Paolo, 1981), interprets the Saghro Group basalts as formed from the mixing of a magmatic melt contaminated by 17 – 18% Paleoproterozoic continental crust (εNd620 = - 16; Ennih and Liégeois, 2008) and 82 – 83% primitive mantle (εNd620 = + 8; Errami et al., 2009). This is further supported by the negative correlation of εNd values with SiO_2, and relatively low εNd values (+ 3.2 to + 4.5), compared to contemporary mantle-derived Saghro inlier basalts (εNd = + 8; Errami et al., 2009).

However, the observed enrichment may stem from either continental crust contamination or mantle source enrichment. The Th/Ce and Th/La ratios for our samples plot linearly near the MORB reservoir, far from the upper continental crust (UCC) field, suggesting limited direct crustal input (Fig. 9a). Moreover, ratios such as (Sm/Yb)N versus (Nb/La)N (Safonova et al., 2016), sensitive to the nature of the mantle source, range from 1.64 to 2.74 and 0.50 to 0.91, respectively. These values place the Saghro Group samples in a transitional domain between MORB and IAB, closer to the field of back-arc basalts (BAB) (Fig. 9b). Similarly, Th/Nb and Ta/Nd ratios (0.12 – 0.30 and 0.03 – 0.06, respectively) indicate a transitional composition between MORB and the mafic lower continental crust (MLCC) (Aldanmaz et al., 2008; Fig. 9c), in alignment with the source diagram (Laurent et al., 2014; Fig. 9d), where all the Saghro Group rocks derived from fractional crystallization and contamination/assimilation of primary mafic lithologies straddling the boundary between high-K to low-K mafic rocks. Overall, the Saghro Group samples originate from the melting of an enriched source transitional between MORB and IAB, followed by fractional crystallization involving ferromagnesian minerals and assimilation of lower Paleoproterozoic continental crust.

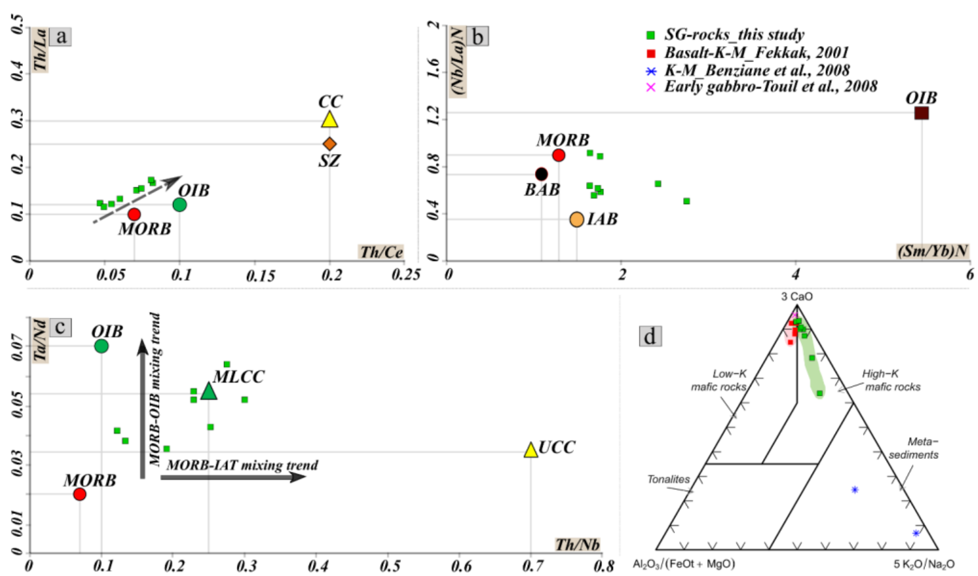

Figure 9: Saghro Group: (a) Th/Ce vs Th/La ratios for SG (Taylor and Mc Lennan, 1995). (b) plot of (Sm/Yb)N vs (Nb/La)N (Safonova et al., 2016). (c) Th/Nb vs Ta/Nd plot (Aldanmaz et al., 2008). (d) The source diagram of Laurent et al., (2014). Abbreviations: K-M: Kelâat M'gouna.

Mis en forme : Police :Gras, Police de script complexe :Gras

5.1.2 The Ouarzazate Group rocks

- **Fractional crystallization and crustal contamination**

The Ouarzazate Group's volcanic and plutonic rocks exhibit chemical evolution that can be explained by fractional crystallization, with decreasing Al2O3, Fe2O3, MgO, CaO, TiO2, and P2O5 vs. rising SiO2. Major elements vs. Zr show no significant correlations (not shown: see supplementary table 4). Selected trace elements, such as Sr, decrease with rising SiO2, typical of plagioclase crystallization. Interestingly, Some trace elements (e.g. Cr, Ni, Ba, Rb, Zr) show disruptions in their patterns with increasing SiO2. Ni uniformly declines then sharply increases, Cr rises steadily then increases, while Ba, Zr, and Rb rise then decline, particularly at 70 wt.% SiO2 (Fig. 10a). These patterns are likely due to a magma recharge event affecting pre-magma's crystallization (Fig. 10a).

Felsic volcanics and plutonics compensate for Sr and P depletion due to plagioclase and apatite fractionation (Fig. 7f). A prominent negative Eu anomaly in rhyolite Zg-106 indicates early calcic phase crystallization, while the absence of an Eu anomaly in dolerites suggests limited plagioclase involvement (Fig. 7e). Additionally, their Pb enrichment indicates crust assimilation (Fig. 7f). The high La (16.4 to 133 ppm) and Ce (33.8 to 284 ppm) values in the Ouarzazate Group samples suggest interaction between parental magma (s) and crust material, indicating enrichment due to either assimilation of continental crust or a combination of assimilation and fractional crystallization during magma ascent (De Paolo, 1981). Further, fractional crystallization relates to correlations between Zr and Th/Nb ratios (Fig. 10b), as most of the Ouarzazate Group felsic volcanics and plutonics show similar Th/Nb and Zr trends, indicating significant assimilation and fractional crystallization in magma evolution. Some plutonics, however, show a limited Th/Nb range, suggesting bulk assimilation control (Fig. 10b). This is supported by the La/Sm versus La diagram (Fig. 10c) indicating source heterogeneity, despite fractional crystallization's dominance. The Y/Nb versus SiO2 wt.% (Fig. 10d) confirms a crustal source with varying differentiation. Depletions in P, Nb, and Ti in Ouarzazate Group rocks (Fig. 7f) suggest crustal contamination and hydrous metasomatism, with P anomalies linked to Nb and Ti depletions (Campbell et al., 1994). In addition, the depletion of HFSEs like Nb and Ti might also indicate magmatic arc signatures and possible crustal contamination during magma processes (Wilson, 1989). All samples show slight K enrichments (Fig. 7f), likely related to fluids from subducted sediments (Beraaouz et al., 2004).

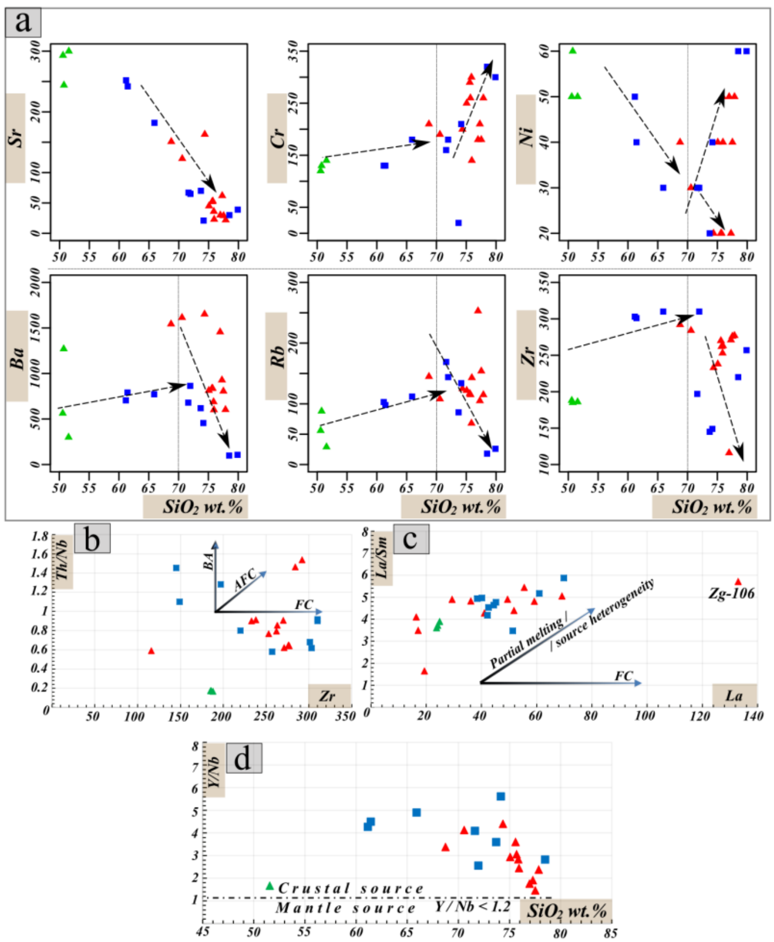

Figure 10: Ouarzazate Group: (a) Harker variation diagrams for selected trace elements (e.g. Sr, Cr, Ni, Ba, Rb, Zr) for the OG rocks. (b) plot of Th/Nb vs Zr. (c) La/Sm vs La plot. (d) Y/Nb vs increasing SiO_2, (Eby, 1990) for the Y/Nb =1.2 discriminating value. Abbreviations: BA: Bulk Assimilation; AFC: Assimilation and Fractional Crystallization; FC: Fractional Crystallization.

- **Magma types and source characteristics**

The coherent negative anomalies in Nb, P, and Ti in the Ouarzazate Group samples might suggest an exclusive crustal origin, with minor discrepancies due to advanced degrees of differentiation. These features may also arise from low partial melting of metasomatized mantle contaminated by continental material (O'Reilly and Griffin, 2013), as supported by εNd values (- 0.9 to + 1.1) indicating juvenile magma contributions. Indeed, trace elements and isotopic compositions can clarify subduction input versus crustal contamination. The Ouarzazate Group rocks show significant LILE and LREE enrichment with Nb-Ta depletion, indicating a metasomatized lithospheric mantle from subduction or assimilation of enriched continental crust (Fig. 7-f). Furthermore, the Th/Yb versus Ta/Yb diagram suggests that the magma source originated from an E-MORB-type mantle, evolving through contamination and Assimilation-Fractional Crystallization, as evidenced by the trend of the samples toward the average upper continental crust (Fig. 12a). This interpretation is consistent with the moderate εNd values and TDM ages that reflect contributions from both mantle and continental crustal components, highlighting the importance of crustal contribution over sediment zone enrichment (Fig. 12b). All in all, the primary magma responsible for the genesis of the Ouarzazate Group rocks sourced from an enriched continental lithospheric mantle, previously underwent metasomatism by fluids from former Neoproterozoic subduction.

5.2 Geodynamic implications and regional correlations

5.2.1 The Saghro Group

Previously, the Saghro Group basin was interpreted as consisting of distal deep marine sediments equivalent to the platform series of Tachdamt Group, formed during the initial rifting associated with the Rodinia breakup (Thomas et al., 2002). However, recent zircon data from the Saghro Group sediments in the Sirwa and Saghro inliers suggest its deposition, post the Bou Azzer–Sirwa ophiolite accretion, during the main Pan-African orogeny (Abati et al., 2010; Errami et al., 2009; Liégeois et al., 2006).

Basaltic samples from the Sirwa inlier (this study) show enrichment in large ion lithophile elements (LILE) and light rare earth elements (LREE) relative to high field strength elements (HFSE) and heavy rare earth elements (HREE). They also exhibit pronounced negative anomalies in Nb, Ta, and Ti, suggesting a subduction zone fluids influence (Wilson, 1989). Despite this, the basalts feature high Zr and relatively low Y concentrations, classifying them as within-plate basalts (WPB) (Fig. 11a). This dual geochemical signature, blending within-plate and active margin characteristics, is further evidenced by their Ti/Y and Zr/Y ratios which plot in transitional field in the geotectonic discrimination diagram (Ti/Y versus Zr/Y; Pearce and Gale, (1977), not shown). Indeed, the coexistence of geotectonic signatures from both active continental margins and within-plate settings is characteristic of magmas generated during back-arc extension (Shinjo and Kato, 2000).

In this context, the subduction-related signature is acquired through mantle metasomatism by sediment/fluid-derived components during arc activity, while the within-plate signature emerges later during back-arc extension processes. This interpretation aligns with the geochemical characteristics of the Saghro Group basalts, which plot within the fields of mid-ocean ridge basalt (MORB) and back-arc basin basalt (BABB) (Fig. 11b). Moreover, the active margin signature is supported by high Th/Nb and low U/Th ratios in the Saghro Group basalts (refer to supplementary table 4). Further, the influence of subduction-related components is further highlighted by the ThN vs NbN ratios, with the basalts plotting above the MORB-OIB array (Fig. 11c). This pattern indicates a mantle source enriched during continental arc processes (Pearce, 1983).

At a regional scale, basaltic flows have been described as interbedded within the sediments of the Saghro Group in the Saghro massif (Errami et al., 2009; Fekkak et al., 2003, 2001). They exhibit diverse geochemical signatures. For a start, the basalts in Sidi Flah (SF) are of Initial Rift Tholeiites (IRT) and Ocean Island Basalts (OIB) character, while those from the Kelâat M'gouna (KM) inlier are Nb-depleted. In contrast, the Anou N'Izem basalts in the Boumalne (BO) inlier possess typical Mid-Ocean Ridge Basalt (MORB) signatures. U-Pb dating of detrital zircons from the Saghro Group in various inliers suggests that this unit was deposited between 640 - 600 Ma across the entire Central-Eastern Anti-Atlas region (Errami et al., 2021a; Abati et al., 2010) (Fig. 13A). This geochemical variation may reflect a single geodynamic event. Specifically, during the evolution of a back-arc basin, the earliest magmas generated often exhibit magmatic arc characteristics due to the proximity of the back-arc to the arc itself. As the back-arc basin evolves and the magma source becomes further removed from the metasomatised mantle, the magmas acquire within-plate geochemical signatures (Vasey et al., 2021; Saunders and Tarney, 1984). Overall, basaltic magmatism in the Saghro Group fits this evolutionary framework. For instance, calc-alkaline basalts from the Sirwa inlier (Thomas et al., 2002; This study), reflect initial stages in back-arc formation. Conversely, and higher in the stratigraphy; IRT, OIB, and MORB-type basalts indicate later stages in back-arc evolution. This interpretation is consistent with sediment geochemistry suggesting back-arc basin deposition (Ouguir et al., 1996). Furthermore, this scenario aligns with the paleogeographic position of the Anti-Atlas during the Ediacaran. During that time, the Anti-Atlas region was dissected in a northward direction (present coordinates) due to south-dipping Cadomian subduction (Fig. 13) (Rojo-Pérez et al., 2024; Stern, 2024; Errami et al., 2021a; Linneman et al., 2014).

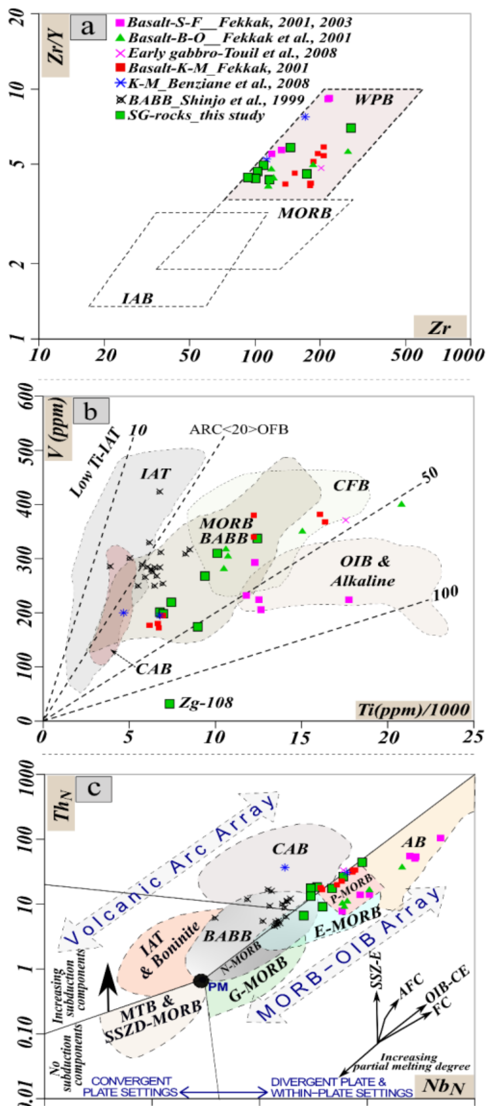
a
Basalt-S-F__Fekkak, 2001, 2003
Basalt-B-O__Fekkak et al., 2001
Early gabbro-Touil et al., 2008
Basalt-K-M_Fekkak, 2001
K-M_Benziane et al., 2008
BABB_Shinjo et al., 1999
SG-rocks_this study
Zr/Y
WPB
MORB
IAB
Zr
b
V (ppm)
Low Ti-IAT
10
ARC<20>OFB
IAT
CFB
50
MORB
BABB
OIB &
Alkaline
100
CAB
Zg-108
Ti(ppm)/1000
c
Th$_N$
Volcanic Arc Array
CAB
AB
P-MORB
E-MORB
BABB
IAT & Boninite
N-MORB
G-MORB
PM
MTB & SSZD-MORB
MORB-OIB Array
SSZ-E
AFC
OIB-CE
FC
Increasing subduction components
No subduction components
Increasing partial melting degree
CONVERGENT PLATE SETTINGS
DIVERGENT PLATE & WITHIN-PLATE SETTINGS
Nb$_N$

Figure 11: Saghro Group: (a) Zr/Y vs Zr plot for basalts of SG (Pearce and Norry, 1979). (b) V vs Ti/1000 plot (Shervais, 1982). (c) plot of Th_N vs Nb_N ratios (Saccani, 2015). Abbreviations: B-O : Boumalne; K-M: Kelâat M'gouna; S-F: Sidi Flah; BABB: Back-arc basin basalts.

5.2.2 The Ouarzazate Group

On the tectonic discrimination diagrams (Fig. 12b-c), the Ouarzazate Group rocks display geochemical characteristics ranging from dominating within-plate to minor active continental margins (oceanic island arcs). Plus, the high Th/Yb ratios > 1 for all rocks refer to a metasomatised mantle source in subduction zone and/or crustal contamination. All in all, the whole accounts for a post-collisional setting (Fig. 12c), involving partial melting of a pre-existing lithospheric source, either a mantle or crust. Hence, controlling the recharge in K_2O and LILE (e.g. Rb, Ba) contents for the majority of our samples (Fig. 11a). Additionally, the alkali-calcic to high-K calc-alkaline signature of our samples is in fact typical to post-collisional events (Liégeois et al., 1998, and reference therein).

The Ediacaran magmatism of the Ouarzazate Group is still debated as being fully post-collisional and linked to asthenospheric rise (upwelling) beneath the WAC during its metacratonic evolution (Belkacim et al., 2017; Gasquet et al., 2008, 2005; Liégeois et al., 2006; Thomas et al., 2002), or related to subduction (Walsh et al., 2012; Benziane, 2007; El Baghdadi et al., 2003), or even representing the Iapetus Ocean opening with ties to the Ediacaran Central Iapetus Magmatic Province (CIMP; Youbi et al., 2020). Nonetheless, subduction-related features can arise in a non-subduction settings without coeval subduction (Morris et al., 2000; M'arquez et al., 1999; Cousens, 1996; Hooper et al., 1995).

Regional correlations with similar magmatism lead us to attribute the Ouarzazate Group to a post-collisional event also exemplified in numerous inliers of the Anti-Atlas (Fig. 13C-D) (Yajioui et al., 2020; Karaoui et al., 2015; Linneman et al., 2014; Toummite et al., 2013; Walsh et al., 2012; Gasquet et al., 2005, 2004; Thomas et al., 2002).

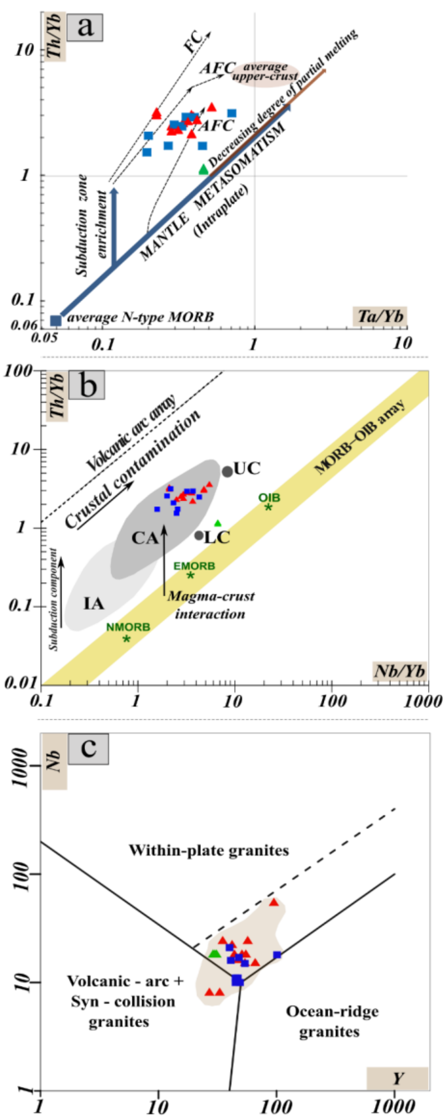
a
Th/Yb
FC
AFC
average upper-crust
Decreasing degree of partial melting
AFC
MANTLE METASOMATISM (Intraplate)
Subduction zone enrichment
average N-type MORB
Ta/Yb
b
Th/Yb
Volcanic arc array
Crustal contamination
UC
MORB-OIB array
OIB
CA
LC
EMORB
IA
Magma-crust interaction
NMORB
Subduction component
Nb/Yb
c
Nb
Within-plate granites
Volcanic - arc + Syn - collision granites
Ocean-ridge granites
Y

Figure 12: (a) Th/Yb vs Ta/Yb plot for OG rocks. (b) Nb/Yb vs Th/Yb diagram of Pearce, (2008). (c) Nb versus Y diagram (Pearce et al., 1984) depicting evolution from volcanic arc granite to within-plate granite.

5.34 Significance of LA-ICP-MS U-Pb data

5.43.12 The Saghro GroupSG detrital age: depositional style and material source

Whether or not the Paleoproterozoic basement exists in the Sirwa massif north of the AAMF, and by consequence the northern margin of the WAC is still debated (Ennih and Liégeois, 2008). Outcrops of this Paleoproterozoic basement have been regarded as being present exclusively in the westernmost part of the Anti-Atlas belt (Choubert, 1963). However, new studies based on TDM ages support the hypothesis that Paleoproterozoic rocks may also be found in both the Central and Eastern segments of the Anti-Atlas (Baidada et al., 2019; Blein et al., 2014; Toummite et al., 2013; Liégeois et al., 2013; Abati et al., 2010; Gasquet et al., 2008; Thomas et al., 2002). Moreover, this hypothesis can be extended to Western Meseta (Pereira et al., 2015, and references therein; Tahiri et al., 2010; Baudin et al., 2003).

During the last decade, the northern boundary of the WAC is considered to be marked by the northernmost outcrops of highly deformed rocks in the southern part of the Bou-Azzer inlier, particularly the Tazagzaout migmatites and gneisses, based on similarities in lithology and deformation degree with the Zenaga Complex in the Western Anti-Atlas (Leblanc and Lancelot, 1980). However, this view has been changed owing to the new U-Pb precision dating obtained from the Tazagzaout gneisses (752 ± $^{+}_{2}$ Ma; D'Lemos et al., (2006), and the Oumlil granite 741 ± 9 Ma; El Hadi et al., (2010)). Furthermore, the positive Nd values of (+ 4.9 to + 6) for the Tazagzaout Complex refer to a juvenile depleted mantle source, not akin to the 2 Ga Eburnean WAC basement (D'Lemos et al., 2006). Consequently, the presence of a WAC basement beneath the Central Anti-Atlas, especially in the Sirwa massif is not clear. Published geochronological data indicate that both the Saghro and Bou Salda groups were deposited approximately 630 to 610 Ma. This deposition occurred during a period of tectonic convergence of the Cadomian arc upon the WAC Iriri-Tazagzaout Complex (Errami et al., 2021a; Walsh et al., 2012; El Hadi et al., 2010). Yet, the precise location of the suture zone marking this collision remains ambiguous. Current interpretations suggest the suture likely corresponds to the Anti-Atlas Major Fault (AAMF) (Hefferan et al., 2014), potentially extending north along the South Atlas Fault (SAF) (Ennih and Liégeois, 2001, 2008).

The existence of a Paleoproterozoic basement in the Sirwa massif and the northern margin of the WAC is debated (Ennih and Liégeois, 2008). While traditionally thought to be confined to the Western Anti-Atlas (Choubert, 1963), recent studies suggest Paleoproterozoic rocks may also be present in the Central and Eastern Anti-Atlas and the Western Meseta (Liégeois et al., 2013; Abati et al., 2010; Gasquet et al., 2008; Pereira et al., 2015, and references therein; Blein et al., 2014). Historically, the WAC's northern boundary was defined by the deformed Tazagzaout migmatites and gneisses in the Bou-Azzer inlier (Leblanc and Lancelot, 1980). However, new U-Pb dating of the Tazagzaout gneisses (752 ± 2 Ma; D'Lemos et al., (2006) and the Oumlil granite (741 ± 9 Ma; El Hadi et al., (2010)) coupled with juvenile Nd signatures (D'Lemos et al., 2006), indicates a juvenile depleted mantle source, not akin to the 2 Ga Eburnean WAC basement.

Commenté [CM16]: This paragraph has been rephrased and shortened based on the comments from Reviewer 2.

Detrital zircon age from our study provides new insights into the basement beneath the Sirwa massif. Sample (Zg-132) from the Imghi Formation of the Saghro Group returned exclusively Paleoproterozoic ages, with a prominent peak at ca. 2100 Ma (Fig. 4-3). Interestingly, no ages younger than 1600 Ma were found in our sample, nor were any zircons dating to the local Pan-African magmatic period in the Anti-Atlas identified. These 883 - 640 Ma Pan-African younger zircons, which are common in outcrops of the Sirwa inlier and have been consistently reported in Saghro Group sediments (Letsch et al., 2018; Abati et al., 2010) are absent in our sample. Indeed, this Paleoproterozoic peak goes in line with the inherited signature from the analyzed zircon population of sediments of the Saghro and Bou Salda groups from the Sirwa massif, for which the obtained maximum depositional ages cluster around 620 – 610 Ma (Abati et al., 2010). Arguably, the authors argued in favor of an exposure of cratonic basement (Paleoproterozoic ?) based on the relatively high proportion of the 610 Ma zircons in regard to Paleoproterozoic zircons in the upper levels of the stratigraphy sequence. Therefore, this suggests that the source of the 610 Ma was eroded favoring the enrichment in Paleoproterozoic ages. Admittedly, the subsequent erosion of the underlying Neoproterozoic rocks (notably synchronous magmatic rocks, and Saghro and Bou Salda groups) might be the source for the prominent 610 Ma peak in the Iberian massif (Chichorro et al., 2022); (Fig. 13A).

The mono-peak at 2.1 Ga can only be accepted to strictly represent Paleoproterozoic. It can be interpreted as representing the material source for the Saghro Group sedimentary units only in the study area (Fig. 13A). Indeed, the returned mono zircon population may reflect insufficient sampling of detrital zircons. However, the number of analyzed zircons (up to 139; see supplementary table 5) is considered adequate to address paleogeographic questions and sediment source areas. In this context, we interpret the Paleoproterozoic mono-peak in our sample to reflect local exposure of Paleoproterozoic basement rocks along the basin margins of the Saghro Group in the study area (Fig. 13A). Consequently, most sediments were derived exclusively from the erosion of these basement rocks in a possible mono Paleoproterozoic paleo-relief without interaction with Cryogenian sediments.

Overall, this evidence argues that during Ediacaran times, the Paleoproterozoic basement was in fact totally or locally exposed in the Sirwa inlier (Fig. 13A). This interpretation is further corroborated by Nd model ages of Ediacaran magmatism from this study (see section Sm-Nd), which yield TDM age of Mesoproterozoic values, indicating a mixing/recycling of older Paleoproterozoic crust with juvenile Ediacaran magma. All in all, and based on these findings, the WAC crust extends beneath the Sirwa massif and likely continues northward far beyond the Anti-Atlas belt. Notably, Paleoproterozoic rhyolites have been reported in the Meseta Block, north of the Anti-Atlas, with a given age of 2050.6 ± 3 Ma (Pereira et al., 2015). These findings do support the extension of the WAC Paleoproterozoic crust northward beyond the AAMF, which was previously considered the northern margin of the craton.

Detrital zircons sourced from the Saghro Group sediments furnishes novel evidence concerning the nature of the underlying basement within the Sirwa massif. The returned 2.1 Ga age mono-peak indicates localized exhumation and exposure of Paleoproterozoic basement lithologies along the Saghro Group basin margins, with no interaction with Cryogenian sediments. These findings substantiate the hypothesis that the Paleoproterozoic crust extends in a northward direction, beyond the Anti-

Atlas Major Fault (AAMF), thereby suggesting that the definitive suture zone may project significantly further to the north, aligning potentially with the South Atlas Fault (SAF).

According to Thomas et al. (2002), the Imghi Formation represents the lower thick beds of greywacke/turbiditic section of SG, and seems to represent a typical flysch succession, which is interpreted as the primary sedimentary fill of a back-arc basin associated with the Khzama ophiolite Complex. For the Zg-132, the alternating patterns (Fig. 3e) suggest fluctuating depositional conditions, specifically changes in hydrodynamic energy and the amount of clay input, consistent with a low-energy, suspension-dominated sedimentation typical of distal turbidites or quiet shallow-marine environment. The calculated MDA at 2025 Ma (n= 3; MSWD = 1.4; Fig. 5A-1) is similar to the ages of syn-to-post-tectonic Eburnean granites in the Central and Western Anti-Atlas (Gasquet et al., 2008, 2005; Aït Malek et al., 1998). Moreover, the detrital zircon age distribution is characterized by a prominent population peaking at ca. 2100 Ma (Fig. 5A-2), reflecting a dominant provenance from the Eburnean-aged basement of the WAC (O'Connor et al., 2010; Gasquet et al., 2008, 2005; Thomas et al., 2002). This primary pulse, coupled with a single Paleo-Archean grain at 3700 Ma, indicates the recycling of ancient cratonic material (Fig. 5A-2). Interestingly, no ages younger than 1600 Ma were found in our sample. In particular 883–640 Ma Pan-African zircons, which are common in outcrops of the Sirwa inlier and have been consistently reported in SG sediments (Letsch et al., 2018; Abati et al., 2010), are absent. Such a narrow gap between the 2100 Ma peak and the 2025 MDA suggests that sedimentation occurred in a basin directly overlaid or adjacent to an uplifted, pristine block of Paleoproterozoic Eburnean basement that acted as the exclusive sediment source without interaction with Ediacaran sediments. Indeed, the returned age may reflect insufficient sampling of detrital zircons. However, the number of analyzed zircons (up to 138; see supplementary table 2) is considered adequate to address paleogeographic questions and sediment source areas (Vermeesch, 2004). Based on these findings, the WAC crust likely extends beneath the Sirwa massif and continues northward far beyond the Anti-Atlas belt. Notably, Paleoproterozoic rhyolites have been reported in the Meseta Block, north of the Anti-Atlas, with a magmatic age of 2050.6 ± 3 Ma (Pereira et al., 2015). These findings do support the presence of the WAC Paleoproterozoic crust northward beyond the AAMF.

Commenté [CM17]: This chapter is completely rewritten based on recommendations from reviewer 2. We have calculated the maximum depositional age, reproduced the zircon images for quality and visibility purposes, and correct the interpretations accordingly.

5.43.21 U-Pb zircon age Magmatic record on magmatic rocks of the OG

Reliable Nnew U-Pb zircon datingages on two magmatic samples (rhyolite Zg-106, and granite Zg-119; Fig. 54), representing the Ouarzazate GroupOG from the Sirwa massif returned ages of 575 ± 3 Ma and the 564 ± 2 Ma, respectively. These ages are consistent with a lower Ouarzazate Group OG affinity, and represent the extension expression of the Ediacaran magmatism previously described in numerous inliers of the Anti-Atlas belt (Yajioui et al., 2020; Karaoui et al., 2015; Hefferan et al., 2014, and references therein; Toummite et al., 2013; Walsh et al., 2012; Gasquet et al., 2005, 2004; Thomas et al., 2002).
Indeed, in the Zgounder Mine RegionZGMR, similar volcanic activity of this type can be bracketed between 620 Ma to 550 Ma (Pelleter et al., 2016; Thomas et al., 2002; This study). For the rhyolite (Zg-106); Pelleter et al., (2016) reported mean age of 578 ± 4 Ma from the Zgounder Mine for the rhyolitic dikes and plugs using the $^{207}Pb/^{206}Pb$ ages. Moreover, in the Sirwa massif, similar U–Pb ages of 579 ± 7 Ma, 571 ± 8 Ma, 577 ± 6 Ma, 579 ± 7, and 575 ± 8 Ma were obtainedproposed for the

Tourcht diorite, the Tikhfist rhyolite (Tiouin Subgroup, Fig. 1C), the Aguins member (Tafrant Subgroup), the Tilsakht granite, and the Askaoun granodiorite, respectively (Thomas et al., 2002). Given that the 575 ± 3 Ma age of our rhyolite is ~~analytically~~ identical within error~~s~~ to the ages of these rocks, ~~thus inferring~~ a rapid sequence of intrusive events ~~that~~ had to occur~~red~~ within a ~~span of a~~ few million years.

For the granite sample (Zg-119); the obtained age of 564 ± 2 Ma is also identical within a margin of error to the ages of the neighbouring Imourkhssen granite dated respectively at 561 ± 3 Ma, ~~and~~ 562 ± 5 Ma, and 558 ± 1 Ma by Toummite et al.~~,~~ (2013), ~~and~~ Thomas et al.~~,~~ (2002), and Ferraq et al. (2024) (Fig. 1C). The Imourkhssen granite ~~on its turn~~ intrudes the lower and older part of the ~~Ouarzazate Group~~OG in the Sirwa massif (Thomas et al., 2002). Additionally, in the Sirwa massif, numerous syn- to late-~~Ouarzazate Group~~OG granites ~~with a sub-alkaline-calcic composition~~ provided ages of c. 560 Ma, making them the Ouarzazate Group's youngest components (Thomas et al., 2002). According to Thomas et al.~~,~~ (2002), these granites belong to the Achkoukchi Complex (Fig. 1C), and grouped into the Amassine Suite (e.g., Bou-Tazart, Aït Nabdas, and Tikitar granites, and the Tazoult Quartz-porphyry at 559 ± 6 Ma). The inherited age of 2156 ± 54 Ma in sample Zg-119 indicates a Paleoproterozoic crustal component, confirming the reworking of ancient Eburnean basement during the genesis of the OG. This result aligns with s~~S~~ignificant inherited Paleoproterozoic zircon population ~~are previously~~ reported for the ~~Ouarzazate Group~~OG rocks ~~all over~~across the Anti-Atlas. For instance, Baidada et al.~~,~~ (2019) reported ~~inherited~~ Paleoproterozoic signature for the Saghro massif granitoids~~.~~, while Blein et al.~~,~~ (2014b) and Thomas et al. (2002) documented similar inheritance in OG ignimbrites from the Agadir Melloul area and syn-extensional granites in the Sirwa massif, respectively.~~proved the existence of Paleoproterozoic inherited zircon in ignimbrite of the Ouarzazate Group in the Agadir Melloul area. Finally, Thomas et al., (2002) highlighted Paleoproterozoic inherited zircons in syn-Ouarzazate Group granites in the Sirwa massif.~~

~~Indeed, the Ouarzazate Group's thick successions of volcano-sedimentary series are dominated by acidic and intermediate high-K calc-alkaline to shoshonitic volcanism (Blein et al., 2014b; Toummite et al., 2013; Walsh et al., 2012; Gasquet et al., 2008, 2005; Benziane, 2007; Thomas et al., 2004; El Baghdadi et al., 2003). Their depositional environment as pull-apart basins with strike-slip faulting conditions and sub-vertical movements favored a high variability in thickness (Walsh et al., 2012, and references therein). Nevertheless, a contemporaneous magmatic activity spanned the 630 to 538 Ma time frame; (Table 1 in Hefferan et al., (2014) for reported precision ages from selected inliers of the Anti-Atlas Mountains). All in all, this activity indicates a prolonged tectono-magmatic event emplaced over multiple pulses over the whole Anti-Atlas belt (Tuduri et al., 2018). In regard to this, Schulte et al., (2022), considered the Ouarzazate Group in the Central and Eastern Anti-Atlas as the relicts of an Ediacaran silicic large igneous province (SLIP) deposited in a strictly continental environment. These huge volumes of mostly felsic magma were emplaced by multiple pulses and occur as a result of a long-lived magmatic event evolving from high-K calc-alkaline at 575–550 Ma to alkaline affinity at 550–540 Ma (Schulte et al., 2022; Blein et al., 2014b; Gasquet et al., 2008). This magmatism is considered to belong to a continental silicic large igneous province (SLIP), referred to as the Ouarzazate Silicic Large Igneous Province (OSLIP), and emplaced over multiple periods at ca. 575 Ma, ca. 560 Ma, and ca. 550 Ma (Tuduri et al., 2018; Blein et al., 2014b). Consequently, the last two pulses at the final stage of the Pan-African~~

Commenté [CM18]: This paragraph has been fused into the new following paragraph on Further discussions (5.5) orogeny (560 to 550 Ma) appear linked to widespread pervasive hydrothermal activity across the whole Anti-Atlas (Tuduri et al., 2018). Regional correlations can be drawn to the extent of the Cadomian orogeny (Linnemann et al., 2014, and references therein). Hence, our samples fall within the age range of 580 to 550 Ma of the Cadomian arc magmatism extended to Iberia (Chichorro et al., 2022, and references therein).

5.5 Further discussions

At a regional scale, basaltic flows have been described as interbedded within the sediments of the SG in the Saghro massif (Errami et al., 2009; Fekkak et al., 2003, 2001). They exhibit diverse geochemical signatures. For a start, the basalts in Sidi Flah (SF) are of Initial Rift Tholeiites (IRT) and Ocean Island Basalts (OIB) character (Fekkak et al., 2001). In contrast, the Anou N'Izem basalts in the Boumalne (BO) inlier possess typical Mid-Ocean Ridge Basalt (MORB) signatures (Errami et al., 2009). U-Pb dating of detrital zircons from the SG in various inliers suggests that this unit was deposited between 640–600 Ma across the entire Central-Eastern Anti-Atlas region (Errami et al., 2021a; Abati et al., 2010).

In liaison, this geochemical variation within the SG likely reflects a single, continuous geodynamic event. Specifically, during the evolution of a back-arc basin, the earliest magmas often exhibit magmatic arc characteristics due to the proximity of the back-arc to the arc itself. As the back-arc matures and the magma source becomes further removed from the metasomatized mantle, the magmas transition toward within-plate (OIB) and MORB-like signatures (Vasey et al., 2021; Saunders and Tarney, 1984). This interpretation is further supported by sediment geochemistry which points toward a back-arc basin depositional environment (Ouguir et al., 1996). In the Anti-Atlas, this footprint is widely ascribed to the activation of a sub continental lithospheric mantle source previously metasomatized during earlier Cryogenian Pan-African subduction events, operating in tandem with distal stress fields from the emerging Cadomian orogenic system (Hefferan et al., 2014). As the basin matured and lithospheric extension advanced, the magma source increasingly tapped deeper, uncontaminated asthenospheric reservoirs, driving a compositional transition toward within-plate (OIB) and MORB-like signatures higher up the stratigraphy. Basaltic magmatism in the SG fits this evolutionary framework: the calc-alkaline basalts from the Sirwa inlier (Thomas et al., 2002; this study) represent the initial stages of back-arc formation, and record the activation of this strongly metasomatized mantle source. Whereas the IRT, OIB, and MORB-type basalts found higher in the stratigraphy indicate a more mature, extensional stage tapping deeper, uncontaminated asthenospheric reservoirs.

The thick volcano-sedimentary successions of the OG are dominated by silicic and intermediate high-K calc-alkaline to shoshonitic volcanism (Blein et al., 2014b; Toummite et al., 2013; Walsh et al., 2012; Gasquet et al., 2008, 2005; Benziane, 2007; Thomas et al., 2004; El Baghdadi et al., 2003). Based on the findings of this study, and regional correlations with similar magmatism (see Table 1 in Hefferan et al. (2014) for reported precise ages from selected inliers of the Anti-Atlas Mountains), we attribute the OG rocks to a widespread post-collisional event exemplified across numerous inliers of the Anti-Atlas (Yajioui et al., 2020; Karaoui et al., 2015; Linnemann et al., 2014; Toummite et al., 2013; Walsh et al., 2012; Gasquet et al., 2005, 2004; Thomas et al., 2002). For the studied OG rocks, high Th/Nb ratios suggest that slab break-off induced a thermal pulse supplying heat to melt the Lower Continental Crust (LCC), with variable input from the metasomatized mantle wedge previously primed during proceeding subduction phase. Moreover, the clustering near and above the Upper Continental Crust (UCC) indicates that lithospheric delamination provided the necessary thermal energy to trigger widespread crustal melting, leading to high-K and shoshonitic signatures of the OG rocks (Bonin, 2004). This period of magmatism was coeval with a Silicic Large Igneous Province (SLIP) recognized all over the Anti-Atlas (Ousbih et al., 2024, and references therein; Schulte et al., 2022).

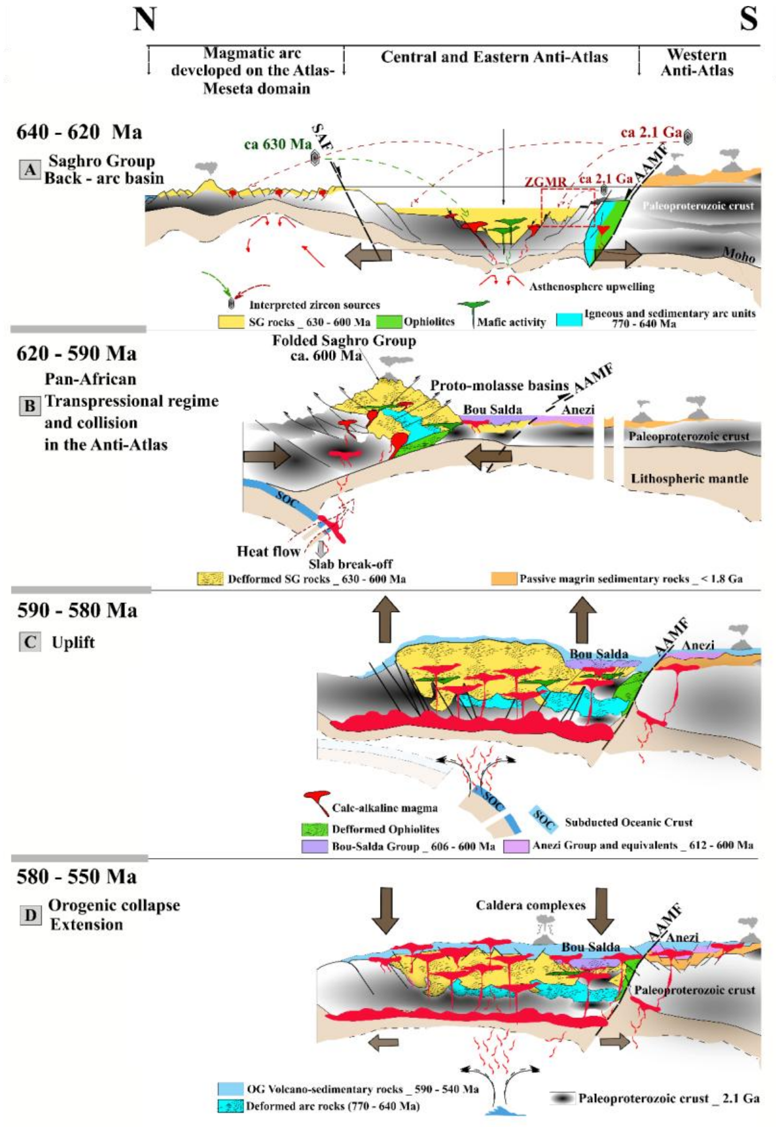
N
S
Magmatic arc developed on the Atlas-Meseta domain
Central and Eastern Anti-Atlas
Western Anti-Atlas
640 - 620 Ma
A Saghro Group Back - arc basin
ca 630 Ma
SAF
ca 2.1 Ga
ZGMR
ca 2.1 Ga
AAMF
Paleoproterozoic crust
Moho
Asthenosphere upwelling
Interpreted zircon sources
SG rocks _ 630 - 600 Ma
Ophiolites
Mafic activity
Igneous and sedimentary arc units 770 - 640 Ma
620 - 590 Ma
B Pan-African Transpressional regime and collision in the Anti-Atlas
Folded Saghro Group ca. 600 Ma
Proto-molasse basins
AAMF
Bou Salda
Anezi
Paleoproterozoic crust
Lithospheric mantle
SOC
Heat flow
Slab break-off
Defformed SG rocks _ 630 - 600 Ma
Passive magrin sedimentary rocks _ < 1.8 Ga
590 - 580 Ma
C Uplift
Bou Salda
AAMF
Anezi
SOC
Calc-alkaline magma
Defformed Ophiolites
Subducted Oceanic Crust
Bou-Salda Group _ 606 - 600 Ma
Anezi Group and equivalents _ 612 - 600 Ma
580 - 550 Ma
D Orogenic collapse Extension
Caldera complexes
Bou Salda
AAMF
Anezi
Paleoproterozoic crust
OG Volcano-sedimentary rocks _ 590 - 540 Ma
Deformed arc rocks (770 - 640 Ma)
Paleoproterozoic crust _ 2.1 Ga

Figure 13: Reconstruction of the geotectonic setting of Saghro Group and Ouarzazate Group during Ediacaran times. (resembled and modified after El Kabouri et al., 2025; Chichorro et al., 2022; Errami et al., 2021a; Abati et al., 2010; Thomas et al., 2002). (A): Saghro Group deposition in a back-arc basin (This study; Ouguir et al., 1996), implying local exposure of the 2.1 Ga Paleoproterozoic crust in the Zgounder Mine Region (This study). (B): Pan-African transpressional regime and collision in the Anti-Atlas, resulting in Saghro Group folding, injection of the 600 Ma calc-alkaline magma (Errami et al., 2021a), and proto molasses basin formation (Thomas et al., 2002). (C): General uplift in the Anti-Atlas. (D): Orogenic collapse favoring the thick Ouarzazate Group sedimentation (e.g. post-tectonic molasse deposition and calc-alkaline magmatism, with coeval acidic rocks).

Commenté [CM19]: We have decided to remove Fig. 13, based on the new interpretations of our data.

6 Conclusions

In the light of the above, the following conclusions can be drawn:

i. LA-ICP-MS U-Pb zircon ages of 575 ± 3 Ma and 564 ± 2 Ma of the OG evidence an expression of a post-collisional syn-orogenic magmatism in the ZGMR. They define a highly rapid sequence of felsic intrusive and extrusive events spanning roughly 11 million years. Detrital zircons from the SG reveal a single-population at ca. 2100 Ma and a MDA of 2025 Ma. This total absence of younger Neoproterozoic/Pan-African zircons demonstrates exclusive sediment derivation from an adjacent, uplifted pristine block of Eburnean basement, confirming the northern extension of the WAC further north of the AAMF.

i. ii. Based on geochemical proxies (major and trace elements), the Saghro Group SG magmatic rocks were emplaced at the early stages of back-arc basin opening, testified by their calc-alkaline affinity, geochemical characteristics and regional correlations. They were derived from contaminated mantle source with an old continental crust. Further, their εNd_{620} εNd (at 620 Ma) = +-3.2 toand +-4.65, and TDM ages of 1.02 and 0.91 Ga 1431 – 1197 Ma reflects a mixed origin, combining mostly mantle-derived magma with limited contribution fromproportion of older crustal material. Thus admitting the existence of an old Paleoproterozoic to even Mesoproterozoic, crust beneathunder the Saghro Group.exhibit both active continental margins and within-plate characteristics. A dual signature characteristic of magmas generated during back-arc extension. Therefore, the recognized subduction-related signature on our samples is acquired through mantle metasomatism by sediment-derived components during arc activity, while the within-plate signature emerges later during back-arc extension processes.

ii. iii. The Saghro Group rocks were emplaced at the early stages of back-arc basin opening, testified by their calc-alkaline affinity, geochemical characteristics and regional correlations. They were derived from contaminated mantle source with an old continental crust. Further, their εNd (at 620 Ma) = + 3.2 to + 4.5, and TDM ages of 1431 – 1197 Ma reflects a mixed origin, combining mostly mantle-derived magma with limited proportion of older crustal material. Thus admitting the existence of an old Paleoproterozoic to even Mesoproterozoic crust under the Saghro Group.

iv. For the Ouarzazate GroupOG magmatic rocks, the evolution in chemical compositions for the suite of high-K calc-alkaline to shoshonitic rocks is was controlled in the most part by fractional crystallization and crustal contamination. They were deposited in a post-collisional setting, and their primary parental magma was sourced from an enriched continental lithospheric mantle, previously underwent metasomatism by fluids from former Neoproterozoic subduction. Further, their εNd_{570} εNd (at 570 Ma) = - -0.98 to +-1.1, and TDM ages of 1526 to 1252 Ma 1.30 to 1.15

Ga imply significant reworking of older, evolved ~~refer to a Mesoproterozoic (and Paleoproterozoic) affinity, implying recycling of~~ Paleoproterozoic continental crustal material during Ediacaran times.

v. Investigation of the OG magmatic rocks within the ZGMR provides insights into how lithospheric delamination and potential slab break-off drove the petrogenesis of post-collisional magmatism, related to the formation of the late Neoproterozoic SLIP along the northwestern edge of the WAC.

~~iii. LA-ICP-MS U-Pb zircon ages on magmatic rocks evince an expression of a post-collisional syn-orogenic magmatism (WACadomian arc), during the emplacement of its first and second pulses at ca. 575 to 560 Ma. This period of magmatism is concordant with a Silicic Large Igneous Province (SLIP) recognized all over the Anti-Atlas.~~

~~iv. The sediment source for the sedimentary succession (Imghi Formation) was sourced from a strictly 2.1 Ga Paleoproterozoic, without interaction with Cryogenian sediments. Thus, implying local exposure of Paleoproterozoic crust in the Sirwa massif, far to the north of the AAMF.~~

Code, data, or code and data availability

Data used in this paper is given in electronic supplements~~will be made available upon request~~.

Supplement link

Author contributions

Abdelhay Ben-Tami: Field work, Sampling and preparation, Thin-sections preparation, Investigation, Data visualization, Data curation, Formal analysis, Writing of original draft, Finalization. **Said Belkacim:** Supervision, Resources, Writing - review and editing. **Jamal El Kabouri:** Data visualization, Writing of original draft. Review and editing. **Joshua H.F.L. Davies and Morgann G. Perrot:** LA-ICP-MS U-Pb data and methodology, writing of original draft, review and editing. **Mariam Ferraq**: Data curation and visualization. **Mohamed Bouabdellah:** review and editing. **Bouchra Baidada, Mohamed Bhilisse** and **Mohamed Assalmi:** Resources, accommodation, field trips, hosting. ~~**David Lalonde:** Resources, Financing, Collaboration. Review, and validation.~~

Competing interests

The authors declare that they have no conflict of interest. Corresponding author (Abdelhay Ben-Tami), discloses an employment relationship with the Zgounder Millenium Silver Mining Company (ZMSM).

Disclaimer

Copernicus Publications remains neutral with regard to jurisdictional claims made in the text, published maps, institutional affiliations, or any other geographical representation in this paper. While Copernicus Publications makes every effort to include appropriate place names, the final responsibility lies with the authors. Views expressed in the text are those of the authors and do not necessarily reflect the views of the publisher.

Acknowledgements

This research represents a component of the corresponding author's thesis project. The authors express their sincere gratitude to the **Zgounder Millenium Silver Mining Company (ZMSM)**, the Moroccan subsidiary of **Aya Gold and Silver (AYA)**, for their essential financial support for this study, as well as for providing accommodation and logistical assistance. Special appreciation is extended to the Exploration geology team at the Zgounder Mine for their valuable facilitation and support during field operations. Official permission to publish this work was granted by **David Lalonde, P. Geo / VP Exploration / Aya Gold and Silver Inc.** ~~Finally, the authors wish to thank the anonymous referees for their constructive feedback and suggestions, which significantly enhanced the quality of this manuscript.~~

Financial support

Financial support for the Whole-rock analysis, Sm-Nd isotopes, U-Pb on zircon, fieldwork and accommodation was guaranteed by the **Zgounder Millenium Silver Mining company (ZMSM)**~~; the Moroccan branch of **Aya Gold and Silver Inc**~~.

Review statement

References

Abati, J., Aghzer, A. M., Gerdes, A., & Ennih, N.: Detrital zircon ages of Neoproterozoic sequences of the Moroccan Anti-Atlas belt. Precambrian Research, 181(1-4), 115–128, https://doi:10.1016/j.precamres.2010.05.018, 2010.

Admou, H., Fekkak, A., Razin, P., Egal, E., Youbi, N., Soulaimani, A., Blein, O., Baudin, T., Chevremont, P.: Carte géologique Maroc (1/50 000), feuille d'Aït Ahmane– Notes et Mémoires Service Géologique Maroc, no. 533, 2012.

~~Ait Lahna, A., Youbi, N., Tassinari, C.C.G., Basei, M.A.S., Ernst, R.E., Chaib, L., Barzouk, A., Mata, J., G¨artner, A., Admou, H., Boumehdi, M.A., S¨oderlund, U., Bensalah, M.K., Bodinier, J.L., Maacha, L., Bekker, A.: Revised stratigraphic framework for the lower Anti-Atlas supergroup based on U–Pb geochronology of magmatic and detrital zircons (Zenaga and Bou Azzer-El Graara inliers, Anti-Atlas Belt, Morocco). Journal of African Earth Sciences. 171, 103946, https://doi.org/10.1016/j.jafrearsci.2020.103946, 2020.~~

Aït Malek, A., Gasquet, D., Bertrand, J.M., Leterrier, J. : Géochronologie U-Pb sur zircon de granitoïdes éburnéens et panafricains dans les boutonnières protérozoïques d'Igherm, du Kerdous et du Bas Drâa (Anti-Atlas occidental, Maroc). Comptes. Rendus. l'Académie des Sciences-Series. IIA–Earth and Planetary Science. 327 (12), 819–826, https://doi.org/10.1016/S1251-8050(99)80056-1, 1998.

Aldanmaz, E., Yaliniz, M. K., Guctekin, A., & Goncuoglu, M. C.: Geochemical characteristics of mafic lavas from the Neotethyan ophiolites in western Turkey: implications for heterogeneous source contribution during variable stages of ocean crust generation. Geological Magazine, 145(1), 37-54, https://doi.org/10.1017/S0016756807003986, 2008.

Álvaro, J.J., Benziane, F., Thomas, R., Walsh, G.J., Yazidi, A.: Neoproterozoic–Cambrian stratigraphic framework of the Anti–Atlas and Ouzellagh promontory (High Atlas), Morocco. Journal of African Earth Sciences. 98, 19–33, https://doi.org/10.1016/j.jafrearsci.2014.04.026, 2014.

Álvaro, J. J., Pouclet, A., Ezzouhairi, H., Soulaimani, A., Bouougri, E. H., Imaz, A. G., and Fekkak, A.: Early Neoproterozoic rift-related magmatism in the Anti-Atlas margin of the West African craton, Morocco. Precambrian Research, 255, 433-442, https://doi.org/10.1016/j.precamres.2014.10.008, 2014b.

Baidada, B., Ikenne, M., Barbey, P., Soulaimani, A., Cousens, B., Haissen, F., Ilmen, Said, Alansari, A.: SHRIMP U–Pb zircon geochronology of the granitoids of the Imiter Inlier: constraints on the Pan-African events in the Saghro massif, Anti-Atlas (Morocco). Journal of African Earth Sciences. 150, 799–810, https://doi.org/10.1016/j. jafrearsci.2018.10.008, 2019.

~~Baidada, B., Cousens, B., Alansari, A., Soulaimani, A., Barbey, P., Ilmen, S., & Ikenne, M.: Geochemistry and Sm–Nd isotopic composition of the Imiter Pan-African granitoids (Saghro massif, eastern Anti-Atlas, Morocco): Geotectonic implications. Journal of African Earth Sciences, 127, 99–112, https://doi:10.1016/j.jafrearsci.2016.08.016, 2017.~~

Bajja, A.: Volcanisme syn à post orogénique du Néoprotérozoïque de l'Anti-Atlas: implications pétrogénétiques et géodynamiques. In: de Wall H., Greiling R.P. (Eds.), Magmatic Evolution of a Neoproterozoic Island-Arc Syn- to Postorogenic Igneous Activity in the Anti-Atlas (Morocco). Forschunszentrum Jülich Gmbh 45, pp. 9–228, 2001.

~~Barbey, P., Nachit, H., and Pons, J.: Magma–host interactions during differentiation and emplacement of a shallow-level, zoned granitic pluton (Tarçouate pluton, Morocco): implications for magma emplacement. Lithos, 58(3-4), 125-143, https://doi.org/10.1016/S0024-4937(01)00053-6, 2001.~~

~~Baudin, T., Chèvremont, P., Razin, P., Youbi, N., Andries, D., Hœpffner, C., and Tegyey, M.: Carte géologique du Maroc au 1/50 000, feuille de Skhour des Rehamna, Mémoire explicatif. Notes Mémoires Services Géologiques. Maroc, 435, 114, 2003.~~

~~Belkacim, S., Gasquet, D., Liégeois, J. P., Arai, S., Gahlan, H. A., Ahmed, H., Ikenne, M.: The Ediacaran volcanic rocks and associated mafic dykes of the Ouarzazate Group (Anti-Atlas, Morocco): Clinopyroxene composition, whole-rock geochemistry and Sr-Nd isotopes constraints from the Ouzellarh-Siroua salient (Tifnoute valley). Journal of African Earth Sciences, 127, 113–135, https://doi:10.1016/j.jafrearsci.2016.08.002, 2017.~~

Ben-Tami, A., Belkacim, S., Baidada, B., El Kabouri, J., Assalmi, M., Bhilisse, M., and Bouabdellah, M.: Lithostratigraphy, Whole-Rock, and Sm–Nd Isotopic Data of the Ediacaran Magmatic Rocks from the Zgounder Ag–Hg Deposit (Siroua Massif, Central Anti-Atlas, Morocco). In international conference on Mediterranean Geosciences Union (pp. 167-171). Cham: Springer Nature Switzerland, https://doi.org/10.1007/978-3-031-48758-3_38, 2024.

Benziane, F., Yazidi, A., Saadane, A., Yazidi, M., El Fahssi, A., Stone, B. D., and Ejjaouani, H.: Carte géologique du Maroc au 1/50 000, feuille KELÂAT M'GOUNA Notice explicative. Notes Mémoires Service Géologique Maroc, 468, 136, 2008.

Benziane, F.: Lithostratigraphie et évolution géodynamique de l'Anti-Atlas (Maroc) du Paléoprotérozoïque au Néoprotérozoïque: exemples de la boutonnière de Tagragra de Tata et du Jbel Saghro. Thèse de doctorat, Université de Savoie CISM, Chambéry, France. 321 pp, 2007.

Beraaouz, E. H., Ikenne, M., Mortaji, A., Madi, A., Lahmam, M., & Gasquet, D.: Neoproterozoic granitoids associated with the Bou-Azzer ophiolitic melange (Anti-Atlas, Morocco): evidence of adakitic magmatism in an arc segment at the NW edge of the West-African craton. Journal of African Earth Sciences, 39(3-5), 285-293, https://doi.org/10.1016/j.jafrearsci.2004.07.040, 2004.

Blein, O., Baudin, T., Chevremont, P., Gasquet, D.: Petrogenesis of late Ediacaran volcanic rocks of the Kerdous and Tagragra d'Akka inliers (Anti-Atlas Morocco): involvement of slab-failure. Journal of African Earth Sciences, 199, 104831, https://doi.org/10.1016/j.jafrearsci.2023.104831, 2023.

Blein, O., Baudin, T., Chèvremont, P., Soulaimani, A., Admou, H., Gasquet, P., … Gombert, P.: Geochronological constraints on the polycyclic magmatism in the Bou Azzer-El Graara inlier (Central Anti-Atlas Morocco). Journal of African Earth Sciences, 99, 287–306, https://doi:10.1016/j.jafrearsci.2014.04.021, 2014.

Blein, O., Baudin, T., Soulaimani, A., Cocherie, A., Chèvremont, P., Admou, H., … Roger, J.: New geochemical, geochronological and structural constraints on the Ediacaran evolution of the south Sirwa, Agadir-Melloul and Iguerda inliers, Anti-Atlas, Morocco. Journal of African Earth Sciences, 98, 47–71, https://doi:10.1016/j.jafrearsci.2014.06.019, 2014b.

Bonin, B.: Do coeval mafic and felsic magmas in post-collisional to within-plate regimes necessarily imply two contrasting, mantle and crustal, sources? A review. Lithos, 78(1-2), 1-24, https://doi.org/10.1016/j.lithos.2004.04.042, 2004.

Bouougri, E. H., Aït Lahna, A., Tassinari, CCG., Basei, MAS., Youbi, N., Admou, H., Saquaque, A., Boumehdi, A., Maacha, L.: Time constraints on early Tonian Rifting and Cryogenian Arc terrane-continent convergence along the northern margin of the West African craton: Insights from SHRIMP and LA-ICP-MS zircon geochronology in the Pan-African Anti-Atlas belt (Morocco). Gondwana Research. 85:169-188, https://doi.org/10.1016/j.gr.2020.03.011, 2020.

Boynton, W. V.: Cosmochemistry of the rare earth elements: meteorite studies. In Developments in geochemistry, Elsevier, (Vol. 2), (pp. 63-114), https://doi.org/10.1016/B978-0-444-42148-7.50008-3, 1984.

Cabanis B, Lecolle M.: Le diagramme La/10–Y/15–Nb/8: un outil pour la discrimination des séries volcaniques et la mise en évidence des processus de mélange et/ou de contamination crustale. Comptes Rendus de l'Académie des Sciences, Paris, Série II 309:2023–2029, 1989.

Campbell McCuaig., Kerrich, R., and Xie, Q.: Phosphorus and high field strength element anomalies in Archean high-magnesian magmas as possible indicators of source mineralogy and depth. Earth and Planetary Science Letters, 124(1-4), 221-239, https://doi.org/10.1016/0012-821X(94)00088-3, 1994.

Chichorro, M., Solá, A. R., Bento dos Santos, T. M., Lains Amaral, J., & Crispim, L.: Cadomian/Pan-African consolidation of the Iberian Massif assessed by its detrital and inherited zircon populations: is the~ 610Ma age peak a persistent Cadomian magmatic inheritance or the key to unravel its Pan-African basement?. Geologica acta, 20, 1-29, https://doi.org/10.1344/GeologicaActa2022.20.15, 2022.

Choubert, G.: Essai de mise au point du problème des “ignimbrites”. Bulletin Volcanologique, 25(1), 123-140, https://doi.org/10.1007/BF02596545, 1963.

Cousens, B.L.: Magmatic evolution of Quaternary mafic magmas at Long Valley Caldera and the Devils Postpile, California: effects of crustal contamination on lithospheric mantle-derived magmas. Journal of Geophysics. Res. 101, https://doi.org/10.1029/ 96JB02093, 27 673–27 689, 1996.

De Beer, C.H., Chevallier, L.P., De Kock, G.S., Gresse, P.G., Thomas, R.J.: Notice Explicative de la Carte Géologique du Maroc au 1/50 000 feuille Sirwa. Notes et Mémoires Service Géologique. Maroc 395, 86, 2000.

Dickinson, W.R., Gehrels, G.E.: Use of U–Pb ages of detrital zircons to infer maximum depositional ages of strata: a test against a Colorado Plateau Mesozoic database. Earth and Planetary Science Letters. 288, 115–125, https://doi.org/10.1016/j.epsl.2009.09.013, 2009.

De Paolo, D.J.: Trace element and isotopic effects of combined wall-rock assimilation and fractional crystallization. Earth and Planetary Science Letters. 53, 189–202, https://doi.org/10.1016/0012-821X(81)90153-9, 1981.

D’Lemos, R. S., Inglis, J. D., and Samson, S. D.: A newly discovered orogenic event in Morocco: Neoproterozoic ages for supposed Eburnean basement of the Bou Azzer inlier, Anti-Atlas Mountains. Precambrian Research, 147(1-2), 65–78, https://doi:10.1016/j.precamres.2006.02.003, 2006.

Eby, G.N.: The A-type granitoids: a review of their occurrence and chemical characteristics and speculations on their petrogenesis. Lithos. 26, 115–134, https://doi.org/10.1016/0024-4937(90)90043-Z, 1990.

Eby, G. N.: Chemical subdivision of the A-type granitoids: petrogenetic and tectonic implications. Geology, 20(7), 641-644, https://doi.org/10.1130/0091-7613(1992)020<0641:CSOTAT>2.3.CO;2, 1992.

El Baghdadi, M., El Boukhari, A., Jouider, A., Benyoucef, A., Nadem, S.: Calc-alkaline arc I-type granitoid associated with S-type granite in the Pan-African belt of eastern Anti-Atlas (Saghro and Ougnat, South Morocco). Gondwana Research. 6 (4), 557–572, https://doi.org/10.1016/S1342-937X(05)71007-8, 2003.

El Bahat, A., Ikenne, M., Cousens, B., Söderlund, U., Ernst, R., Klausen, M. B., and Youbi, N.: New constraints on the geochronology and Sm-Nd isotopic characteristics of Bas-Drâa mafic dykes, Anti-Atlas of Morocco. Journal of African Earth Sciences, 127, 77-87, https://doi.org/10.1016/j.jafrearsci.2016.09.003, 2017.

El Hadi, H., Simancas, J.F., Martínez-Poyatos, D., Azor, A., Tahiri, A., Montero, P., Fanning, C.M., Bea, F., Gonzalez-Lodeiro, F.: Structural and geochronological constraints on the evolution of the Bou Azzer Neoproterozoic ophiolite (Anti-Atlas, Morocco). Precambrian Research. 182 (1–2), 1–14, https://doi.org/10.1016/j. precamres.2010.06.011, 2010.

El Haibi, H., Hadi, H. E., Tahiri, A., Poyatos, D. M., Gasquet, D., Pérez-Cáceres, I., and Mehdioui, S.: Geochronology and isotopic geochemistry of Ediacaran high-K calc-alkaline felsic volcanism: an example of a Moroccan perigondwanan

(Avalonian?) remnant in the El Jadida horst (Mazagonia). Journal of African Earth Sciences, 163, 103669, https://doi.org/10.1016/j.jafrearsci.2019.103669, 2020.

El Kabouri, J., Triantafyllou, A., Errami, E., Belkacim, S., Calassou, E., Zouicha, A., and Linnemann, U.: Revising the lithostratigraphic framework of the Ediacaran succession of the Anti-Atlas belt: correlation across the Cadomian domain of the West African Craton. Journal of African Earth Sciences, 105696, https://doi.org/10.1016/j.jafrearsci.2025.105696, 2025.

Ennih, N., and Liégeois, J. P.: The boundaries of the West African craton, with special reference to the basement of the Moroccan metacratonic Anti-Atlas belt. Geological Society, London, Special Publications, 297(1), 1–17, https://doi.org/10.1144/SP297.1, 2008.

Ennih, N., and Liégeois, J.P.: The Moroccan Anti-Atlas: the West African craton passive margin with limited Pan-African activity. Implications for the northern limit of the craton. Precambrian Research. 112 (3–4), 289–302, https://doi.org/10.1016/S0301-9268 (01)00195-4, 2001.

Errami, E., Linnemann, U., Hofmann, M., G¨artner, A., Zieger, J., G¨artner, J., Mende, K., El Kabouri, J., Gasquet, D., Ennih, N.: From pan-african transpression to cadomian transtension at the west african margin: New U-Pb zircon ages from the eastern saghro inlier (anti-atlas, Morocco). Geological Society. Special Publications. 503, 209–233, https://doi.org/10.1144/SP503-2020-105, 2021a.

Errami, E., Bonin, B., Laduron, D., Lasri, L.: Petrology and geodynamic significance of the post-collisional Pan-African magmatism in the Eastern Saghro area (Anti- Atlas, Morocco). Journal of African Earth Sciences. 55 (1–2), 105–124, https://doi.org/10.1016/j. jafrearsci.2009.02.006, 2009.

Faure, G.: Isotope systematics in two-component mixtures. Principles of isotope geology, 2 edn. John Wiley & Sons, Chichester, 141-153, 1986.

Fekkak, A., Pouclet, A., & Benharref, M.: The middle Neoproterozoic sidi flah group (Anti-Atlas, Morocco): syn-rift deposition in a Pan-African continent/ocean transition zone. Journal of African Earth Sciences, 37(1-2), 73-87, https://doi.org/10.1016/S0899-5362(03)00049-6, 2003.

Fekkak, A., Pouclet, A., & Badra, L.: The pre-Pan-African rifting of Saghro (Anti-Atlas, Morocco): example of the middle Neoproterozoic basin of Boumalne. Bulletin de la Société géologique de France, 173(1), 25-35, https://doi.org/10.2113/173.1.25, 2002.

Fekkak, A., Pouclet, A., Ouguir, H., Ouazzani, H., Badra, L., Gasquet, D.: Géochimie et signification géotectonique des volcanites du Cryogénien inférieur du Saghro (Anti-Atlas oriental, Maroc) /Geochemistry and geotectonic significance of Early Cryogenian volcanics of Saghro (Eastern Anti-Atlas, Morocco). Geodinamica. Acta, 14 (6), 373–385, https://doi.org/10.1080/09853111.2001.10510730, 2001.

Ferraq, M., Belkacim, S., Cheng, L. Z., Davies, J. H., Perrot, M. G., Ben-Tami, A., & Bouabdellah, M.: New Geochemical and Geochronological Constraints on the Genesis of the Imourkhssen Cu±Mo±Au±Ag Porphyry Deposit (Ouzellagh-Siroua Salient, Anti-Atlas, Morocco): Geodynamic and Metallogenic Implications. Minerals, 14(8), 832, https://doi.org/10.3390/min14080832, 2024.

Frost, B. R., Barnes, C. G., Collins, W. J., Arculus, R. J., Ellis, D. J., and Frost, C. D.: A geochemical classification for granitic rocks. Journal of petrology, 42(11), 2033-2048, https://doi.org/10.1093/petrology/42.11.2033, 2001.

Garfunkel, Z.: The relations between Gondwana and the adjacent peripheral Cadomian domain—constrains on the origin, history, and paleogeography of the peripheral domain. Gondwana Research, 28(4), 1257-1281, https://doi.org/10.1016/j.gr.2015.05.011, 2015.

Gasquet, D., Ennih, N., Liégeois, J.P., Soulaimani, A., Michard, A.: The Pan-African Belt. In: Michard, A., Saddiqi, O., Chalouan, A., Frizon de Lamotte, D. (Eds.), Continental evolution: the geology of Morocco. Lect. Notes Earth Sci. 116, 33–64, https://doi.org/10.1007/978-3-540-77076-3_2, 2008.

Gasquet, D., Levresse, G., Cheilletz, A., Azizi-Samir, M. R., and Mouttaqi, A.: Contribution to a geodynamic reconstruction of the Anti-Atlas (Morocco) during Pan-African times with the emphasis on inversion tectonics and metallogenic activity at the Precambrian–Cambrian transition. Precambrian Research, 140(3-4), 157–182, https://doi:10.1016/j.precamres.2005.06.009, 2005.

Gasquet, D., Chevremont, P., Baudin, T., Chalot-Prat, F., Guerrot, C., Cocherie, A., and Cheilletz, A.: Polycyclic magmatism in the tagragra d'akka and kerdous–tafeltast inliers (western Anti-Atlas, Morocco). Journal of African Earth Sciences, 39(3-5), 267-275, https://doi.org/10.1016/j.jafrearsci.2004.07.062, 2004.

Goldstein, S. L., O'nions, R. K., and Hamilton, P. J.: A Sm-Nd isotopic study of atmospheric dusts and particulates from major river systems. Earth and planetary Science letters, 70(2), 221-236, https://doi.org/10.1016/0012-821X(84)90007-4, 1984.

Green, T. H.: Significance of Nb/Ta as an indicator of geochemical processes in the crust-mantle system. Chemical geology, 120(3-4), 347-359, https://doi.org/10.1016/0009-2541(94)00145-X, 1995.

Gresse, P.G., De Beer, C.H., Chevallier, L.P., De Kock, G.S., Thomas, R.J. : Notice Explicative de la Carte Géologique du Maroc au 1/50 000 feuille Tachoukacht. Notes et Mémoires Service Géologique. Maroc 393, 106, 2000.

Hastie, A.R., Kerr, A.C., Pearce, J.A., Mitchell, S.F.: Classification of altered volcanic island arc rocks using immobile trace elements: development of the Th–Co discrimination diagram. Journal of Petrology. 48 (12), 2341–2357, https://doi.org/10.1093/ petrology/egm062, 2007.

Hefferan, K., Soulaimani, A., Samson, S. D., Admou, H., Inglis, J., Saquaque, A., … Heywood, N.: A reconsideration of Pan African orogenic cycle in the Anti-Atlas Mountains, Morocco. Journal of African Earth Sciences, 98, 34–46, https:// doi:10.1016/j.jafrearsci.2014.03.007, 2014.

Hefferan, K., Samson, S., Hietpas, J., Admou, H., Inglis, J., Saquaque, A., & Heywood, N.: A ~ 604 Ma depositional age for the Tiddiline conglomerate, Bou Azzer inlier, Morocco based on U–Pb dating of detrital zircon. Geol. Soc. Am, 44, 285, 2012.

Hodel, F., Triantafyllou, A., Berger, J., Macouin, M., Baele, J.M., Mattielli, N., Monnier, C., Trindade, R.I.F., Ducea, M.N., Chatir, A., Ennih, N., Langlade, J., Poujol, M.: The Moroccan Anti-Atlas ophiolites: Timing and melting processes in an intra-oceanic arc-back-arc environment. Gondwana Research. 86, 182–202, https://doi.org/10.1016/j.gr.2020.05.014, 2020.

Hofmann, A. W., Jochum, K. P., Seufert, M., and White, W. M.: Nb and Pb in oceanic basalts: new constraints on mantle evolution. Earth and Planetary science letters, 79(1-2), 33-45, https://doi.org/10.1016/0012-821X(86)90038-5, 1986.

Hooper, P.R., Bailey, D.G., McCarley Holder, G.A.: Tertiary calc-alkaline magmatism associated with lithospheric extension in the Pacific Northwest. J. Geophysical Research. 100 (B6), https://doi.org/10.1029/94JB03328, 10,303–10,319, 1995.

Horstwood, M. S., Košler, J., Gehrels, G., Jackson, S. E., McLean, N. M., Paton, C., ... and Schoene, B.: Community-derived standards for LA-ICP-MS U-(Th-) Pb geochronology–Uncertainty propagation, age interpretation and data reporting. Geostandards and Geoanalytical Research, 40(3), 311-332, https://doi.org/10.1111/j.1751-908X.2016.00379.x, 2016.

Hughes, C. J.: Spilites, keratophyres, and the igneous spectrum. Geological Magazine, 109(6), 513-527, https://doi.org/10.1017/S0016756800042795, 1972.

Ikenne, M., Ennaciri, A., Ouguir, H., Cousens, B., Ziyadi, R., Mouhagir, M., & El-Gaouzi, A.: Geochemical Signature And Geodynamic Significance Of An Ag-Hg Mineralized Dyke Swarm In The Neoproterozoic Inlier Of Imiter - Anti-Atlas (Morocco). Ofioliti, 32(2), 109–118, https://doi.org/10.4454/ofioliti.v32i2.351, 2007.

Ikenne, M., Söderlund, U., Ernst, R. E., Pin, C., Youbi, N., El Aouli, E. H., and Hafid, A.: A c. 1710 Ma mafic sill emplaced into a quartzite and calcareous series from Ighrem, Anti-Atlas — Morocco: Evidence that the Taghdout passive margin sedimentary group is nearly 1 Ga older than previously thought. Journal of African Earth Sciences. 127, 62–76, https://doi:10.1016/j.jafrearsci.2016.08.020, 2017.

Inglis, J.D., D'Lemos, R.S., Samson, S.D., Admou, H.: Geochronological constraints on Late Precambrian intrusion, metamorphism, and tectonism in the anti-atlas mountains. Journal of Geology. 113, 439–450, https://doi.org/10.1086/430242, 2005.

Janoušek, V., Farrow, C. M., & Erban, V.: Interpretation of whole-rock geochemical data in igneous geochemistry: introducing Geochemical Data Toolkit (GCDkit). Journal of Petrology, 47(6), 1255-1259, https://doi.org/10.1093/petrology/egl013, 2006.

Janoušek, V., Moyen, J. F., Martin, H., Erban, V., & Farrow, C.: Geochemical modelling of igneous processes: principles and recipes in R language. Bringing the Power of R to a Geochemical Community. Springer, Berlin, https://doi.org/10.1007/978-3-662-46792-3, 2016.

Karaoui, B., Breitkreuz, C., Mahmoudi, A., Youbi, N., Hofmann, M., Gärtner, A., & Linnemann, U.: U–Pb zircon ages from volcanic and sedimentary rocks of the Ediacaran Bas Draâ inlier (Anti-Atlas Morocco): Chronostratigraphic and provenance implications. Precambrian Research. 263, 43–58, https://doi:10.1016/j.precamres.2015.03.003, 2015.

Karaoui, B., Breitkreuz, C., Mahmoudi, A., and Youbi, N.: Physical volcanology, geochemistry and basin evolution of the Ediacaran volcano-sedimentary succession in the Bas Draâ inlier (Ouarzazate Supergroup, Western Anti-Atlas, Morocco). Journal of African Earth Sciences. 99, 307-331, https://doi.org/10.1016/j.jafrearsci.2014.06.022, 2014.

Large, R.R., Gemmell, J.B., Paulick, H., Huston, D.L.: The alteration box plot: a simple approach to understanding the relationship between alteration mineralogy and lithogeochemistry associated with volcanic-hosted massive sulfide deposits. Economic Geology. 96 (5), 957–971, https://doi.org/10.2113/gsecongeo.96.5.957, 2001.

Laurent, O., Martin, H., Moyen J.F., Doucelance, R.: The diversity and evolution of late-Archean granites: Evidence for the onset of a "modern-style" plate tectonics between 3.0 and 2.5 Ga. Lithos, 205, (pp. 208-235), https://doi.org/10.1016/j, 2014.

Labanieh, S.; Chauvel, C.; Germa, A.; Quidelleur, X.: Martinique: a Clear Case for Sediment Melting and Slab Dehydration as a Function of Distance to the Trench. Journal of Petrology, 53(12), 2441–2464. https://doi:10.1093/petrology/egs055, 2012.

Leblanc, M., & Lancelot, J. R.: Interprétation géodynamique du domaine pan-africain (Précambrien terminal) de l'Anti-Atlas (Maroc) à partir de données géologiques et géochronologiques. Canadian Journal of Earth Sciences, 17(1), 142–155, https://doi:10.1139/e80-012, 1980.

Letsch, D., Houicha, M. E., von Quadt, A., and Winkler, W.: missing link in the peri-Gondwanan terrane collage: the Precambrian basement of the Moroccan Meseta and its lower Paleozoic cover. Canadian Journal of earth sciences, 55(1), 33-51, https://doi.org/10.1139/cjes-2017-0086, 2018.

Liégeois, J.P., Abdelsalam, M.G., Ennih, N., Ouabadi, A.: Metacraton: nature, genesis and behavior. Gondwana Res. 23 (1), 220–237, https://doi.org/10.1016/j. gr.2012.02.016, 2013.

Liégeois, J.P., Fekkak, A., Bruguier, O., Errami, E., Ennih, N.: The Lower Ediacaran (630–610 Ma) Saghro group: an orogenic transgressive basin development during the early metacratonic evolution of the Anti-Atlas (Morocco). In: IGCP485 4th meeting, Algiers, p. 57, 2006.

Liégeois, J. P., Navez, J., Hertogen, J., and Black, R.: Contrasting origin of post-collisional high-K calc-alkaline and shoshonitic versus alkaline and peralkaline granitoids. The use of sliding normalization. Lithos, 45(1-4), 1-28, https://doi.org/10.1016/S0024-4937(98)00023-1, 1998.

Liew, T. C., & Hofmann, A. W.: Precambrian crustal components, plutonic associations, plate environment of the Hercynian Fold Belt of central Europe: indications from a Nd and Sr isotopic study. Contributions to Mineralogy and Petrology, 98(2), 129-138, https://doi.org/10.1007/BF00402106, 1988.

Linnemann, U., Ovtcharova, M., Schaltegger, U., Gärtner, A., Hautmann, M., Geyer, G., and Smith, J.: New high-resolution age data from the Ediacaran–Cambrian boundary indicate rapid, ecologically driven onset of the Cambrian explosion. Terra Nova, 31(1), 49-58, https://doi.org/10.1111/ter.12368, 2019.

Linnemann, U., Gerdes, A., Hofmann, M., Marko, L.: The Cadomian Orogen: Neoproterozoic to Early Cambrian crustal growth and orogenic zoning along the periphery of the West African Craton-Constraints from U-Pb zircon ages and Hf isotopes (Schwarzburg Antiform, Germany). Precambrian Research. 244, 236–278, https://doi.org/10.1016/j.precamres.2013.08.007, 2014.
Linnemann, U., Gerdes, A., Hofmann, M., Marko, L.: The Cadomian Orogen: Neoproterozoic to Early Cambrian crustal growth and orogenic zoning along the periphery of the West African Craton-Constraints from U-Pb zircon ages and Hf isotopes (Schwarzburg Antiform, Germany). Precambrian Research. 244, 236–278, https://doi.org/10.1016/j.precamres.2013.08.007, 2014.
Linnemann, U., Pereira, F., Jeffries, T.E., Drost, K., Gerdes, A.: The Cadomian Orogeny and the opening of the Rheic Ocean: the diacrony of geotectonic processes constrained by LA-ICP-MS U–Pb zircon dating (Ossa-Morena and Saxo-Thuringian Zones, Iberian and Bohemian Massifs). Tectonophysics 461, 21–43, https://doi.org/ 10.1016/j.tecto.2008.05.002, 2008.

M'arquez, A., Oyarzun, R., Doblas, M., and Verma, S. P.: Alkalic (ocean-island basalt type) and calc-alkalic volcanism in the Mexican volcanic belt: a case for plume-related magmatism and propagating rifting at an active margin?. Geology, 27(1), 51-54, https://doi.org/10.1130/0091-7613(1999)027<0051:AOIBTA>2.3.CO;2, 1999.

Michard, A., Soulaimani, A., Ouanaimi, H., Raddi, Y., Brahim, L.A., Rjimati, E.C., Saddiqi, O.: Saghro Group in the Ougnat Massif (Morocco), an evidence for a continuous Cadomian basin along the northern West African Craton. Comptes Rendus Géosciences. 349 (2), 81–90, https://doi.org/10.1016/j.crte.2017.01.001, 2017.

Michard, A., Saddiqi, O., Chalouan, A., and de Lamotte, D. F. (Eds.).: Continental evolution: The geology of Morocco: Structure, stratigraphy, and tectonics of the Africa-Atlantic-Mediterranean triple junction (Vol. 116). Berlin: Springer, 2008.

Morris, G.A., Larson, P.B., Hooper, P.R.: 'Subduction style' magmatism in a non-subduction setting: the Colville Igneous Complex, NE Washington State, USA. Journal of Petrology. 41, 43–67, https://doi.org/10.1093/petrology/41.1.43, 2000.

Middlemost, E. A.: Naming materials in the magma/igneous rock system. Earth-science reviews, 37(3-4), 215-224, https://doi.org/10.1016/0012-8252(94)90029-9, 1994.

Mrini, Z.: Chronologie (Rb-Sr, U-Pb), traçage isotopique (Sr-Nd-Pb) des sources de roches magmatiques éburnéenne, panafricaine et hercynienne du Maroc. Un-published thesis. University of Marrakech, Morocco, 200 p, 1993.

Nance, R. D., Murphy, J. B., Strachan, R. A., Keppie, J. D., Gutiérrez-Alonso, G., Fernández-Suárez, J., ... & Pisarevsky, S. A.: Neoproterozoic–early Palaeozoic tectonostratigraphy and palaeogeography of the peri-Gondwanan terranes: Amazonian v. West African connections. Geological Society, London, Special Publications, 297, 345–383, https://doi.org/10.1144/SP297.17, 2008.

O'Connor, E.A., Barnes, R.P., Beddoe-Stephens, B., Fletcher, T., Gillespie, M.R., Hawkins, M.P., Loughlin, S.C., Smith, M., Smith, R.A., Waters, C.N., Williams, M.: Geology of the Drâa, Kerdous, and Boumalne Districts, Anti-Atlas. Keyworth, Nottingham British Geological Survey, Morocco, p. 324, 2010.

O'Reilly, S. Y., and Griffin, W. L.: Mantle metasomatism. Metasomatism and the chemical transformation of rock, 471-533, 2013.

Ouabid, M., Garrido, C.J.: Widespread Cadomian–Pan-African Ediacaran magmatism across the Moroccan Meseta: implication for the geodynamic evolution of the NW Gondwana margin. Precambrian Research. 387, https://doi.org/ 10.1016/j.precamres.2023.106992, 2023.

Ougadire, M., Askkour, F., Favier, A., Ousbih, M., Ikenne, M., & Géraud, Y.: Petrogenesis of the late Ediacaran A-type granites of the western part of the Moroccan Anti-Atlas belt: Insights from U–Pb dating, geochemistry and Sr–Nd isotopes of the Sidi El Houssein, Tafraout and Taourgha intrusions. Journal of African Earth Sciences, 203, 104947, https://doi.org/10.1016/j.jafrearsci.2023.104947, 2023.

Ouguir, H., Macaudière, J., Dagallier, G. : Le Protérozoïque supérieur d'Imiter, Saghro oriental, Maroc : un contexte géodynamique d'arrière-arc. Journal of African Earth Sciences. 22 (2), 173–189, https://doi.org/10.1016/0899-5362(96)00002-4, 1996.

Ousbih, M., Ikenne, M., Cousens, B., Chelle-Michou, C., El Bilali, H., Gaouzi, A., ... & Ernst, R.: Stratigraphy, geochronology, geochemistry and Nd isotopes of the Ouarzazate Group, Anti-Atlas, Morocco: Evidence of a Late Neoproterozoic LIP in the northwestern part of the West African Craton. Lithos, 474, 107593., https://doi.org/10.1016/j.lithos.2024.107593, 2024.

Pearce JA, Ernst RE, Peate DW, Rogers C.: LIP printing: use of immobile element proxies to characterize Large Igneous Provinces in the geologic record. Lithos 392–393:106068, https://doi.org/10.1016/j.lithos.2021.106068, 2021.

Pearce, J. A.: Geochemical fingerprinting of oceanic basalts with applications to ophiolite classification and the search for Archean oceanic crust. Lithos, 100(1-4), 14-48, https://doi.org/10.1016/j.lithos.2007.06.016, 2008.

Pearce, J.: Sources and settings of granitic rocks. Episodes, 19, 120-125, 1996.

Pearce, J. A., Harris, N. B., and Tindle, A. G.: Trace element discrimination diagrams for the tectonic interpretation of granitic rocks. Journal of petrology, 25(4), 956-983, https://doi.org/10.1093/petrology/25.4.956, 1984.

Pearce, J. A.: Role of the sub-continental lithosphere in magma genesis at active continental margins. Hawkesworth, C.J. and Norry, M.J., eds. Continental basalts and mantle xenoliths, Nantwich, Cheshire: Shiva Publications, pp. 230-249, 1983.

Pearce, J. A., and Norry, M. J.: Petrogenetic implications of Ti, Zr, Y, and Nb variations in volcanic rocks. Contributions to mineralogy and petrology, 69(1), 33-47, https://doi.org/10.1007/BF00375192, 1979.

Pearce, J. A., and Gale, G. H.: Identification of ore-deposition environment from trace-element geochemistry of associated igneous host rocks. Geological Society, London, Special Publications, 7(1), 14-24, https://doi.org/10.1144/GSL.SP.1977.007.01.03, 1977.

Pelleter, E., Cheilletz, A., Gasquet, D., Mouttaqi, A., Annich, M., Camus, Q., Deloule, E., Ouazzani, L., Bounajma, H., Ouchtouban, L.: U/Pb ages of magmatism in the Zgounder Epithermal Ag–Hg Deposit, Sirwa Window, Anti-Atlas, Morocco. In: Mineral Deposits of North Africa. Springer, pp. 143–165, https://doi.org/10.1007/978-3-319-31733-5_5, 2016.

Pereira, M. F., El Houicha, M., Chichorro, M., Armstrong, R., Jouhari, A., El Attari, A., and Silva, J. B.: Evidence of a Paleoproterozoic basement in the Moroccan Variscan belt (Rehamna massif, western Meseta). Precambrian Research, 268, 61-73, https://doi.org/10.1016/j.precamres.2015.07.010, 2015.

Pereira, M.F., Linnemann, U., Hofmann, M., Chichorro, M., Solá, A.R., Medina, J., Silva, J.B.: The provenance of Late Ediacaran and Early Ordovician siliciclastic rocks in the Southwest Central Iberian Zone: constraints from detrital zircon data on northern Gondwana margin evolution during the late Neoproterozoic. Precambrian Research. 192, 166-189, https://doi.org/10.1016/j.precamres.2011.10.019, 2012a.

Rojo-Pérez, E., Arenas, R., Fuenlabrada, J. M., Novo-Fernández, I., Martínez, S. S., Moreno-Martín, D., and Fernández, R. D.: Lower Cambrian magmatism in the SW Iberian sector of the African–Gondwana margin: geochemical and isotopic keys to incipient tectonic switching, https://doi.org/10.1144/SP542-2022-294, 2024.

Saadi, A.: Contribution à l'étude écologique de deux hydrosystèmes temporaires saumâtres du Maroc : Zima et Sedd-El-Messjoun (Bassin de la Bahira). PhD thesis, Semlalia Faculty, University of Cady Ayyad, Marrakech, Morocco, 1985.

Saccani, E.: A new method of discriminating different types of post-Archean ophiolitic basalts and their tectonic significance using Th-Nb and Ce-Dy-Yb systematics. Geoscience Frontiers, 6(4), 481-501, https://doi.org/10.1016/j.gsf.2014.03.006, 2015.

Safonova, I., Maruyama, S., Kojima, S., Komiya, T., Krivonogov, S., and Koshida, K.: Recognizing OIB and MORB in accretionary complexes: A new approach based on ocean plate stratigraphy, petrology and geochemistry. Gondwana Research, 33, 92-114, https://doi.org/10.1016/j.gr.2015.06.013, 2016.

Samson, S. D., Inglis, J. D., D'Lemos, R. S., Admou, H., Blichert-Toft, J., and Hefferan, K.: Geochronological, geochemical, and Nd–Hf isotopic constraints on the origin of Neoproterozoic plagiogranites in the Tasriwine ophiolite, Anti-Atlas orogen, Morocco. Precambrian Research, 135(1-2), 133–147, https://doi:10.1016/j.precamres.2004.08.003, 2004.

Saunders, A. D., and Tarney, J.: Geochemical characteristics of basaltic volcanism within back-arc basins. Geological Society, London, Special Publications, 16(1), 59-76, https://doi.org/10.1144/GSL.SP.1984.016.01.05, 1984.

Schulte, B., Boger, S.D., Benziane, F., Yazidi, A., Fanning, C.M.: The Ouarzazate Supergroup and its plutonic keel: the relics of an Ediacaran silicic large igneous province in North Africa. Journal of the Geological Society. London. 179, 5, https://doi.org/10.1144/ jgs2021-114, 2022.

Shand, S. J.: Eruptive rocks; their genesis, composition, classification, and their relation to ore-deposits with a chapter on meteorite. New York: John Wiley & Sons, 1943.

Sharman, G. R., and Malkowski, M. A.: Modeling apparent Pb loss in zircon U–Pb geochronology. Geochronology, 6(1), 37-51, https://doi.org/10.5194/gchron-6-37-2024, 2024.

Shervais, J. W.: The petrogenesis of modern and ophiolitic lavas reconsidered: Ti-V and Nb-Th. Geoscience Frontiers, 13(2), 101319, https://doi.org/10.1016/j.gsf.2021.101319, 2022.

Shervais, J. W.: Ti-V plots and the petrogenesis of modern and ophiolitic lavas. Earth and planetary science letters, 59(1), 101-118, https://doi.org/10.1016/0012-821X(82)90120-0, 1982.

Shinjo, R., and Kato, Y.: Geochemical constraints on the origin of bimodal magmatism at the Okinawa Trough, an incipient back-arc basin. Lithos, 54(3-4), 117-137, https://doi.org/10.1016/S0024-4937(00)00034-7, 2000.

Soulaimani, A., Ouanaimi, H., Saddiqi, O., Baidder, L., and Michard, A.: The Anti-Atlas Pan-African Belt (Morocco): Overview and pending questions. Comptes Rendus Géoscience, https://doi:10.1016/j.crte.2018.07.002, 2018.

Stern, R. J.: A reinterpretation of the past 2.5 billion years of Earth's tectonic history: Two episodes each of plate and single-lid tectonics. Geological Society of America Bulletin, https://doi.org/10.1130/B37966.1, 2024.

Sun, S. S., and McDonough, W. F.: Chemical and isotopic systematics of oceanic basalts: implications for mantle composition and processes. Geological Society, London, Special Publications, 42(1), (pp. 313-345), https://doi.org/10.1144/GSL.SP.1989.042.01.19, 1989.

Tahiri, A., Montero, P., El Hadi, H., Poyatos, D. M., Azor, A., Bea, F., and Lodeiro, F. G.: Geochronological data on the Rabat–Tiflet granitoids: their bearing on the tectonics of the Moroccan Variscides. Journal of African Earth Sciences, 57(1-2), 1-13, https://doi.org/10.1016/j.jafrearsci.2009.07.005, 2010.

Taylor, S. R., and McLennan, S. M.: The geochemical evolution of the continental crust. Reviews of geophysics, 33(2), 241-265, https://doi.org/10.1029/95RG00262, 1995.

Thomas, R. J., Fekkak, A., Ennih, N., Errami, E., Loughlin, S. C., Gresse, P. G., Liégeois, J.-P.: A new lithostratigraphic framework for the Anti-Atlas Orogen, Morocco. Journal of African Earth Sciences, 39(3-5), 217–226, https://doi:10.1016/j.jafrearsci.2004.07.046, 2004.

Thomas, R. ., Chevallier, L. ., Gresse, P. ., Harmer, R. ., Eglington, B. ., Armstrong, R. ., Ingram, B.: Precambrian evolution of the Sirwa Window, Anti-Atlas Orogen, Morocco. Precambrian Research, 118(1-2), 1–57, https://doi:10.1016/s0301-9268(02)00075-x, 2002.

Thomas, R.J., De Beer, C.H., Chevallier, L.P., De Kock, G.S., Gresse, P.G.: Notice Explicative de la Carte Géologique du Maroc au 1/50 000 feuille Assarag. Notes et Mémoires Service Géologique. Maroc 392, 84, 2000a.

Touil, A., Hafid, A., Moutte, J., and El Boukhari, A.: Petrology and geochemistry of the Neoproterozoic Siroua granitoids (central Anti-Atlas, Morocco): evolution from subduction-related to within-plate magmatism. Geological Society, London, Special Publications, https://doi.org/10.1144/SP297.13, 2008.

Touil, A., El-Boukhari, A., Bilal, E., and Moutte, J. : Les tholeiites a affinité alcaline du secteur ouest du Siroua (Anti-Atlas central, Maroc): témoins d'une distension au Néoprotérozoïque. Journal of African Earth Sciences, 29(4), 699-713, https://doi.org/10.1016/S0899-5362(99)00125-6, 1999.

Toummite, A., Liégeois, J.P., Gasquet, D., Bruguier, O., Beraaouz, E.H., Ikenne, M.: Field, geochemistry and Sr-Nd isotopes of the Pan-African granitoids from the Tifnoute Valley (Sirwa, Anti-Atlas, Morocco): a post-collisional event in a metacratonic setting. Mineralogy and Petrology. 107 (5), 739–763, https://doi.org/10.1007/ s00710-012-0245-3, 2013.

Triantafyllou, A., Berger, J., Baele, J.-M., Diot, H., Ennih, N., Plissart, G., Vandycke, S.: The Tachakoucht–Iriri–Tourtit arc complex (Moroccan Anti-Atlas): Neoproterozoic records of polyphased subduction-accretion dynamics during the Pan-African orogeny. Journal of Geodynamics, 96, 81–103, https://doi.org/10.1016/j.jog.2015.07.004, 2016.

Tuduri, J., Chauvet, A., Barbanson, L., Bourdier, J.L., Labriki, M., Ennaciri, A., Badra, L., Dubois, M., Ennaciri-Leloix, Ch., Sizaret, S., Maacha, L.: The Jbel Saghro au (–Ag, Cu) and Ag–Hg Metallogenetic Province: product of a Long-Lived Ediacaran Tectono-Magmatic Evolution in the Moroccan Anti-Atlas. Minerals, 8 (12), 592, https://doi.org/10.3390/min8120592, 2018.

Vasey, D. A., Cowgill, E., & Cooper, K. M.: A preliminary framework for magmatism in modern continental back-arc basins and its application to the Triassic-Jurassic tectonic evolution of the Caucasus. Geochemistry, Geophysics, Geosystems, 22(6), e2020GC009490, https://doi.org/10.1029/2020GC009490, 2021.

Vermeesch, P.: IsoplotR: A Free and Open Toolbox for Geochronology. Geoscience Frontiers. 9 (5), 1479–1493, https://doi.org/10.1016/j.gsf.2018.04.001, 2018.

Vermeesch, P.: How many grains are needed for a provenance study?. Earth and Planetary Science Letters, 224(3-4), 441-451, https://doi.org/10.1016/j.epsl.2004.05.037, 2004.

Walsh, G.J., Aleinikoff, J.N., Harrison, R.W., Yazidi, A., Burton, W.C., Quick, J.E., Benziane, F., Yazidi, A., Saadane, A.: Neoproterozoic tectonic evolution of the Jebel Saghro and Bou Azzer—El Graara inliers, eastern and central Anti-Atlas, Morocco. Precambrian Research. 216, 23–62, https://doi.org/10.1016/j. precamres.2012.06.010, 2012.

Walsh, G. J., Aleinikoff, J. N., Benziane, F., Yazidi, A., & Armstrong, T. R.: U–Pb zircon geochronology of the Paleoproterozoic Tagragra de Tata inlier and its Neoproterozoic cover, western Anti-Atlas, Morocco. Precambrian Research, 117(1-2), 1-20, https://doi.org/10.1016/S0301-9268(02)00044-X, 2002.

Wilson, M. (Ed.).: Igneous petrogenesis. Dordrecht: Springer Netherlands, 1989.

Winchester, J. A., and Floyd, P. A.: Geochemical discrimination of different magma series and their differentiation products using immobile elements. Chemical geology, 20, (pp. 325-343), https://doi.org/10.1016/0009-2541(77)90057-2, 1977.

~~Wood, D. A.: The application of a Th-Hf-Ta diagram to problems of tectonomagmatic classification and to establishing the nature of crustal contamination of basaltic lavas of the British Tertiary Volcanic Province. Earth and planetary science letters, 50(1), 11-30, https://doi.org/10.1016/0012-821X(80)90116-8, 1980.~~

Yajioui, Z., Karaoui, B., Chew, D., Breitkreuz, C., Mahmoudi, A.: U–Pb zircon geochronology of the Ediacaran volcano-sedimentary succession of the NE Saghro inlier (Anti-Atlas, Morocco): chronostratigraphic correlation on the northwestern margin of Gondwana. Gondwana Research. 87, 263–277, https://doi.org/10.1016/j. gr.2020.06.015, 2020.

Youbi, N., Ernst, R.E., Soderlund, U., Boumehdi, M.A., Ait Lahna, A., Tassinari, C.C.G., El Moume, W., Bensalah, M.K.: The Central Iapetus magmatic province: an updated review and link with the ca. 580 Ma Gaskiers glaciation. In: Adatte, T., Bond, D.P.G., Keller, G. (Eds.), Mass Extinctions, Volcanism, and Impacts: New Developments: Geological Society of America Special Paper, 544, pp. 35–66, https://doi.org/10.1130/2020.2544(02), 2020.